University of Alberta

HUMAN UBIQUITIN-CONJUGATING ENZYME VARIANT HUEV1A: STRUCTURE, DYNAMICS, AND CATALYTIC MECHANISM

by

David Duong Hau

A thesis submitted to the Faculty of Graduate Studies and Research in partial fulfillment of the requirements for the degree of **Master of Science**.

Department of Biochemistry

Edmonton, Alberta
Fall 2006

Library and Archives Canada

Published Heritage Branch

395 Wellington Street
Ottawa ON K1A 0N4
Canada

Bibliothèque et Archives Canada

Direction du Patrimoine de l'édition

395, rue Wellington
Ottawa ON K1A 0N4
Canada

Your file Votre référence
ISBN: 978-0-494-22282-9
Our file Notre référence
ISBN: 978-0-494-22282-9

NOTICE:
The author has granted a non-exclusive license allowing Library and Archives Canada to reproduce, publish, archive, preserve, conserve, communicate to the public by telecommunication or on the Internet, loan, distribute and sell theses worldwide, for commercial or non-commercial purposes, in microform, paper, electronic and/or any other formats.

The author retains copyright ownership and moral rights in this thesis. Neither the thesis nor substantial extracts from it may be printed or otherwise reproduced without the author's permission.

AVIS:
L'auteur a accordé une licence non exclusive permettant à la Bibliothèque et Archives Canada de reproduire, publier, archiver, sauvegarder, conserver, transmettre au public par télécommunication ou par l'Internet, prêter, distribuer et vendre des thèses partout dans le monde, à des fins commerciales ou autres, sur support microforme, papier, électronique et/ou autres formats.

L'auteur conserve la propriété du droit d'auteur et des droits moraux qui protège cette thèse. Ni la thèse ni des extraits substantiels de celle-ci ne doivent être imprimés ou autrement reproduits sans son autorisation.

In compliance with the Canadian Privacy Act some supporting forms may have been removed from this thesis.

While these forms may be included in the document page count, their removal does not represent any loss of content from the thesis.

Conformément à la loi canadienne sur la protection de la vie privée, quelques formulaires secondaires ont été enlevés de cette thèse.

Bien que ces formulaires aient inclus dans la pagination, il n'y aura aucun contenu manquant.

Canada

Abstract

Since the late 1970's, the protein ubiquitin and, in particular, protein modification by covalent attachment of ubiquitin have been extensively studied due to their role in a multiplicity of cellular processes. Covalent attachment of a chain of ubiquitins, linked through isopeptide results in altered activity or fate for the protein substrate. Polyubiquitin chains linked through Lys^{63} have been associated with such processes as immunity, DNA repair, endocytosis, and translation. The polyubiquitination of the signalling adapter proteins TRAF6 and TRAF2 are important events within the signal cascade responsible for the activation of NF-κB, JNK, and p38. Polyubiquitination of TRAF2/6 requires a heterodimer composed of an E2 known as hUbc13 and an E2 variant known as hUev1a. This dissertation documents research involving the structure determination of hUev1a by NMR, studies concerning the protein interactions of hUev1a, and some insights into the atomic mechanism of ubiquitin conjugation.

Acknowledgements

I would like to thank:

1) The Canadian Institutes for Health Research (CIHR), the Alberta Heritage Foundation for Medical Research (AHFMR), and the University of Alberta for financial support.

2) Dr. Leo Spyracopoulos for giving me the opportunity to study god by NMR.

3) Mike Lewis and Linda Saltibus for their friendship and knowhow.

4) Ryan Hoffman, Pascal Mercier, Roman Eisner, and Xu Wang for their expertise.

5) My family and friends for their support.

For my parents

Contents

1 Introduction 1

1.1 Ubiquitin . . . 1
1.2 Ubiquitination . . . 1
1.2.1 Lys^{63}-linked Polyubiquitin Chains . . . 2
1.3 The Ubiquitination Machinery . . . 2
1.3.1 Ubiquitin-Activating Enzymes . . . 3
1.3.2 Ubiquitin-Conjugating Enzymes . . . 3
1.3.3 Ubiquitin-Conjugating Enzyme Variants . . . 4
1.3.4 Ubiquitin Ligases . . . 6
1.4 The hMms2·hUbc13 Heterodimer . . . 6
1.4.1 Biological Function . . . 6
1.4.2 Structure . . . 8
1.4.3 Model for Ubiquitin Conjugation . . . 8
1.5 hUev1a: a Human Ubiquitin-Conjugating Enzyme Variant . . . 10
1.5.1 Biological Function . . . 10
1.5.2 Characteristics of hUev1a . . . 14
1.6 Overview . . . 15

2 NMR Solution Structure of hUev1a 25

2.1 Introduction . . . 25
2.2 Experimental Procedures . . . 25
2.2.1 Cloning and Expression . . . 25
2.2.2 NMR Spectroscopy . . . 26
2.2.3 Structure Calculations . . . 27
2.3 Results . . . 28
2.4 Discussion . . . 29
2.4.1 Structural Comparison to hMms2 . . . 29

3 Main Chain Dynamics of hUev1a 36

3.1 Introduction . . . 36
3.2 Experimental Procedures . . . 36
3.3 Results . . . 37
3.4 Discussion . . . 39

4 Protein-Protein Interactions of hUev1a with Ub and hUbc13 **41**
4.1 Introduction 41
4.2 Experimental Procedures 41
4.2.1 Cloning and Expression 41
4.2.2 Titration of hUbc13 into [U-^{15}N]-hUev1a 41
4.2.3 Chemical shift mapping of [U-15N]-hUev1a upon titration with Ub 42
4.3 Results 42
4.3.1 Chemical shift mapping of [U-^{15}N]-hUev1a upon titration with hUbc13 42
4.3.2 Chemical shift mapping of [U-^{15}N]-hUev1a upon titration with Ub . 43
4.4 Discussion 43
4.4.1 Interaction with hUbc13 43
4.4.2 Interaction with Ubiquitin 46
4.4.3 Potential E3 Interactions 46

5 Molecular Dynamics Simulations for the Ub·hUev1a·hUbc13~Ub Tetramer **53**
5.1 Introduction 53
5.2 Experimental Procedures 53
5.2.1 Model-building for the hUev1a·(Ub-Gly-Gly^{76}~Cys^{87}-hUbc-13)·Ub tetramer 53
5.3 Results 55
5.4 Discussion 56

6 Conclusion **62**
6.1 Conclusion 62

A hUev1a Chemical Shifts **68**

B Python Scripting **88**

List of Tables

2.1 Characteristics of the Ensemble of Structures for hUev1a 30

A.1 Backbone Amide ^{15}N and ^{1}H Chemical Shifts 68
A.2 ^{13}C Chemical Shifts 72
A.3 $^{1}H_{\alpha}$ and $^{1}H_{\beta}$ Chemical Shifts 77
A.4 $^{1}H_{\gamma}$, $^{1}H_{\delta}$, and $^{1}H_{\epsilon}$ Chemical Shifts 81
A.5 Aromatic Sidechain ^{13}C, ^{15}N, and ^{1}H Chemical Shifts 85
A.6 Sidechain Amide ^{15}N and ^{1}H Chemical Shifts 87

List of Figures

1.1 Mechanism of E1 Ubiquitin Activation 4
1.2 Common Core Structure for E2 Enzymes 5
1.3 Structure of RING Domains 7
1.4 Model for Ub Conjugation and Structure of Ub-bound hMms2 9
1.5 hUev1a-mediated Pathways for NF-κB and JNK\p38 Activation 13
1.6 Sequence Alignment of hUev1a and hMms2 15

2.1 Solution Structure for the Core Domain of hUev1a 29

3.1 Rotational Diffusion Tensors for hUev1a 38
3.2 Main Chain Dynamics for hUev1a 38

4.1 Protein-Protein Interactions for hUev1a 44
4.2 Chemical Shift Maps for hUev1a upon Binding of Ub and hUbc13 45
4.3 Surface Representations of hUev1a and Cognate Protein Binding Partners . 47
4.4 Sequence Alignment of RING Domains from TRAF6, TRAF2, and c-Cbl . 48
4.5 Sequence Alignment of UbcH7 and hUbc13 48
4.6 Sequence Alignment of RING Domains from TRAF6 and c-Cbl 49
4.7 Sequence Alignment of UbcH7 and hUbc13 49
4.8 Structure of the c-Cbl·UbcH7 Heterodimer and Model of the hUev1a·hUbc13·TRAF6 RING Domain Trimer 50

5.1 Instantaneous ΔpK_a Values for the Lys^{63} ϵ-nitrogen of Acceptor Ub 55
5.2 Model for Synthesis of Lys^{63}-linked polyUb Chains 58

6.1 Differences in Core Residues Between hUev1a and hMms2 65
6.2 Models for Polyubiquitin-Chain Synthesis 66

List of Symbols, Nomenclature, Acronyms, and Abbreviations

2D	two-dimensional
3D	three-dimensional
AIC	Akaike's information criteria
AMP	adenosine monophosphate
APF-1	ATP-dependent proteolysis factor 1
ATP	adenosine triphosphate
Bcl	B-cell CLL/lymphoma
Cbl	casitas B-lineage lymphoma
C-terminal	carboxy terminal
CARMA	CARD-containing MAGUK
CHIP	C-terminal of Hsp70-interacting protein
DNA	deoxyribonucleic acid
DSS	2,2-dimethyl-2-silapentane-5-sulfonate
DTT	dithiothreitol
E1	ubiquitin-activating enzyme
E2	ubiquitin-conjugating enzyme
E3	ubiquitin ligase
E. coli	*Escherichia coli*
FHSQC	fast HSQC
GST	glutathione S-transferase
HECT	homologous to E6AP C-terminus
Hsp	heat shock protein
HSQC	heteronuclear single quantum coherence
IKK	IκB kinase
IL-1β	interleukin-1β
IPTG	isopropyl-β-D-thiogalactopyranoside
IRAK	IL-1β receptor associated kinase
JNK	jun N-terminal kinase
K_D	dissociation constant
L	loop
LB	Luria-Bertani broth
MALT	mucosa-associated lymphoid tissue

MAPK	mitogen-activated protein kinase
MAPKK	MAPK kinase
MAPKKK	MAPKK kinase
MKK	MAPKK
Mms	methyl methanesulfonate
mRNA	messenger ribonucleic acid
MyD	myeloid differentiation factor
N-terminal	amino terminal
NEMO	NF-κB essential modulator
Nf-κB	nuclear factor kappa B
NMR	nuclear magnetic resonance
NOE	nuclear Overhauser effect
NOESY	nuclear Overhauser effect spectroscopy
PBS	phosphate-buffered saline
PCNA	proliferating cell nuclear antigen
PD	Parkinson's disease
PKC	protein kinase C
PolyUb	polyubiquitin
PP_i	pyrophosphate
RAD	ras associated with diabetes
RING	really interesting new gene
RIP	receptor interacting protein
RMSD	root mean square deviation
S^2	generalized order parameter
TAB	tubulin antisense-binding
TAK	TGFβ-activated kinase
TNFα	tumour necrosis factor α
TNFR	tumor necrosis factor receptor
TOCSY	total correlated spectroscopy
TRADD	TNFR-associated death domain
TRAF	TNFR-associated factor
Ub	ubiquitin
Ubc	ubiquitin-conjugating enzyme
UEV	ubiquitin-conjugating enzyme variant
UV	ultraviolet

E2s	hUbc13, UbcH7
UEVs	hUev1a, hMms2
E3s	TRAF6, TRAF2, c-Cbl

Chapter 1

Introduction

1.1 Ubiquitin

The search for thymic polypeptide hormones [30] from extracts which recovered immunological functioning in athymic mice led to the discovery of ubiquitin (Ub) [53]. First isolated from bovines, the 8.5 kDa ubiquitin protein was found to induce T and B cell differentiation *in vitro*, and was subsequently dubbed 'ubiquitin' since it was found in the cells of yeast, higher plants, insects, and animals (including humans) [30, 89, 25]. Two interesting facets regarding the characterization of the 76 residue ubiquitin protein [72] are that it is highly conserved [25, 89] and exceedingly stable over a wide range of pH and temperature values [67].

1.2 Ubiquitination

Ubiquitin was accidentally discovered during studies of T and B cell differentiation [30]. Subsequently, the function of ubiquitin was discovered through research examining the ATP requirement for protein degradation [92, 36]. The protein APF-1 was known to form covalent bonds to target proteins in an ATP-dependent reaction, and conjugation was thought to be a necessary requirement for the degradation of target proteins [16, 15]. Interestingly, APF-1 is now known as ubiquitin [103], and subsequent research strongly supported ubiquitin ligation as a requirement for breakdown of numerous proteins in mammalian, yeast, and plant cells [35]. Furthermore, the ubiquitin molecules were attached to the target protein as polyubiquitin chains [38] linked through an isopeptide bond consisting of the C-terminus of one ubiquitin and the side chain amine group from Lys^{48} of another

ubiquitin [11]. The process of ubiquitination will be discussed in Section 1.3. The 26S proteasome complex is responsible for the degradation of ubiquitinated proteins [40, 45, 46], whereby the target protein is unfolded, using energy derived from ATP hydrolysis, and hydrolysed into small peptides [6].

Ubiquitin-dependent proteolysis of proteins is integral to many cellular processes, including the regulation of cell cycle and division, differentiation and development, the cellular response to stress and extracellular effectors, morphogenesis of neuronal networks, modulation of cell surface receptors, ion channels and the secretory pathway, DNA repair, transcriptional regulation, transcriptional silencing, long-term memory, circadian rhythms, regulation of the immune and inflammatory responses, and biogenesis of organelles. [28]

1.2.1 Lys^{63}-linked Polyubiquitin Chains

Of the seven lysine residues on ubiquitin, only Lys^{48} is essential [94]. Of the remaining six lysine residues, four have been found to be involved in polyubiquitin chains, with chains linked through Lys^{63} being the most well understood [82].

Lys^{63}-linked polyubiquitin chains were first discovered in yeast and were important for stress responses [4]. Over the past decade, Lys^{63}-linked polyubiquitin chains have been shown to be important for various cellular processes such as post-replicative DNA repair [94, 43], NF-κB activation [20], p38 and JNK activation [102], translation [93], and endocytosis [24]. However, the mechanisms by which Lys^{63}-linked polyubiquitin chains function in these processes remains to be fully understood. A key determinant for the distinct functional differences between Lys^{48}-linked and Lys^{63}-linked polyubiquitin chains is thought to be due to a difference in chain topologies [100].

1.3 The Ubiquitination Machinery

The process by which a polyubiquitin chain is covalently assembled onto a target protein has multiple steps and requires a host of enzymes [82]. The first step involves the covalent attachment of Ub to a Ub-activating enzyme (E1), which is driven by energy derived from ATP hydrolysis. The carboxy terminus of Ub forms a thioester bond with a cysteine on the E1. Subsequently, the activated Ub is transferred to a Ub-conjugating enzyme (E2

or Ubc), which is also attached to Ub through a similar thioester linkage. Next, a Ub ligase catalyzes the transfer of Ub from the E2 to the target protein, forming an isopeptide bond between the C-terminus of the Ub and the sidechain amine group of a lysine on the target protein. Further Ub molecules may be attached to one of several lysine residues found on the existing Ub, and this process is repeated to produce a poly-Ub chain [36, 54, 41].

In the following subsections, the E1, E2, and E3 protein families will be discussed in further detail.

1.3.1 Ubiquitin-Activating Enzymes

In the search for the enzyme(s) responsible for the production of polyubiquitin chains, the first identified enzyme was the ubiquitin-activating enzyme, or E1 [15, 14]. E1 proteins function as homodimers, composed of two 105 kDa subunits [14]. The mechanism by which the E1 activates ubiquitin can be broken down into three steps. First, ATP and ubiquitin form a ubiquitin adenylate (AMP-Ub), which is tightly bound to the E1. Next, the ubiquitin is transferred from the adenylate to the E1, releasing AMP. The C-terminus of ubiquitin forms a thioester bond with a cysteine thiol group on the E1. In the third step, an additional ubiquitin molecule is adenylated, resulting in an E1 subunit that is covalently bound to one ubiquitin molecule and non-covalently bound to a ubiquitin adenylate [31, 32]. The covalently bound ubiquitin molecule is then transferred to a ubiquitin-conjugating enzyme, or E2, in a transthioesterification reaction, whereby the C-terminus of the ubiquitin forms a thioester bond with the active site cysteine on the E2 [39] (Figure 1.1). The role of the E1 is to essentially imbue the ubiquitin molecule with enough ATP-derived chemical potential to drive subsequent reactions [98].

The human E1 protein is found in the cytosol and nucleus of all cells [34], and, like the other enzymes in the ubiquitin system, is highly conserved in evolution [36].

1.3.2 Ubiquitin-Conjugating Enzymes

In general, ubiquitin-conjugating enzymes are a family of proteins whose function is to mediate the transfer of ubiquitin from the E1 to the protein substrate, with or without the assistance of a ubiquitin ligase, or E3 [36] (Section 1.3.4). The specific E2/E3 pair determines which target protein is ubiquitinated and therefore the biological process in

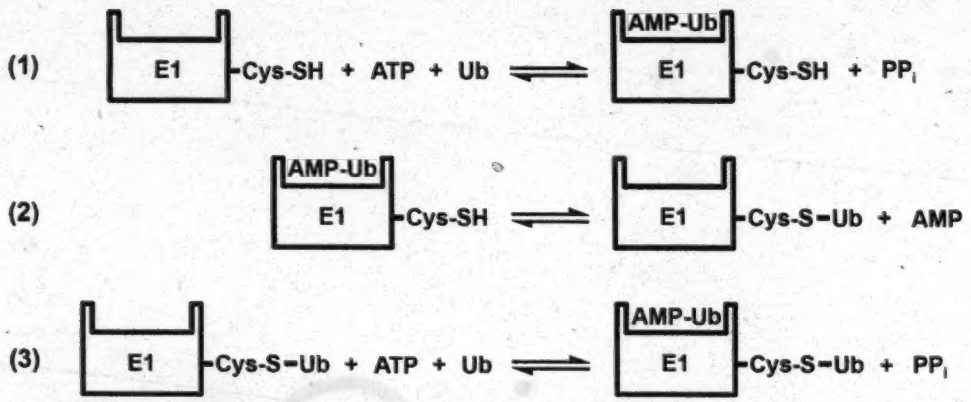

Figure 1.1: **Mechanism of E1 Ubiquitin Activation.** The mechanism can be broken down into three steps: (1) the formation of a non-covalently bound ubiquitin-adenylate, (2) transfer of the ubiquitin to the thiol group on the active site cysteine, releasing AMP, and (3) binding of an additional ubiquitin-adenylate. Adapted from [32].

which the ubiquitin is involved [82, 37].

Evidence indicates that interactions between E1 and E2 bring E1-bound ubiquitin within catalytic proximity to the E2 [83].

The human genome project indicates that there are more than 40 different E2s [104]. Class I E2 proteins are the most well studied and share a common core structure consisting of a four stranded anti-parallel β-sheet, a short 3_{10} helix, and four α helices [17, 105, 55, 78, 50, 79, 44, 71]. E2s contain a conserved active site cysteine residue whose thiol group forms a covalent bond with the carboxy terminus of activated ubiquitin molecules transferred from the E1 [82]. The recently discovered class II E2 protein [77] is not relevant to the work presented herein and will not be discussed.

In this thesis, all experiments involving E2 enzymes were conducted exclusively with the E2 hUbc13.

1.3.3 Ubiquitin-Conjugating Enzyme Variants

Ubiquitin-conjugating enzyme variant (UEV) proteins structurally resemble E2s, but lack the active site cysteine residue [83]. UEVs heterodimerize with E2s to produce polyubiquitin chains linked through Lys^{63} [43, 20]. More specifically, UEVs bind to both Ub and

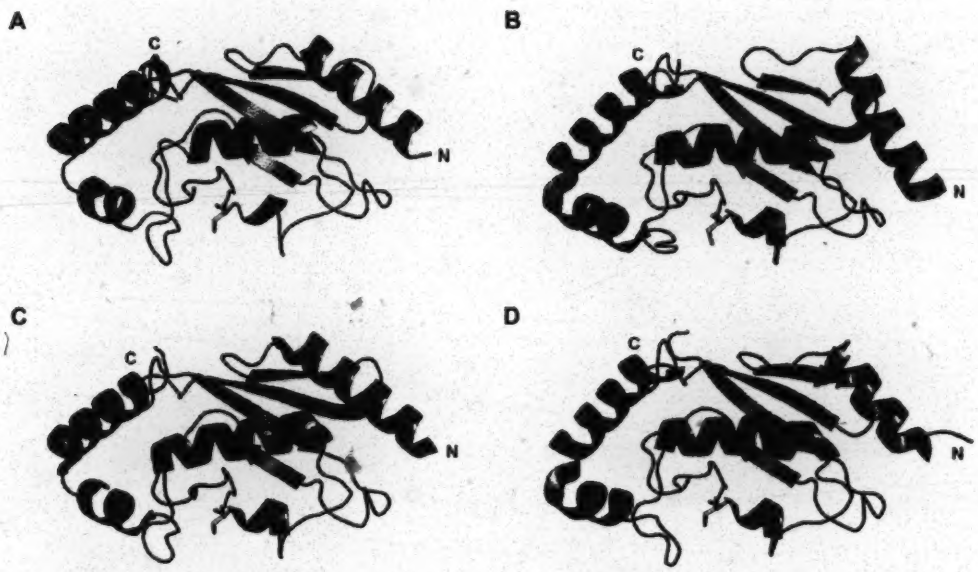

Figure 1.2: **Common Core Structure for E2 Enzymes** E2 protein structures of clam E2-C (A), yeast Ubc4 (B), human UbcH10 (C), and human Ubc13 (D) [55, 17, 79, 71]. The tertiary structure of E2s is conserved, consisting of a four strand anti parallel β-sheet, a short 3_{10} helix, and four α helices. Active site cysteine residues are shown in yellow.

the E2, aligning Lys^{63} of Ub near the active site of the E2 [99, 76, 68].

To date, only two UEVs have been studied, hUev1a and hMms2. We will focus on these two UEVs in Sections 1.4 and 1.5.

1.3.4 Ubiquitin Ligases

Ubiquitin ligases, or E3s, may cooperate with one or more E2s, and may ubiquitinate more than one type of substrate [82]. In general, E3s act as a scaffolding protein, bringing together E2s and the target proteins, thereby facilitating the transfer of Ub [83]. It is estimated that there are more than 300 E3 proteins [104], which would account for the diversity of cellular processes in which ubiquitination is involved.

There are three known E3 families: Homologous to E6AP Carboxy Terminus (HECT), Really Interesting New Gene (RING), and UFD2 homology (U-box) proteins [83].

In this report, we will only touch on E3s possessing RING domains; a brief description follows.

RING Domains

RING domains are characterized by a short motif containing conserved cysteine and histidine residues, which are required to coordinate two zinc ions [7]. Apart from the conserved zinc-coordinating residues, the primary sequence of RING domains are not highly conserved [83]. The structure of RING domains are characterized by a central α-helix and two small β-strands [7] (Figure 1.3). Evidence of direct interactions between RING domains and E2s as well as structures of these dimers have been produced [2, 9, 108]. The biological importance of E2·RING domain interactions has also been extensively characterized and includes such processes as DNA repair, transcription control, cell cycle regulation, and apoptosis [57].

1.4 The hMms2·hUbc13 Heterodimer

1.4.1 Biological Function

DNA is highly susceptible to damage that results in strand lesions. During replication of DNA, lesions are able to stall the replication machinery [86]. One mechanism by which

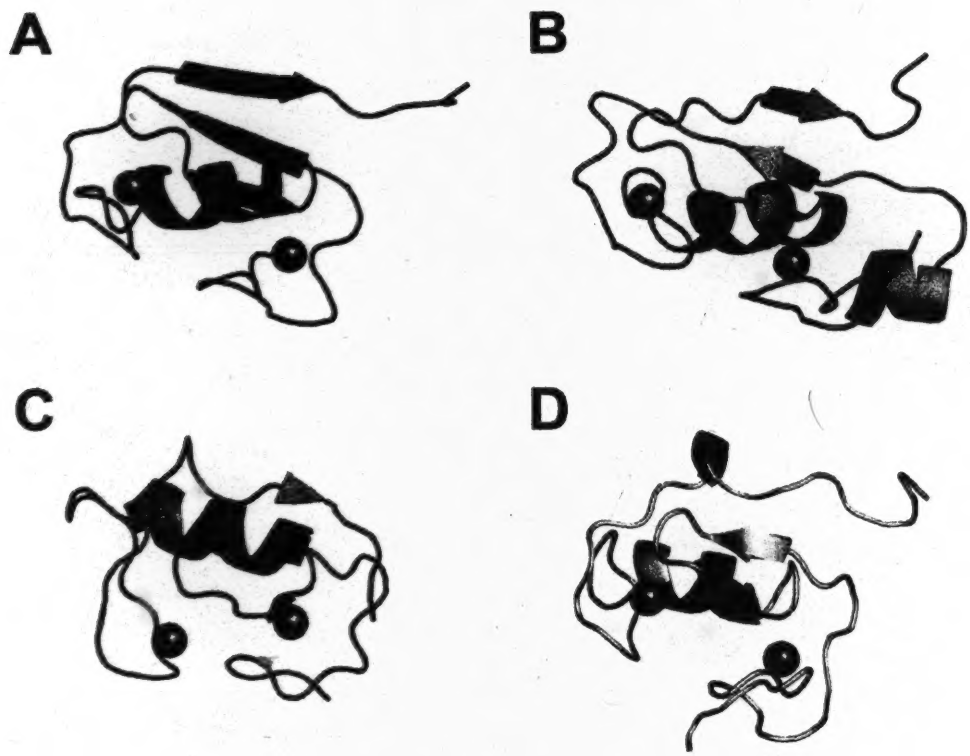

Figure 1.3: **Structure of RING Domains.** Structures of RING domains from: the EHV-63 protein of equine herpes virus 1 (A) [5], human MAT1 protein (B) [26], human BRCA1 protein (C) [10], and human TRAF6 (D) (Mercier, not yet published). The typical tertiary structure of RING domains are characterized by a central α-helix and at least two small β-strands. Coordinated zinc atoms are depicted as gray spheres.

the lesion is overcome and replication is resumed involves ubiquitination of proliferating cell nuclear antigen (PCNA), which functions as a trimer to tether DNA polymerases to DNA [66]. The polyubiquitination of PCNA occurs in two steps; first, an E2/E3 complex, RAD6/RAD18, ligates the first ubiquitin to PCNA, providing the substrate for an E2/UEV/E3 complex, hUbc13/hMms2/RAD5, to attach further ubiquitin molecules, producing a Lys^{63}-linked polyubiquitin chain [42]. It is thought that the polyubiquitination of PCNA destabilizes the DNA polymerase δ complex such that it is able to reassemble on the daughter strand of the sister duplex and use it as template, thus overcoming the lesion [8].

1.4.2 Structure

Both the yeast [99] and human [79] Mms2·Ubc13 structures have been determined. The structure of Ubc13 is that of a typical E2 as described in Section 1.3.2 (Figure 1.2D). The structure of Mms2 is composed of a central four strand, antiparallel β sheet flanked by two α helices and a 3_{10} helix [79].

1.4.3 Model for Ubiquitin Conjugation

A structural model for the hUbc13·hMms2 heterodimer complexed with two ubiquitin molecules has been produced, using chemical shift mapping and a docking program [75] (Figure 1.4A). The donor ubiquitin is bound to hUbc13 while the other ubiquitin, the acceptor Ub, noncovalently interacts with both hUbc13 and hMms2 such that Lys^{63} of the acceptor is proximal to the active site cysteine on hUbc13. Thus, the model suggests how the hMms2·hUbc13 heterodimer positions ubiquitin molecules for conjugation.

However, since the model is based predominately on chemical shift maps, the resolution and accuracy of the tetamer is compromised. Recently, a high resolution structure of Ub-bound hMms2 has been produced, which supports the tetramer model in that hMms2 binds Ub similarly in both structures [68] (Figure 1.4B).

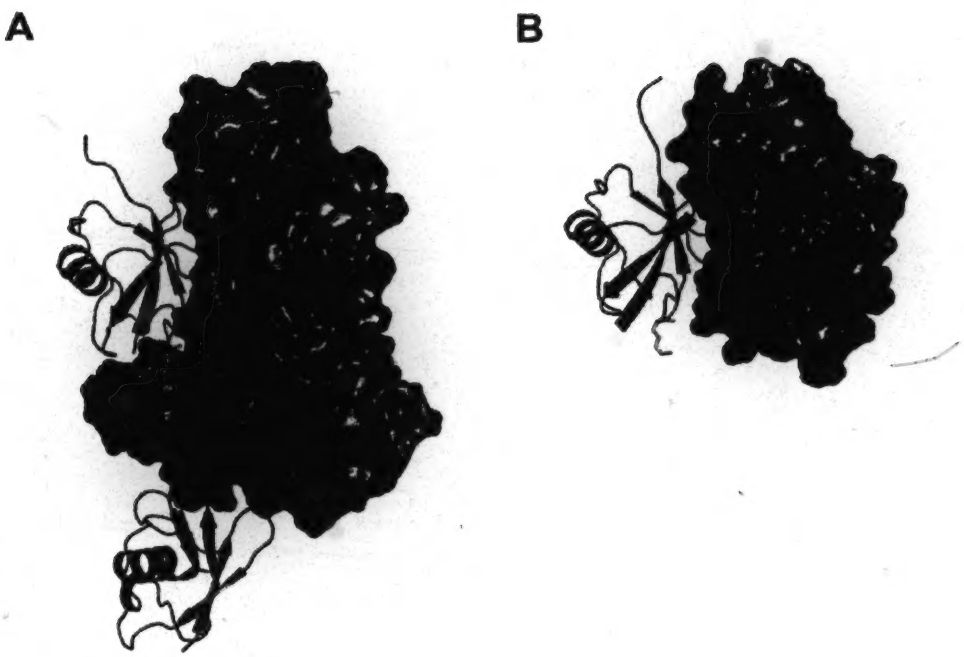

Figure 1.4: **Model for Ub Conjugation and Structure of Ub-bound hMms2.** The tetramer model for Ub conjugation (A) [75] and the NMR-derived solution state structure of hMms2 bound to Ub (B) [68]. hMms2, hUbc13, and Ub are shown in orange, purple, and green, respectively, while Lys^{63} is shown in yellow.

1.5 hUev1a: a Human Ubiquitin-Conjugating Enzyme Variant

1.5.1 Biological Function

The human ubiquitin-conjugating enzyme variant hUev1a dimerizes with hUbc13 to function as an E2, catalyzing Lys^{63}-linked polyubiquitin chains. hUev1a·hUbc13 activity is important for the activation of NF-κB, p38, and JNK [12]. Moreover, recent research has suggested that hUev1a-hUbc13 activity may play a role in Parkinson's disease pathogenesis [22] as well as in the cellular machinery that handles misfolded proteins [90].

In the following subsections, systems in which hUev1a is directly, or potentially, involved in will be summarized.

NF-κB Activation

Recognition of pathogens by innate or adaptive immune cells (eg. macrophages, dendritic cells, and lymphocytes) leads to the activation of these cells. Activation results in the expression and secretion of cytokines, which in turn activate other cells to culminate an immune response [27]. Among the numerous cytokines that are produced, tumour necrosis factor α (TNFα) and interleukin-1β (IL-1β), upon binding to their respective cell-surface receptors, induce a signal cascade that eventually results in transcriptional activation of various genes by the NF-κB protein dimer [27]. These genes encode for proteins involved in a wide range of processes, including inflammatory responses, development of the immune system, and apoptosis [27]. Deviations from standard NF-κB functioning are the source of certain chronic inflammatory diseases [106] and cancers [1, 84].

The mammalian NF-κB family of proteins consists of c-Rel, RelA (p65), RelB, NF-κB1 (p50), and NF-κB2 (p52). Homodimeric and heterodimeric combinations of these proteins result in a functional NF-κB protein [27]. Most dimers activate transcription (the most common being p65/p50), though certain combinations repress transcription [109]. In unstimulated cells, IκB binds NF-κB, occluding the nuclear localization sequence of NF-κB such that it is localized in the cytosol [101]. However, stimulation by a cytokine activates signal transduction pathways, resulting in the phosphorylation of IκB by IκB kinase (IKK) and subsequent degradation through Lys^{48}-linked polyubiquitination. The

released NF-κB translocates to the nucleus to alter the transcription rates of various genes [73].

The three IKK activation pathways relevent to the focus of this dissertation will now be discussed. The first and better understood pathway is that of IKK activation by the cytokine IL-1β(Figure 1.5). Binding of IL-1β to the IL-1β receptor or Toll-like receptors (TLRs) results in the recruitment of MyD88, which recruits two other proteins, IL-1β receptor associated kinases (IRAK) 1 and 4 [12]. IRAK1 binds to the TNFR-associated factor (TRAF) 6 protein, promoting oligomerization of TRAF6, thereby activating its ubiquitin ligase activity [12]. In cooperation with the hUbc13·hUev1a E2 complex, TRAF6 autopolyubiquitinates itself with Lys^{63}-linked polyubiquitin chains [20]. TAB2 or TAB3 then binds to the polyubiquitin chain and this binding event allows the TAB protein to activate TAK1 (TGFβ-activated kinase), which then phosphorylates IKK, thus activating it [102, 58].

Though not definitively known, TRAF2 may also play a role in IKK activation (Figure 1.5). Binding of TNFα to the TNF receptor 1 protein results in the recruitment of the adaptor protein TRADD [49], which subsequently recruits and activates TRAF2 [48]. Mutation of hUbc13 has been shown to block NF-κB activation by TRAF2 [20]. Also, TRAF2 has been found to polyubiquitinate itself with the participation of the hUbc13·hUev1a heterodimer [91]. Thus, TRAF2 may activate IKK through the same TAB/TAK1 mechanism as TRAF6.

In addition to TRAF2, TRADD recruits the RIP protein, which is also important for NF-κB activation [47]. TRAF2 ubiquitinates RIP, which recruits ubiquitinated TAK1, activating NF-κB [65]. Though definitive proof that RIP polyubiquitination is necessary for TNFα signaling is still lacking. Moreover, it is not known if hUbc13·hUev1a is involved in the formation of the polyubiquitin chains on RIP.

The third relevant NF-κB activation pathway involves the stimulation of antigen receptors on T and B cells, a critical step in adaptive immunity, which requires the Bcl10 protein [88]. Stimulation of the antigen receptors results in activation of PKCθ, which recruits a complex composed of CARMA1, Bcl10, and MALT1 [97]. Bcl10 and MALT1, in coordination with hUbc13·hUev1a, then induce the formation of Lys^{63}-linked polyubiquitin chains on the NF-κB essential modulator (NEMO), a non-catalytic subunit of IKK, activating NF-κB [110, 95]. Currently, the mechanism by which polyubiquitination of

NEMO results in IKK activation is not understood; it is thought that polyubiquitination might serve to recruit IKK kinase, an activator of IKK, or cause a conformational shift in IKK that results in its activation [110]. *In vitro* studies indicate that TRAF6 is involved in the ubiquitination reaction, and that TRAF2 and TRAF6 are redundant in this pathway [95]. However, the validity of these *in vitro* observations in an *in vivo* context has yet to be determined.

In summary, formation of Lys^{63}-linked polyubiquitin chains facilitated by hUbc13·hUev1a is important for IL-1β-, Bcl10-, and potentially TNFα-mediated NF-κB-activation.

JNK and p38 Activation

p38 and c-Jun N-terminal kinase (JNK) belong to a family of proteins called mitogen-activated protein kinases (MAPKs) [81]. MAPKs are activated by MAPK kinases (MAPKKs or MKKs), which phosphorylate two residues, a Thr and a Tyr, on MAPKs. MAPKKs are in turn activated by phosphorylation by MAPKK kinases (MAPKKKs) [63]. The specific MAPKKK and MAPKK involved in the activation of p38 or JNK depends on the stimulation source [64]. Evidence suggests that, depending on the cell type and stimulus, brief stimulation of MAPK is responsible for gene expression, proliferation, and differentiation, while extended activation promotes apoptosis [80].

Outside of cytokine stimulation, JNK and p38 can also be activated by conditions such as UV irradiation, hyperosmolarity, exposure to toxins, and heat shock [81, 59]. JNK phosphorylates a number of proteins, some of which are transcription factors [70] involved in such processes as cell proliferation, differentiation, apoptosis, migration, and cytoskeletal integrity [81].

Activation of p38 results in induction of transcription [96], increased mRNA stability for certain mRNA [61], and altered protein translation rates [63]. The genes and gene products that are affected by p38 activation are typically those of cytokines [63]. p38 is important for cell adhesion, migration [61, 51], and microtubule dynamics [19].

Activation of TAK1 mediated by TRAF6, and possibly TRAF2, by mechanisms described in Section 1.5.1, results in the phosphorylation of MKK6, which in turn activates the JNK and p38 pathways [102] (Figure 1.5). Lys^{63}-linked polyubiquitination of TRAF2 is required for activation of JNK [91], which supports the hypothesis that TAK1 mediates

JNK/p38 activation by TNFα. The redundant role of TRAF5 renders TRAF2 non-essential for JNK and NF-κB activation [33, 12]. However, TRAF2 is essential for p38 activation [33].

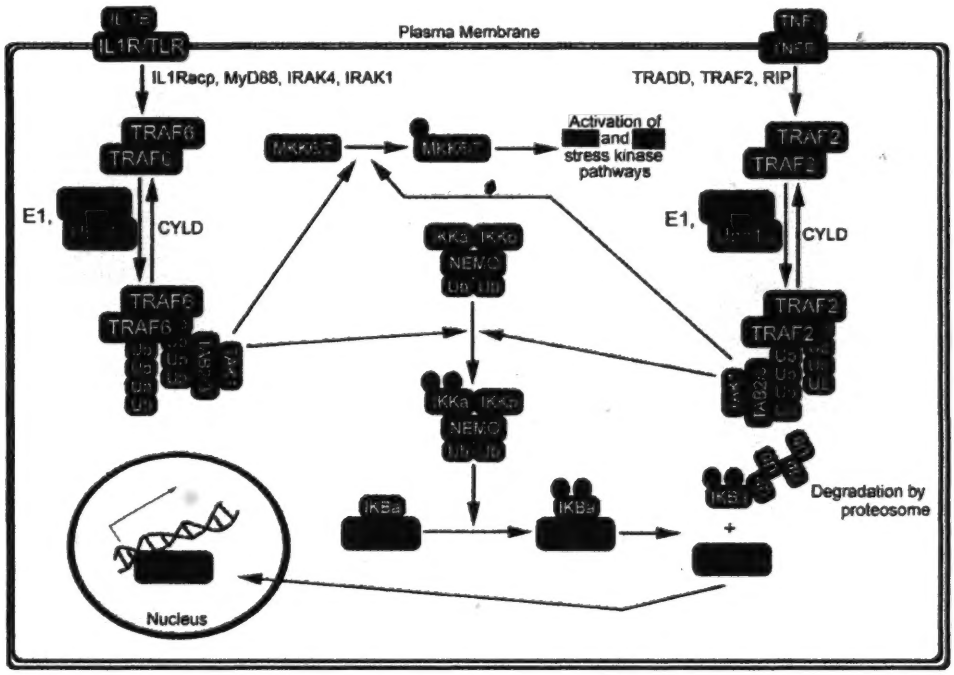

Figure 1.5: **hUev1a-mediated Pathways for NF-κB and JNK\ p38 Activation.** A schematic representation of a cell and the signal transduction pathways for hUev1a-required activation of NF-κB, JNK, and p38.

Potential Importance in Parkinson's Disease

Parkinson's disease (PD) is caused by degeneration of dopaminergic neurons in the midbrain and brain stem, resulting in loss of balance, resting tremors, and slow movements [23]. The neurons found in adult-onset PD are characterized by Lewy bodies, which are inclusion bodies containing a substantial amount of aggregated α-synuclein protein [87].

Parkin is a ubiquitin ligase genetically linked to PD [52, 60]. Parkin functions as a dual specificity ubiquitin ligase as it is able to produce Lys^{48}-linked polyubiquitin chains with two E2s, UbcH7 and UbcH8, as well as Lys^{63}-linked chains with hUbc13·hUev1a

[69, 22]. Parkin polyubiquitinates, through Lys^{63}, synphilin-1, an α-synuclein interacting protein and a component of Lewy bodies [13, 69]. α-synuclein is also a PD-linked protein [62, 85] that stimulates Lys^{63}-linked polyubiquitin assembly through an as yet unknown mechanism [22].

Much more work is required to understand if Lys^{63}-linked polyubiquitin chains play a role in PD pathogenesis. The current observations indicate that Lys^{63}-linked polyubiquitin chains are important in development of PD and that hUbc13·hUev1a may be involved.

Potential Involvement with CHIP

Abnormal or misfolded proteins are recognized and refolded by chaperones such as the heat shock proteins (Hsps) family. Unsuccessfully refolded proteins are believed to be directed towards the proteasome for degradation [90].

The C-terminal of Hsp70-interacting protein (CHIP) interacts with Hsp90 and Hsp70 [90]. CHIP contains a U box domain which is structurally similar to RING domains (section 1.3.4) with the exception that the structure is stabilized by hydrogen bonds instead of zinc binding [90]. While CHIP has been shown to catalyze Lys^{48}-linked polyubiquitination in conjunction with UbcH5 [90], it has been recently shown that CHIP binds hUbc13·hUev1a and functions to catalyze free Lys^{63}-linked polyubiquitin chains *in vitro* [107]. Moreover, CHIP ubiquitinates Hsp70 with Lys^{63}-linked chains [56]. Thus, Lys^{63}-linked polyubiquitination may play a role in the handling of misfolded proteins and diseases associated with this process.

1.5.2 Characteristics of hUev1a

hUev1a is a 170 residue protein. Residues 26-170 of hUev1a share approximately 93% sequence identity with those of hMms2 (Figure 1.6). Comparisons of 2D ^{15}N-HSQC experiments for hMms2 and hUev1a show a high degree of similarity [74], suggesting that hUev1a might possess a tertiary structure akin to that of hMms2. Moreover, the ^{15}N-HSQC of hUev1a reveals a significant number of crosspeaks with low chemical shift dispersion [74]. This observation combined with the fact that efforts to crystallize hUev1a have been unsuccessful (Moraes, personal communication), suggest that the first 20-30 residues of hUev1a are unstructured. Interestingly, despite the high sequence similarity

between hUev1a and hMms2, and the fact that both dimerize with hUbc13 to form a functional E2, hUev1a and hMms2 are involved in distinct cellular processes [3] as outlined in Sections 1.4.1 and 1.5.1.

1.6 Overview

The first objective of this project was to determine the structure and dynamics of hUev1a by NMR spectroscopy. Therefore, we mapped hUev1a residues affected by interactions with hUbc13 and Ub. Finally, we propose a model for the catalytic mechanism of ubiquitin conjugation.

The information concerning the structure, dynamics, and chemical shifts of hUev1a determined herein should be invaluable in the elucidation of the mechanism of hUev1a-based Lys^{63}-linked polyubiquitination.

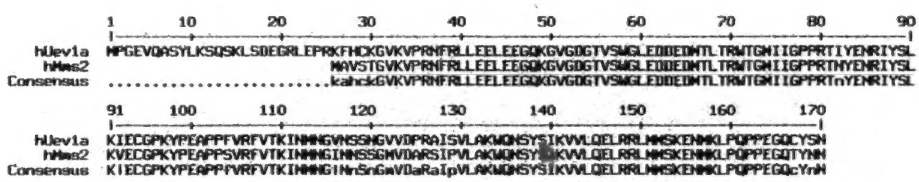

Figure 1.6: **Sequence Alignment of hUev1a and hMms2.** Alignment of the sequences of two UEV proteins, hUev1a and hMms2. Conserved positions are shown in red. The sequences were aligned with the program Multalin [18].

Bibliography

[1] B. B. Aggarwal. Nuclear Factor-κB: The Enemy Within. *Cancer Cell*, 6:203–206, 2004.

[2] T. K. Albert, H. Hanzawa, Y. Legtenberg, M. de Ruwe, F. van den Heuvel, M. Collart, R. Boelens, and H. Timmers. Identification of a Ubiquitin-protein Ligase Subunit within the CCR4-NOT Transcription Repressor Complex. *EMBO J.*, 21:355–364, 2002.

[3] P. L. Andersen, H. Zhou, L. Pastushok, T. Moraes, S. McKenna, B. Ziola, M. J. Ellison, V. M. Dixit, and W. Xiao. Distinct Regulation of Ubc13 Functions by the Two Ubiquitin-Conjugating Enzyme Variants Mms2 and Uev1a. *J. Cell Bio.*, 147:138–146, 2000.

[4] T. Arnason and M. J. Ellison. Stress Resistance in *Saccharomyces cerevisiae* is Strongly Correlated with Assembly of a Novel Type of Multiubiquitin Chain. *Mol. Cell. Biol.*, 14:7876–7883, 1994.

[5] P. N. Barlow, B. Luisi, A. Milner, M. Elliott, and R. Everett. Structure of the C3HC4 Domain by 1H-nuclear Magnetic Resonance Spectroscopy. A New Structural Class of Zinc-finger. *J. Mol. Biol.*, 237:201–211, 1994.

[6] W. Baumeister, J. Walz, F. Zuhl, and E. Seemuller. The Proteasome: Paradigm of a Self-compartmentalizing Protease. *Cell*, 92:367–380, 1998.

[7] Katherine L. B. Borden. RING Domains: Master Builders of Molecular Scaffolds? *J. Mol. Biol.*, 295:1103–1112, 2000.

[8] D. Branzei, M. Seki, and T. Enomoto. Rad18/Rad5/Mms2-mediated Polyubiquitination of PCNA is Implicated in Replication Completion During Replication Stress. *Genes Cells*, 9:1031–1042, 2004.

[9] P. S. Brzovic, J. R. Keeffe, H. Nishikawa, K. Miyamoto, D. Fox, M. Fukuda, T. Ohta, and R. Klevit. Binding and Recognition in the Assembly of an Active BRCA1/BARD1 Ubiquitin-ligase Complex. *Proc. Natl. Acad. Sci. U. S. A.*, 100:5646–5651, 2003.

[10] P. S. Brzovic, P. Rajagopal, D. W. Hoyt, M. C. King, and R. E. Klevit. Structure of a BRCA1-BARD1 Heterodimeric RING-RING Complex. *Nat. Struct. Biol.*, 8:822–824, 2001.

[11] V. Chau, J. W. Tobias, A. Bachmair, D. Marriott, D. J. Ecker, D. K. Gonda, and A. Varshavsky. A Multiubiquitin Chain is Confined to Specific Lysine in a Targeted Short-lived Protein. *Science*, 243:1576–1583, 1989.

[12] Z. J. Chen. Ubiquitin Signalling in the NF-κB Pathway. *Nat. Cell Biol.*, 7:758–765, 2005.

[13] K. K. Chung, Y. Zhang, and K. L. Lim. Parkin Ubiquitinates the α-synuclein-interacting Protein, synphilin-1: Implications for Lewy-body Formation in Parkinson Disease. *Nat. Med.*, 7:1144–1150, 2001.

[14] A. Ciechanover, S. Elias, H. Heller, and A. Hershko. "Covalent Affinity" Purification of Ubiquitin-activating Enzyme. *J. Biol. Chem.*, 257:2537–2542, 1982.

[15] A. Ciechanover, H. Heller, S. Elias, A. L. Haas, and A. Hershko. ATP-dependent Conjugation of Reticulocyte Proteins with the Polypeptide Required for Protein Degradation. *Proc. Natl. Acad. Sci. U.S.A.*, 77:1365–1368, 1980.

[16] A. Ciechanover, Y. Hod, and A. Hershko. A Heat-stable Polypeptide Component of an ATP-dependent Proteolytic System from Reticulocytes. *Biochem. Biophys. Res. Commun.*, 81:1100–1105, 1978.

[17] W. J. Cook, L. C. Jeffrey, Y. Xu, and V. Chau. Tertiary Structures of Class I Ubiquitin-conjugating Enzymes are Highly Conserved: Crystal Structure of Yeast Ubc4. *Biochemistry*, 32:13809–13817, 1993.

[18] F. Corpet. Multiple Sequence Alignment with Heirarchical Clustering. *Nucl. Acids. Res.*, 16:10881–10890, 1988.

[19] P. A. Curmi, O. Gavet, E. Charbaut, S. Ozon, S. Lachkar-Comerauer, V. Manceau, S. Siavoshian, A. Maucuer, and A. Sobel. Stathmin and its Phosphoprotein Family: General Properties, Biochemical and Functional Interaction with Tubulin. *Cell Struct. Funct.*, 24:345–357, 1999.

[20] L. Deng, C. Wang, E. Spencer, L. Yang, A. Braun, J. You, C. Slaughter, C. Pickart, and Z. Chen. Activation of the IκB Kinase Complex by TRAF6 Requires a Dimeric Ubiquitin-Conjugating Enzyme Complex and a Unique Polyubiquitin Chain. *Cell*, 103:361–381, 2000.

[21] J. F. Dice. Peptide Sequences that Target Cytosolic Proteins for Lysosomal Proteolysis. *Trends. Biochem. Sci.*, 15:305–309, 1990.

[22] E. W. Doss-Pepe, L. Chen, and K. Madura. α-Synuclein and Parkin Contribute to the Assembly of Ubiquitin Lysine 63-linked Multiubiquitin Chains. *J. Biol. Chem.*, 280:16619–16624, 2005.

[23] L. S. Forno. Neuropathology of Parkinson's Disease. *J. Neuropathol. Exp.*, 55:259–272, 1996.

[24] J. M. Galan and R. Haguenauer-Tsapis. Ubiquitin Lys63 is Involved in Ubiquitination of a Yeast Plasma Membrane Protein. *EMBO J.*, 16:5847–5854, 1997.

[25] J. G. Gavilanes, G. Gonzalez de Buitrago, R. Perez-Castells, and R. Rodriguez. Isolation, Characterization, and Amino Acid Sequence of a Ubiquitin-like Protein from Insect Eggs. *J. Biol. Chem.*, 257:10267–10270, 1982.

[26] V. Gervais, D. Busso, E. Wasielewski, A. Poterszman, J. M. Egly, J. C. Thierry, and B. Kieffer. Solution Structure of the N-terminal Domain of the Human TFIIH MAT1 Subunit: New Insights into the RING Finger Family. *J. Biol. Chem.*, 276:7457–7464, 2001.

[27] S. Ghosh, M. J. May, and E. B. Kopp. NF-κB and Rel Proteins: Evolutionarily Conserved Mediators of Immune Responses. *Annu. Rev. Immunol.*, 16:225–260, 1998.

[28] M. H. Glickman and A. Ciechanover. The Ubiquitin-Proteasome Proteolytic Pathway: Destruction for the Sake of Construction. *Physiol. Rev.*, 82:373–428, 2002.

[29] A. L. Goldberg. ATP-dependent Proteases in Prokaryotic and Eukaryotic Cells. *Semin. Cell. Biol.*, 1:423–32, 1990.

[30] G. Goldstein, M. Scheid, U. Hammerling, E. A. Boyse, D. H. Schlesinger, and H. D. Niall. Isolation of a Polypeptide that has Lymphocyte-Differentiating Properties and is Probably Represented Universally in Living Cells. *Proc. Nat. Acad. Sci.*, 72:11–15, 1975.

[31] A. L. Haas, J. V. B. Warms, A. Hershko, and I. A. Rose. Ubiquitin-activating Enzyme. *J. Biol. Chem.*, 257:2543–2548, 1982.

[32] A. L. Haas, J. V. B. Warms, and I. A. Rose. Ubiquitin Adenylate: Structure and Role in Ubiquitin Activation. *Biochemistry*, 22:4388–4394, 1983.

[33] H. Habelhah, S. Takahashi, S.-G. Cho, T. Kadoya, T. Watanabe, and Z. Ronai. Ubiquitination and Translocation of TRAF2 is Required for Activation of JNK but not of p38 or NF-κB. *EMBO*, 23:322–332, 2004.

[34] P. M. Handley, M. Mueckler, N. R. Siegel, A. Ciechanover, and A. L. Schwartz. Molecular Cloning, Sequence, and Tissue Distribution of the Human Ubiquitin-activating Enzyme E1. *Proc. Natl. Acad. Sci. U. S. A.*, 88:258–262, 1991.

[35] A. Hershko. Ubiquitin-mediated Protein Degradation. *J. Biol. Chem.*, 263:15237–15240, 1988.

[36] A. Hershko and A. Ciechanover. The Ubiquitin System for Protein Degradation. *Annu. Rev. Biochem.*, 61:761–807, 1992.

[37] A. Hershko and A. Ciechanover. The Ubiquitin System. *Annu. Rev. Biochem.*, 67:425–479, 1998.

[38] A. Hershko and H. Heller. Occurence of a Polyubiquitin Structure in Ubiquitin-protein Conjugates. *Biochem. Biophys. Res. Commun.*, 128:1079–1086, 1985.

[39] A. Hershko, H. Heller, S. Elias, and A. Ciechanover. Components of Ubiquitin-Protein Ligase System. *J. Biol. Chem.*, 258:8206–8214, 1983.

[40] A. Hershko, E. Leshinsky, D. Ganoth, and H. Heller. ATP-dependent Degradation of Ubiquitin-protein Conjugates. *Proc. Natl. Acad. Sci. U. S. A.*, 81, 1619-1623.

[41] M. Hochstrasser. Ubiquitin-dependent Protein Degradation. *Annu. Rev. Genet.*, 30:405–439, 1996.

[42] C. Hoege, B. Pfander, G.-L. Moldovan, G. Pyrowolakis, and S. Jentsch. RAD6-dependent DNA Repair is Linked to Modification of PCNA by Ubiquitin and SUMO. *Nature*, 419:135–141, 2002.

[43] R. M. Hofmann and C. M. Pickart. Noncanonical MMS2-encodd Ubiquitin-conjugating Enzyme Functions in Assembly of Novel Polyubiquitin Chains for DNA Repair. *Cell*, 96:645–653, 1999.

[44] K. Houben, C. Dominguez, H. T. van Schaik, F. M.and Timmers, A. M. Bonvin, and R. Boelens. Solution Structure of the Ubiquitin-conjugating Enzyme UbcH5B. *J. Mol. Biol.*, 344:513–526, 2004.

[45] R. Hough, G. Pratt, and M. Rechsteiner. Ubiquitin-lysozye Conjugates. Identification and Characterization of an ATP-dependent Protease from Rabbit Reticulocyte Lysates. *J. Biol. Chem.*, 261:2400–2408, 1986.

[46] R. Hough, G. Pratt, and M. Rechsteiner. Purification of two high molecular weight proteases from rabbit reticulocyte lysate. *J. Biol. Chem.*, 262, 8303-8313.

[47] H. Hsu, J. Huang, H. B. Shu, V. Baichwal, and D. V. Goeddel. TNF-dependent Recruitment of the Protein Kinase RIP to the TNF Receptor-1 Signaling Complex. *Immunity*, 4:387–396, 1996.

[48] H. Hsu, H.-B. Shu, M.-G. Pan, and D. V. Goeddel. TRADD-TRAF2 and TRADD-FADD Interactions Define Two Distinct TNF Receptor 1 Signal Transduction Pathways. *Cell*, 84:299–308, 1996.

[49] H. Hsu, J. Xiong, and D. V. Goeddel. The TNF Receptor 1-associated Protein TRADD Signals Cell Death and NF-κB Activation. *Cell*, 81:495–504, 1995.

[50] L. Huang, E. Kinnucan, G. Wang, S. Beaudenon, P. M. Howley, J. M. Huibregtse, and N. P. Pavletich. Structure of an E6AP-UbcH7 Complex: Insights into Ubiquitination by the E2-E3 Enzyme Cascade. *Science*, 286:1321–1326, 1999.

[51] X. Huang, S. Chen, L. Xu, Y. Liu, D. K. Deb, L. C. Platanias, and R. C. Bergan. Genistein Inhibits p38 Map Kinase Activation, Matrix Metalloproteinase Type 2, and Cell Invasion in Human Prostate Epithelial Cells. *Cancer Res.*, 65:3470–3478, 2005.

[52] Y. Imai, M. Soda, and R. Takahashi. Parkin Suppresses Unfolded Protein Stress-induced Cell Death through Its E3 Ubiquitin-protein Ligase Activity. *J. Biol. Chem.*, 275:35661–35664, 2000.

[53] B. D. Jankovic, K. Isakovic, and J. Horvat. Effect of a Lipid Fraction from Rat Thymus on Delayed Hypersensitivity Reactions of Neonatally Thymectomized Rats. *Nature*, 208:356–357, 1965.

[54] S. Jentsch. The Ubiquitin-conjugating System. *Annu. Rev. Genet.*, 26:179–207, 1992.

[55] F. Jiang and R. Basavappa. Crystal Structure of the Cyclin-specific Ubiquitin-conjugating Enzyme from Clam, E2-C, at 2.0 Å Resolution. *Biochemistry*, 38:6471–6478, 1999.

[56] J. Jiang, C. A. Ballinger, Y. Wu, Q. Dai, D. M. Cyr, J. Hohfeld, and C. Patterson. CHIP is a U-box-dependent E3 Ubiquitin Ligase. *J. Biol. Chem.*, 276:42938–42944, 2001.

[57] C. Joazeiro and A. Weissman. RING Finger Proteins: Mediators of Ubiquitin Ligase Activity. *Cell*, 102:549–552, 2000.

[58] A. Kanayama, R. B. Seth, L. Sun, C.-K. Ea, M. Hong, A. Shaito, Y.-H. Chiu, L. Deng, and Z. J. Chen. TAB2 and TAB3 Activate the NF-κB Pathway through Binding to Polyubiquitin Chains. *Mol. Cell*, 15:535–548, 2004.

[59] E. Katsoulidis, Y. Li, H. Mears, and L. Platanias. The p38 Mitogen-activated Protein Kinase Pathway in Interferon Signal Transduction. *J. Interferon Cytokine Res.*, 25:749–756, 2005.

[60] T. Kitada, S. Asakawa, N. Hattori, H. Matsumine, Y. Yamamura, S. Minoshima, M. Yokochi, Y. Mizuno, and N. Shimizu. Mutations in the parkin gene cause autosomal recessive juvenile parkinsonism. *Nature*, 392:606–608, 1998.

[61] A. Kotlyarov and M. Gaestel. Is MK2 (Mitogen-activated Protein Kinase-activated Protein Kinase 2) the Key for Understanding Post-transcription Regulation of Gene Expression? *Biochem. Soc. Trans.*, 30:959–963, 2002.

[62] R. Krüger, W. Kuhn, T. Müller, D. Woitalla, M. Graeber, S. Kösel, H. Przuntek, J. T. Epplen, L. Schols, and O. Riess. Ala30Pro Mutation in the Gene Encoding α-Synuclein in Parkinson's Disease. *Nat. Genet.*, 18:106–108, 1998.

[63] S. Kumar, J. Boehm, and J. C. Lee. p38 Map Kinases: Key Signalling Molecules as Therapeutic Targets for Inflammatory Diseases. *Nat. Rev. Drug Discov.*, 2:717–726, 2003.

[64] J. M. Kyriakis and J. Avruch. Mammalian Mitogen-activated Protein Kinase Signal Transduction Pathways Activated by Stress and Inflammation. *Physiol. Rev.*, 81:807–869, 2001.

[65] T. H. Lee, J. Shank, N. Cuson, and M. A. Kelliher. The Kinase Activity of RIP1 is not Required for Tumor Necrosis Factor-α-induced IκB Kinase or p38 MAP Kinase Activation or for the Ubiquitination of RIP1 by TRAF2. *J. Biol. Chem.*, 279:33185–33191, 2004.

[66] A. R. Lehmann. Clubbing Together on Clamps: The Key to Translesion Synthesis. *DNA Repair*, 5:404–407, 2006.

[67] R. E. Lenkinski, D. M. Chen, J. D. Glickson, and G. Goldstein. Nuclear Magnetic Resonance Studies of the Denaturation of Ubiquitin. *Biochim. Biophys. Acta.*, 494:126–130, 1977.

[68] M. J. Lewis, L. F. Saltibus, D. D. Hau, W. Xiao, and L. Spyracopoulos. Structural Basis for Non-covalent Interaction between Ubiquitin and the Ubiquitin Conjugating Enzyme Variant Human MMS2. *J. Biomol. NMR.*, 34:89–100, 2006.

[69] K.-L. Lim, V. L. Dawson, and T. M. Dawson. Parkin-mediated Lysine 63-linked Polyubiquitination: A Link to Protein Inclusions Formation in Parkinson's and other Conformational Diseases? *Neurobiol. Aging*, Paper in Press., 2005.

[70] A. Lin. Activation of the JNK Signaling Pathway: Breaking the Brake on Apoptosis. *Bioessays*, 25:17–24, 2003.

[71] Y. Lin, W. C. Hwang, and R. Basavappa. Structural and Functional Analysis of the Human Mitotic-specific Ubiquitin-Conjugating Enzyme, UbcH10. *J. Biol. Chem.*, 277:21913–21921, 2002.

[72] P. K. Lund, B. M. Moats-Staats, J. G. Simmons, E. Hoyt, A. J. D'Ercole, F. Martin, and J. J. Van Wyk. Nucleotide Sequence Analysis of a cDNA Encoding Human Ubiquitin Reveals that Ubiquitin is Synthesized as a Precursor. *J. Biol. Chem.*, 260:7609–7613, 1985.

[73] T. Maniatis. A Ubiquitin Ligase Complex Essential for the NF-κB, Wnt/Wingless, and Hedgehog Signaling Pathways. *Genes Dev.*, 13:505–510, 1999.

[74] S. McKenna, J. Hu, T. Moraes, W. Xiao, M. J. Ellison, and L. Spyracopoulos. Energetics and Specificity of Interactions within Ub·Uev·Ubc13 Human Ubiquitin Conjugation Complexes. *Biochemistry*, 42:7922–7930, 2003.

[75] S. McKenna, T. Moraes, L. Pastushok, C. Ptak, W. Xiao, L. Spyracopoulos, and M. J. Ellison. An NMR-based Model of the Ubiquitin-bound Human Ubiquitin Conjugation Complex Mms2-Ubc13. *J. Biol. Chem.*, 278:13151–13158, 2003.

[76] S. McKenna, L. Spyracopoulos, T. Moraes, L. Pastushok, C. Ptak, W. Xiao, and M. J. Ellison. Noncovalent Interaction between Ubiquitin and the Human DNA Repair Protein Mms2 Is Required for Ubc13-mediated Polyubiquitination. *J. Biol. Chem.*, 276:40120–40126, 2001.

[77] N. Merkley and G. S. Shaw. Solution Structure of the Flexible Class II Ubiquitin-conjugating Enzyme Ubc1 Provides Insight for Polyubiquitin Chain Assembly. *J. Biol. Chem.*, 279:139–47, 2004.

[78] T. Miura, W. Klaus, B. Gsell, C. Miyamoto, and H. Senn. Characterization of the Binding Interface between Ubiquitin and Class I Human Ubiquitin-conjugating Enzyme 2b by Multidimensional Heteronuclear NMR Spectroscopy in Solution. *J. Mol. Biol.*, 290:213–228, 1999.

[79] T. F. Moraes, R. A. Edwards, S. McKenna, L. Pastushok, W. Xiao, J. N. M. Glover, and M. J. Ellison. Crystal Structure of the Human Ubiquitin Conjugating Enzyme Complex, hMms2-hUbc13. *Nat. Struct. Biol.*, 8:669–673, 2001.

[80] H. Nakano, A. Nakajima, S. Sakon-Komazawa, J.-h. Piao, X. Xue, and K. Okumura. Reactive Oxygen Species Mediate Crosstalk Between NF-κB and JNK. *Cell Death Differ.*, Print in Press, 2005.

[81] H. Nishina, T. Wada, and T. Katada. Physiological Roles of SAPK/JNK Signaling Pathway. *J. Biochem.*, 136:123–126, 2004.

[82] C. M. Pickart. Mechanisms Underlying Ubiquitination. *Annu. Rev. Biochem.*, 70:503–533, 2001.

[83] C. M. Pickart and M. J. Eddins. Ubiquitin: Structures, Functions, Mechanisms. *BBA-Mol. Cell Res.*, 1695:55–72, 2004.

[84] E. Pikarsky, R. M. Porat, I. Stein, R. Abramovitch, S. Amit, S. Kasem, E. Gutkovich-Pyest, S. Urieli-Shoval, E. Galun, and Y. Ben-Neriah. NF-κB Functions as a Tumour Promoter in Inflammation-associated Cancer. *Nature*, 431:461–466, 2004.

[85] M. H. Polymeropoulos, C. Lavedan, E. Leroy, S. E. Ide, A. Dehejia, A. Dutra, B. Pike, H. Root, J. Rubenstein, R. Boyer, E. S. Stenroos, S. Chandrasekharappa, A. Athanassiadou, T. Papapetropoulos, W. G. Johnson, A. M. Lazzarini, R. C. Duvoisin, G. Di Iorio, L. I. Golbe, and R. L. Nussbaum. Mutation in the α-Synuclein Gene Identified in Families with Parkinson's Disease. *Science*, 276:2045–2047, 1997.

[86] S. Prakash, P. Sung, and L. Prakash. DNA Repair Genes and Proteins of *Saccharomyces cerevisiae*. *Annu. Rev. Genet.*, 27:33–70, 1993.

[87] C. A. Ross and M. A. Poirier. Protein Aggregation and Neurodegenerative Disease. *Nat. Med.*, 10 Suppl:S10–S17, 2004.

[88] J. Ruland, G.S. Duncan, A. Elia, I. del Barco Barrantes, L. Nguyen, S. Plyte, D. G. Millar, D. Bouchard, A. Wakeham, P. S. Ohashi, and T. W. Mak. Bcl10 is a Positive Regulator of Antigen Receptor-induced Activation of NF-κB and Neural Tube Closure. *Cell*, 104:33–42, 2001.

[89] D. H. Schlesinger and G. Goldstein. Molecular Conservation of 74 Amino Acid Sequence of Ubiquitin between Cattle and Man. *Nature*, 255:423–424, 1975.

[90] B. A. Schulman and Z. J. Chen. Protein Ubiquitination: CHIPping Away the Symmetry. *Mol. Cell*, 20:653–655, 2005.

[91] C.-S. Shi and J. H. Kehrl. Tumor Necrosis Factor (TNF)-induced Germinal Center Kinase-related (GCKR) and Stress-activated Protein Kinase (SAPK) Activation Depends upon the E2/E3 Complex Ubc13-Uev1A/TNF Receptor-associated Factor 2 (TRAF2). *J. Biol. Chem.*, 278:15429–15434, 2003.

[92] M. V. Simpson. Control of Enzyme Levels in Animal Tissues. *J. Biol. Chem.*, 20:143–154, 1953.

[93] J. Spence, R. R. Gali, G. Dittmar, F. Sherman, M. Karin, and D. Finley. Cell Cycle-Regulated Modification of the Ribosome by a Variant Multiubiquitin Chain. *Cell*, 102:67–76, 2000.

[94] J. Spence, S. Sadis, A. L. Haas, and D. Finley. A Ubiquitin Mutant with Specific Defects in DNA Repair and Multiubiquitination. *Mol. Cell Biol.*, 15:1265–1273, 1995.

[95] L. Sun, L. Deng, C.-K. Ea, Z.-P. Xia, and Z. J. Chen. The TRAF6 Ubiquitin Ligase and TAK1 Kinase Mediate IKK Activation by BCL10 and MALT1 in T Lymphocytes. *Mol. Cell*, 14:289–301, 2004.

[96] Y. Tan, J. Rouse, A. Zhang, S. Cariatis, P. Cohen, and M. J. Comb. FGF and Stress Regulate CREB and ATF-1 via a Pathway Involving p38 MAP Kinase and MAPKAP Kinase-2. *EMBO J.*, 15:4629–4642, 1996.

[97] M. Thome and J. Tschopp. TCR-induced NF-κB Activation: a Crucial Role for Carma1, Bcl10 and MALT1. *Trends Immunol.*, 24:419–424, 2003.

[98] A. P. VanDemark and C. P. Hill. E1 on the Move. *Mol. Cell*, 17:474–475, 2005.

[99] A. P. VanDemark, R. M. Hofmann, C. Tsui, C. M. Pickart, and C. Wolberger. Molecular Insights into Polyubiquitin Chain Assembly: Crystal Structure of the Mms2/Ubc13 Heterodimer. *Cell*, 105:711–720, 2001.

[100] R. Varadan, M. Assfalg, A. Haririnia, S. Raasi, C. Pickart, and D. Fushan. Solution Conformation of Lys^{63}-linked Di-ubiquitin Chain Provides Clues to Functional Diversity of Polyubiquitin Signaling. *J. Biol. Chem.*, 279:7055–7063, 2004.

[101] I. M. Verma, J. K. Stevenson, E. M. Schwarz, D. Van Antwerp, and S. Miyamoto. Rel/NF-κB/IκB Family: Intimate Tales of Association and Dissociation. *Genes Dev.*, 9:2723–2735, 1995.

[102] C. Wang, L. Deng, M. Hong, G. R. Akkaraju, J. Inoue, and Z. J. Chen. TAK1 is a Ubiquitin-dependent Kinase of MKK and IKK. *Nature*, 412:346–351, 2001.

[103] K. D. Wilkinson, M. K. Urban, and A. L. Haas. Ubiquitin is the ATP-dependent Proteolysis Factor I of Rabbit Reticulocytes. *J. Biol. Chem.*, 255:7529–7532, 1980.

[104] B. R. Wong, F. Parlati, K. Qu, S. Demo, T. Pray, J. Huang, D. G. Payan, and M. K. Bennett. Drug Discovery in the Ubiquitin Regulatory Pathway. *Drug Discov. Today*, 8:746–754, 2003.

[105] D. K. Worthylake, S. Prakash, L. Prakash, and C. P. Hill. Crystal Structure of the *Saccharomyces cerevisiae* Ubiquitin-conjugating Enzyme Rad6 at 2.6 Å Resolution. *J. Biol. Chem.*, 273:6271–6276, 1998.

[106] Y. Yamamoto and R. B. Gaynor. Therapeutic Potential of Inhibition of the NF-κB Pathway in the Treatment of Inflammation and Cancer. *J. Clin. Invest.*, 107:135–142, 2001.

[107] M. Zhang, M. Windheim, S. M. Roe, P. Cohen, C. Prodromou, and L. H. Pearl. Chaperoned Ubiquitylation - Crystal Structures of the CHIP U Box E3 Ubiquitin Ligase and a CHIP-Ubc13-Uev1a Complex. *Mol. Cell*, 20:525–538, 2005.

[108] N. Zheng, P. Wang, P. D. Jeffrey, and N. P. Pavletich. Structure of a C-Cbl-UbcH7 Complex: RING Domain Function in Ubiquitin-Protein Ligases. *Cell*, 102:533–539, 2000.

[109] H. Zhong, M. J. May, E. Jimi, and S. Ghosh. The Phosphorylation Status of Nuclear NF-κB Determines Its Association with CBP/p300 or HDAC-1. *Mol. Cell*, 9:625–636, 2002.

[110] H. Zhou, I. Wertz, K. O'Rourke, M. Ultsch, S. Seshagiri, M. Eby, W. Xiao, and V. M. Dixit. Bcl10 Activates the NF-κB Pathway through Ubiquitination of NEMO. *Nature*, 427:167–171, 2004.

Chapter 2

NMR Solution Structure of hUev1a

2.1 Introduction

hUbc13 dimerizes with a UEV protein to form a functional E2 enzyme that catalyzes the formation of Lys^{63}-linked polyUb chains on target proteins [14, 5]. Lys^{63}-linked polyUb chains affect the fate/activity of a number of target proteins involved in cellular processes such as DNA repair [14], NF-κB activation [9], and JNK/p38 activation [34].

Recent work has demonstrated that hUev1a is the requisite UEV [1] for Interleukin-1 (IL-1) [9] and TNFα-induced [31] activation of NF-κB, JNK, and p38. It is also essential for Bcl10-mediated NF-κB activation [41]. Moreover, hUbc13·hUev1a activity may play a role in Parkinson's disease pathogenesis [10] as well as within the cellular mechanism that deals with misfolded proteins [39].

To better understand the mechanism of Lys^{63} polyubiquitination and to provide a basis for understanding how hMms2 and hUev1a are involved in different processes (and yet catalyze the same basic reaction), the solution structure of hUev1a was determined, as described in this chapter.

2.2 Experimental Procedures

2.2.1 Cloning and Expression

hUev1a was cloned as a GST fusion protein as previously described [21]. Expression of hUev1a is as previously described for hMms2 [32] with the following exceptions. For production of [U-^{15}N; U-^{13}C]-hUev1a, the M9 minimal media [30] contained 2 g/L [^{13}C,

99%] D-glucose and 1 g/L [^{15}N, 98%] ammonium sulfate as the only carbon and nitrogen sources, respectively. For all protein purification buffers containing NaCl, the NaCl concentration was 250 mM.

The protocol for the production of [U-^{15}N] or [U-^{15}N; U-10% ^{13}C]-hUev1a was identical to the protocol for [U-^{15}N; U-^{13}C]-hUev1a with the exception that 2 g/L [^{13}C, 99%] D-glucose in the minimal media was substituted by 4g/L ^{12}C D-glucose or 0.2 g/L [^{13}C, 99%] D-glucose with 1.8 g/L ^{12}C D-glucose, respectively. The protocol for unlabelled hUev1a expression was identical to that detailed above with the exception that LB media, containing 50 μg/mL ampicillin and 25 μg/mL chloramphenicol, was used instead of the M9 minimal media.

2.2.2 NMR Spectroscopy

For all NMR experiments, full length hUev1a, including five N-terminal vestigial residues (Gly-Pro-Leu-Gly-Ser) from a cloning artifact, was used. All samples contained 9:1 H_2O:D_2O buffer with 50 mM NaH_2PO_4, 250 mM NaCl, 0.9 mM DTT, and 1.7 mM DSS at pH 7.0. For NMR experiments involving [U-^{15}N; U-^{13}C]-hUev1a, the protein concentration was $\sim$1 mM for 300 μL samples in Shigemi microcell NMR tubes. For all other samples, standard 5 mm i.d. NMR tubes were used with protein concentrations of $\sim$0.75 mM for [U-^{15}N; U-10% ^{13}C]-hUev1a and $\sim$0.5 mM for all other experiments.

All NMR spectra were collected on a Varian Unity INOVA 600 MHz NMR spectrometer with the exception of ^{15}N-separated 3D NOESY HSQC [40] and ^{15}N/^{13}C-separated 3D NOESY HSQC [28] spectra, which were recorded on a Varian Unity INOVA 800 MHz NMR spectrometer. All NMR experiments were performed at 30 °C. Spectra were processed and analyzed with the NMRPipe [7] and NMRView [17] programs, respectively.

Sequential resonance assignments were accomplished using a combination of the HNCACB [26, 36], CBCA(CO)NH [13, 36], and HNCA [16] experiments. Assignment of ^{1}Hα, and side chain ^{1}H and ^{13}C atoms, excluding those found on aromatic and methionine methyl groups, were accomplished with the (H)CC(CO)NNH-TOCSY [12], H(C)CC(CO)NNH-TOCSY [12, 24], HCCH-TOCSY [3, 18], MQ-(H)CC$_m$H$_m$-TOCSY [38], HNHA [33], and HNHB [2] experiments. Aromatic atoms were assigned using the (HB)CB(CGCD)HD [37], (HB)CB(CGCDCE)HE [37], (H)CCH-TROSY [22, 23], aromatic 2D ^{1}H-^{13}C

HSQC [29], ^{15}N-separated 3D NOESY HSQC [40], and ^{13}C-separated 3D NOESY HSQC [28] experiments, in conjunction with structures determined late in the refinement process. Resonances for methionine methyl groups were determined using the 2D ^{1}H-^{13}C HSQC, ^{15}N-separated 3D NOESY HSQC, and ^{15}N/^{13}C-separated 3D NOESY HSQC experiments, with analyses of structures during the refinement process. A non-constant time 2D ^{1}H-^{13}C HSQC experiment using [U-^{15}N; U-10% ^{13}C]-hUev1a was used to stereospecifically assign the side chain methyl groups of valine and leucine residues [27].

2.2.3 Structure Calculations

Interproton distance restraints were obtained from the ^{15}N-separated 3D NOESY HSQC [40] and ^{13}C-separated 3D NOESY HSQC [28] experiments. A total of 2080 distance restraints were obtained from NOE resonance peak intensities and were calibrated within the range of 1.7- 6.0 Å as previously described [11]. Due to resonance peak overlap, twenty restraints were lengthened by an additional 0.07 - 1.37 Å.

$^{3}J_{HNH\alpha}$ coupling constants obtained from the HNHA experiment were used to calculate restraints for the main chain ϕ dihedral angle [33]. The error assigned to each coupling constant was 1 Hz. Additional ϕ and ψ dihedral restraints were generated by the TALOS program using $^{1}H_{\alpha}$, $^{13}C_{\alpha}$, $^{13}C_{\beta}$, and main chain ^{15}N chemical shifts [6]. The error of each predicted restraint was set to twice the standard deviation of the predicted angle. For residues that the TALOS program was unable to predict a ψ dihedral restraint, restraints were produced using the $d_{N\alpha}/d_{\alpha N}$ intensity ratio obtained from the ^{15}N-separated 3D-NOESY HSQC experiment and the error was set to $\pm 100°$ [11]. Main chain dihedral restraints were imposed only if the residue did not show a resonance peak in a 2D ^{1}H-^{15}N CLEANEX-PM FHSQC [15] NMR spectrum with a 100 ms mixing time and the dihedral restraint was within the range of angles observed in structures determined only with NOE distance restraints.

In addition to distance and dihedral angle restraints, main chain hydrogen bond restraints were included for α-helical or β-strand regions as follows: hydrogen bonds were predicted from working structures using the program VADAR [35] and O-H_N distance restraints were set to 2.05 $\pm$ 0.25 Å. In addition, hydrogen bond restraints were imposed only if a residue did not display a resonance peak in a 100 ms mixing time 2D ^{1}H-^{15}N

CLEANEX-PM FHSQC NMR spectrum. The experimental NMR-derived restraints are given in Table 1.

Following structure refinement, two hundred structures were calculated using the torsion angle-based simulated annealing protocol in CNS 1.1 [4], starting from an extended conformation for hUev1a that lacked the vestigial residues from the cloning artifact. The final NMR ensemble consisted of the fifteen lowest energy structures. Structural statistics were calculated using the programs AQUA and PROCHECK-NMR [20], in-house written scripts, PyMOL [8], and MOLMOL [19]. Molecular structure graphics were produced with the program PyMOL.

2.3 Results

Of the total ^{1}H, ^{13}C, and ^{15}N chemical shift resonances, 87% were assigned. Most of the valine and leucine methyl groups were stereospecifically assigned with the exception of Val^{130}, Leu^{10}, and Leu^{16} (due to chemical shift overlap). Of the 200 structures that were calculated, the 15 lowest energy structures were selected for the ensemble (Figure 2.1). The solution state structure of hUev1a indicates that the N-terminal region of the protein (35 residues) is unstructured, whereas the bulk of the remaining residues form a core domain with a typical UEV fold. The N-terminal region of the structure shows an average main chain rmsd value of 9 ± 3 Å upon superposition to the average structure. The lack of structure for the N-terminus is supported by three observations. First, residues within the N-terminal region are deficient in NOE restraints, despite the fact that 86% of the atoms within this region have been assigned; residues within the N-terminal region have an average of three NOEs per residue compared to the structured UEV core region that has an average of fifteen NOEs per residue. Second, nearly all of the 35 N-terminal residues give rise to a resonance peak in a 100 ms mixing time 2D ^{1}H-^{15}N CLEANEX-PM FHSQC experiment, indicating that the main chain amide protons for these residues are in fast exchange with water. Thus, these residues are likely to be solvent accessible, and presumably unstructured. Finally, the main chain amide ^{1}H chemical shifts from these residues are found within a narrow region from 7.8 to 8.5 ppm, consistent with a lack of secondary structure.

The core structured region displays a typical UEV fold, composed of an N-terminal α helix, α1 (36-49), which is followed by a four strand, antiparallel β sheet (β1: 56-59, β2: 69-77, β3: 86-94, and β4: 104-107) and two C-terminal α helices (α2: 140-152 and α3: 154-157), with α2 forming extensive contacts with one face of the β sheet (Figure 2.1). For the ensemble of fifteen structures, the main chain atoms within the structured region have an rmsd value of 0.98 $\pm$ 0.15 Å, where regions of secondary structure have a main chain rmsd value of 0.43 $\pm$ 0.07 Å. Structural statistics are summarized in Table 2.1.

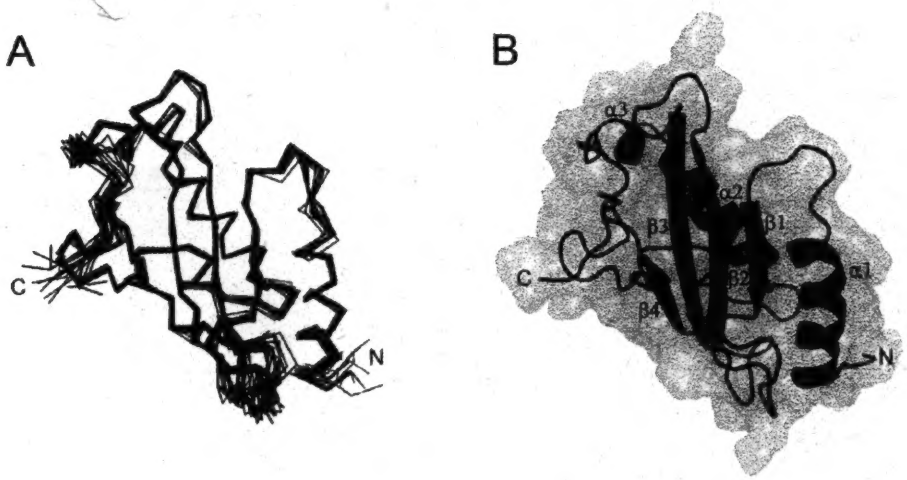

Figure 2.1: **Solution Structure for the Core Domain of hUev1a.** (A) Backbone superposition of the fifteen structures for the core of hUev1a (residues 33-170). (B) Ribbon representation of the minimized average structure of hUev1a (residues 33-170), depicting secondary structural elements.

2.4 Discussion

2.4.1 Structural Comparison to hMms2

hMms2 is ~90% identical in sequence to residues 26-170 of hUev1a. Therefore, it is expected that the structured core region of hUev1a should adopt a similar tertiary structure to that of hMms2. Alignment of the main chain atoms of residues 35-170 of the minimized average structure of hUev1a with residues 10-145 of hMms2 (PDB ID: 1J74) [25] gives an rmsd value of 1.3 Å, indicating that the two structures are similar. The functional

Table 2.1: **Characteristics of the Ensemble of Structures for hUev1a** [1] All 15 structures in the final ensemble were included in the calculations. [2] Calculated for residues 36-170. [3] Calculated for residues 36-49, 56-59, 69-77, 86-94, 104-107, 140-152, 154-157.

Distance Restraints	
total	2080
intraresidue	843
medium ($1 \leq \|i\text{-}j\| \leq 4$)	659
long ($\|i\text{-}j\| \geq 5$)	578
hydrogen bonds	36
Dihedral Restraints	
$^3J_{HNH\alpha}$-derived ϕ	56
TALOS-derived ϕ	69
TALOS-derived ψ	68
$d_{N\alpha}/d_{\alpha N}$-derived ψ	4
Restraint Violations[1]	
distance restraints (> 0.3 Å)	0%
distance restraints (≥ 0.1 Å, ≤ 0.3 Å)	0.2%
distance restraints (< 0.1 Å)	5.7%
dihedral restraints (> 0 °)	6.5%
maximum dihedral violation (°)	2.6
Ramachandran Plot	
allowed region	97.6%
generously allowed region	1.9%
disallowed region	0.5%
rmsd (Å)[2]	
heavy atoms	1.6 ± 0.1
backbone atoms	1.0 ± 0.2
2° structure backbone atoms[3]	0.43 ± 0.07
RMSD from Ideal Covalent Geometry	
bonds (Å)	0.00147 ± 0.00005
angles (°)	0.329 ± 0.003
impropers (°)	0.193 ± 0.007

differences between hMms2 and hUev1a may be a consequence of the presence of the N-terminal tail of hUev1a that is not present in hMms2. The results presented herein indicate that the N-terminal tail is not involved in interactions with hUbc13 or Ub, and therefore may be involved in interactions with the cognate E3 Ub ligase (Section 5).

Bibliography

[1] P. L. Andersen, H. Zhou, L. Pastushok, T. Moraes, S. McKenna, B. Ziola, M. J. Ellison, V. M. Dixit, and W. Xiao. Distinct Regulation of Ubc13 Functions by the Two Ubiquitin-Conjugating Enzyme Variants Mms2 and Uev1a. *J. Cell Bio.*, 147:138–146, 2000.

[2] S. J. Archer, M. Ikura, D. A. Torchia, and A. Bax. An Alternative 3D NMR Technique for Correlating Backbone Nitrogen-15 with Side-Chain Hβ Resonances in Larger Proteins. *J. Magn. Reson.*, 95:636–641, 1991.

[3] A. Bax, G.M. Clore, and A.M. Gronenborn. Proton-Proton Correlation via Isotropic Mixing of ^{13}C Magnetization, a New Three-Dimensional Approach for Assigning Proton and ^{13}C spectra of ^{13}C-Enriched Proteins. *J. Magn. Reson.*, 88:425–431, 1990.

[4] A. T. Brunger, P. D. Adams, G. M. Clore, W. L. DeLano, P. Gros, R. W. Grosse-Kunstleve, J.-Ss Jiang, J. Kuszewski, M. Nilges, N. S. Pannu, R. J. Read, L. M. Rice, T. Simonson, and G. L. Warren. Crystallography & NMR System: A New Software Suite for Macromolecular Structure Determination. *Acta. Cryst.*, D 54:905–921, 1998.

[5] Z. J. Chen. Ubiquitin Signalling in the NF-κB Pathway. *Nat. Cell Biol.*, 7:758–765, 2005.

[6] G. Cornilescu, F. Delaglio, and A. Bax. Protein Backbone Angle Restraints from Searching a Database for Chemical Shift and Sequence Homology. *J. Biomol. NMR.*, 13:289–302, 1999.

[7] F. Delaglio, S. Grzesiek, G. Zhu, G. W. Vuister, J. Pfeifer, and A. Bax. NMRPipe: a Multidimensional Spectral Processing System Based on UNIX Pipes. *J. Biomol. NMR.*, 6:227–293, 1995.

[8] W. L. DeLano. The PyMOL Molecular Graphics System. http://www.pymol.org, 2002.

[9] L. Deng, C. Wang, E. Spencer, L. Yang, A. Braun, J. You, C. Slaughter, C. Pickart, and Z. Chen. Activation of the IκB Kinase Complex by TRAF6 Requires a Dimeric Ubiquitin-Conjugating Enzyme Complex and a Unique Polyubiquitin Chain. *Cell*, 103:361–381, 2000.

[10] E. W. Doss-Pepe, L. Chen, and K. Madura. α-Synuclein and Parkin Contribute to the Assembly of Ubiquitin Lysine 63-linked Multiubiquitin Chains. *J. Biol. Chem.*, 280:16619–16624, 2005.

[11] S. M. Gagné, M. X. Li, and B. D. Sykes. Mechanism of Direct Coupling between Binding and Induced Structural Change in Regulatory Calcium Binding Proteins. *Biochemistry*, 36:4386–4392, 1997.

[12] S. Grzesiek, J. Anglister, and A. Bax. Correlation of Backbone Amide and Aliphatic Side-Chain Resonances in $^{13}C/^{15}N$-Enriched Proteins by Isotropic Mixing of ^{13}C Magnetization. *J. Magn. Reson.*, B 101:114–119, 1993.

[13] S. Grzesiek and A. Bax. Correlating Backbone Amide and Side Chain Resonances in Larger Proteins by Multiple Relayed Triple Resonance NMR. *J. Am. Chem. Soc.*, 114:6291–6293, 1992.

[14] C. Hoege, B. Pfander, G.-L. Moldovan, G. Pyrowolakis, and S. Jentsch. RAD6-dependent DNA Repair is Linked to Modification of PCNA by Ubiquitin and SUMO. *Nature*, 419:135–141, 2002.

[15] T.-L. Hwang, P. C. M. van Zijl, and S. Mori. Accurate Quantitation of Water-Amide Proton Exchange Rates Using the Phase-Modulated CLEAN Chemical EXchange (CLEANEX-PM) Approach with a Fast-HSQC (FHSQC) Detection Scheme. *J. Biomol. NMR.*, 11:221–226, 1998.

[16] M. Ikura, L. Kay, and A. Bax. A Novel Approach for Sequential Assignment of ^{1}H, ^{13}C, ^{15}N Spectra of Larger Proteins: Heteronuclear Triple-Resonance Three-Dimensional NMR Spectroscopy. Application to Calmodulin. *Biochemistry*, 29:4659–4667, 1990.

[17] B. A. Johnson and R. A. Blevins. NMR View: A Computer Program for the Visualization and Analysis of NMR Data. *J. Biomol. NMR.*, 5:603–614, 1994.

[18] L. E. Kay, G.-Y. Xu, A. U. Singer, D. R. Muhandiram, and J. D. Forman-Kay. A Gradient-Enhanced HCCH-TOCSY Experiment for Recording Side-Chain ^{1}H and ^{13}C Correlations in H_2O Samples of Proteins. *J. Magn. Reson.*, B 101:333–337, 1993.

[19] R. Koradi, M. Billeter, and K. Wüthrich. MOLMOL:a Program for Display and Analysis of Macromolecular Structures. *J. Mol. Graphics*, 14:51–55, 1996.

[20] R. A. Laskowski, J. A. Rullmannn, M. W. MacArthur, R. Kaptein, and J. M. Thornton. AQUA and PROCHECK-NMR: Programs for Checking the Quality of Protein Structures Solved by NMR. *J. Biomol. NMR.*, 8:477–486, 1996.

[21] S. McKenna, L. Spyracopoulos, T. Moraes, L. Pastushok, C. Ptak, W. Xiao, and M. J. Ellison. Noncovalent Interaction between Ubiquitin and the Human DNA Repair Protein Mms2 Is Required for Ubc13-mediated Polyubiquitination. *J. Biol. Chem.*, 276:40120–40126, 2001.

[22] A. Meissner and O. W. Sorensen. Optimization of Three-Dimensional TROSY-Type HCCH NMR Correlation of Aromatic ^{1}H-^{13}C Groups in Proteins. *J. Magn. Reson.*, 139:447–450, 1999.

[23] A. Meissner and O. W. Sorensen. Suppression of Diagonal Peaks in Three-Dimensional Protein NMR TROSY-Type HCCH Correlation Experiments. *J. Magn. Reson.*, 144:171–174, 2000.

[24] G. T. Montelione, B. A. Lyons, S. D. Emerson, and M. Tashiro. An Efficient Triple Resonance Experiment Using Carbon-13 Isotropic Mixing for Determining Sequence-Specific Resonance Assignments of Isotopically-Enriched Proteins. *J. Am. Chem. Soc.*, 114:10974–10975, 1992.

[25] T. F. Moraes, R. A. Edwards, S. McKenna, L. Pastushok, W. Xiao, J. N. M. Glover, and M. J. Ellison. Crystal Structure of the Human Ubiquitin Conjugating Enzyme Complex, hMms2-hUbc13. *Nat. Struct. Biol.*, 8:669–673, 2001.

[26] D. R. Muhandiram and L. E. Kay. Gradient-enhanced Triple-resonance 3-Dimensional NMR Experiments with Improved Sensitivity. *J. Magn. Reson.*, B 103:203–216, 1994.

[27] D. Neri, T. Szyperski, G. Otting, H. Senn, and K. Wuthrich. Stereospecific Nuclear Magnetic Resonance Assignments of the Methyl Groups of Valine and Leucine in the DNA-Binding Domain of the 434 Repressor by Biosynthetically Directed Fractional ^{13}C Labeling. *Biochemistry*, 28:7510–7516, 1989.

[28] S. M. Pascal, D. R. Muhandiram, T. Yamazaki, J. D. Forman-Kay, and L. E. Kay. Simultaneous Acquisition of ^{15}N- and ^{13}C-Edited NOE Spectra of Proteins Dissolved in H_2O. *J. Magn. Reson.*, B 103:197–201, 1994.

[29] K. Pervushin, R. Riek, G. Wider, and K. Wuthrich. Transverse Relaxation-optimized Spectroscopy (TROSY) for NMR Studies of Aromatic Spin Systems in C-13-labeled Proteins. *J. Am. Chem. Soc.*, 120:6394–6400, 1998.

[30] S. Sambrook, E. F. Fritch, and T. Maniatis. Molecular Cloning: A Laboratory Manual. pages Cold Spring Harbor Laboratory Press, New York, NY, 1989.

[31] C.-S. Shi and J. H. Kehrl. Tumor Necrosis Factor (TNF)-induced Germinal Center Kinase-related (GCKR) and Stress-activated Protein Kinase (SAPK) Activation Depends upon the E2/E3 Complex Ubc13-Uev1A/TNF Receptor-associated Factor 2 (TRAF2). *J. Biol. Chem.*, 278:15429–15434, 2003.

[32] L. Spyracopoulos, M. J. Lewis, and L. F. Saltibus. Main Chain and Side Chain Dynamics of the Ubiquitin Conjugating Enzyme Variant Human Mms2 in the Free and Ubiquitin-Bound States. *Biochemistry*, 44:8770–8781, 2005.

[33] G. W. Vuister and A. Bax. Quantitative J Correlations: A New Approach for Measuring Homonuclear Three-Bond $J(H^{N}H^{\alpha})$ Coupling Constants in ^{15}N-Enriched Proteins. *J. Am. Chem. Soc.*, 115:7772–7777, 1993.

[34] C. Wang, L. Deng, M. Hong, G. R. Akkaraju, J. Inoue, and Z. J. Chen. TAK1 is a Ubiquitin-dependent Kinase of MKK and IKK. *Nature*, 412:346–351, 2001.

[35] L. Willard, A. Ranjan, H. Zhang, H. Monzavi, R. F. Boyko, B. D. Sykes, and D. S. Wishart. VADAR: a Web Server for Quantitative Evaluation of Protein Structure Quality. *Nucleic Acids Res.*, 31:3316–3319, 2003.

[36] M. Wittekind and L. Mueller. HNCACB, a High-Sensitivity 3D NMR Experiment to Correlate Amide-Proton and Nitrogen Resonances with the Alpha- and Beta-Carbon Resonances in Proteins. *J. Magn. Reson.*, B 101:201–205, 1993.

[37] T. Yamazaki, J. D. Forman-Kay, and L. E. Kay. Two-Dimensional NMR Experiments for Correlating $^{13}C\beta$ and $^{1}H\delta/\epsilon$ Chemical Shifts of Aromatic Residues in ^{13}C-Labeled Proteins via Scalar Couplings. *J. Am. Chem. Soc.*, 115:11054–11055, 1993.

[38] D. Yang, Y. Zheng, D. Liu, and D. F. Wyss. Sequence-Specific Assignments of Methyl Groups in High-Molecular Weight Proteins. *J. Am. Chem. Soc.*, 126:3710–3711, 2004.

[39] M. Zhang, M. Windheim, S. M. Roe, P. Cohen, C. Prodromou, and L. H. Pearl. Chaperoned Ubiquitylation - Crystal Structures of the CHIP U Box E3 Ubiquitin Ligase and a CHIP-Ubc13-Uev1a Complex. *Mol. Cell*, 20:525–538, 2005.

[40] O. Zhang, L. E. Kay, J. P. Olivier, and J. D. Forman-Kay. Backbone $^{1}H$and ^{15}Nresonance assignments of the N-terminal SH3 domain of drk in folded and unfolded states using enhanced-sensitivity pulsed field gradient NMR techniques. *J. Biomol. NMR.*, 4:845–858, 1994.

[41] H. Zhou, I. Wertz, K. O'Rourke, M. Ultsch, S. Seshagiri, M. Eby, W. Xiao, and V. M. Dixit. Bcl10 Activates the NF-κB Pathway through Ubiquitination of NEMO. *Nature*, 427:167–171, 2004.

Chapter 3

Main Chain Dynamics of hUev1a

3.1 Introduction

To validate the overall fold of the solution structure of hUev1a determined herein (see Chapter 2), a series of experiments were performed to measure main chain amide ^{15}N-T_1, T_2, and NOE values for hUev1a, and used to determine the rotational diffusion parameters. The calculated diffusion parameters were compared with theoretical values calculated using the structure. The agreement between the observed and calculated rotational diffusion parameters supports the accuracy of the overall fold.

Moreover, the flexibility of the hUev1a main chain was assessed through NMR-based measurement of order parameters, or S^2 values, for main chain ^{1}H-^{15}N pairs [3]. S^2 values represent the amplitude of spatial restriction for a main chain ^{1}H-^{15}N bond vector. Characterization of the S^2 values of free hUev1a allows for assessment of regions of flexibility within a protein, and detection of specific changes in protein flexibility, or entropy, upon interaction with ligands [2, 3].

3.2 Experimental Procedures

^{15}N-T_1, ^{15}N-T_2, and $\{^1$H$\}^{15}$N NOE data were collected, processed and analyzed as previously described [3]. NMR spectra were acquired at 30 °C and two magnetic field strengths (600 and 500 MHz). For the T_1 data, spectra were acquired with the following relaxation delays: 10, 50, 120, 200, 300, 400, 500, 700, and 800 ms; the same delays were used for the T_1 data collected at 600 MHz, with the exception that an additional spectrum with a relaxation delay of 1 s was collected. Delays of 10, 30, 50, 70, 90, 110, 130, and

150 ms were used for the measurement of T_2 at 500 and 600 MHz. The delays between transients were 1.2 s and 3.0 s for the T_1 and T_2 pulse sequences, respectively, at both magnetic field strengths. $\{^1H\}^{15}N$ NOEs were measured as previously described [3]. An analysis of rotational diffusion anisotropy, and a Lipari-Szabo model-free analysis were conducted using the program Mathematica [6], using an approach similar to that recently described [3].

3.3 Results

Main chain amide ^{15}N NMR relaxation data were obtained at 500 and (600) MHz for 118 (118) of a total of 170 residues. Uncharacterized residues were either prolines, in rapid exchange with water, or partially/completely overlapped in the 2D ^1H-^{15}N-HSQC NMR spectra. The average T_1 for all residues is 562 $\pm$ 61 (721 $\pm$ 98) ms, with an average error of 26 (24) ms. The average T_2 for all residues is 97 $\pm$ 45 (90 $\pm$ 41) ms, with an average error of 3 (5) ms. The average NOE for all residues is 0.65 $\pm$ 0.24 (0.75 $\pm$ 0.17), with an average error of 0.08 (0.05). The theoretical values for T_1, T_2, and NOE are 652 (844) ms, 88 (83) ms, and 0.74 (0.75), respectively, and correspond closely to the experimental averages. The theoretical values were determined using τ_m, τ_f, and S^2 values of 9.84 ns, 25 ps, and 0.85, respectively.

The isotropic, axially symmetric prolate, and axially symmetric oblate rotational diffusion models were used in conjunction with T_1/T_2 ratios to analyze the overall tumbling of hUev1a [4, 5]. Given the flexible nature of the N-terminal residues, only the atomic coordinates of residues 36-170 of the minimized average structure of hUev1a were used in the analysis of rotational diffusion. Analysis of the T_1/T_2 ratios at 500 and (600) MHz indicates that hUev1a undergoes axially symmetric prolate rotational diffusion. The AIC values for the isotropic, prolate, and oblate diffusion models are 246 (319), 184 (154), and 217 (186), respectively. The rates of diffusion for the axially symmetric prolate model are $D_{xx} = D_{yy} = 16.9\ (15.7)\ \mu s^{-1}$, $D_{zz} = 20.4\ (22.2)\ \mu s^{-1}$, and $2D_{zz}/(D_{xx} + D_{yy}) = 1.21\ (1.41)$. The HYDRONMR program [1] was used to calculate D_{xx}, D_{yy}, D_{zz}, and $2D_{zz}/(D_{xx} + D_{yy})$ values of 17.7 μs^{-1}, 17.0 μs^{-1}, 22.7 μs^{-1}, and 1.31, respectively, for the core domain of hUev1a (residues 35-170). The angle between the experimental and theoretical D_{zz} values

is 11 ° (6 °) (Figure 3.1).

S^2 values were calculated for main chain amide groups from data obtained at 500 and 600MHz (Figure 3.2). The average S^2 value is 0.8 $\pm$ 0.1. Loop 1 (L1) and the extreme C-terminal residue display low S^2 values. Due to peak overlap or poor signal to noise ratio, many S^2 values were not calculated for the N-terminal tail (residues 1-35).

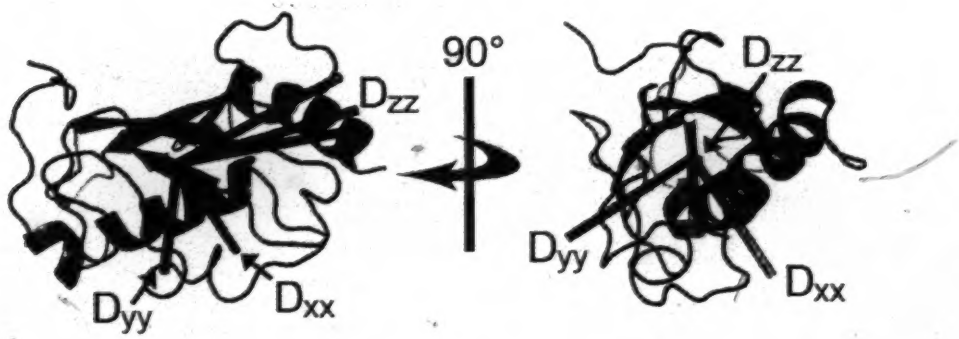

Figure 3.1: **Rotational Diffusion Tensor of hUev1a.** A comparison of the theoretical rotational diffusion tensor (green) with observed diffusion tensors at 500 (yellow) and 600 (red) MHz. The theoretical diffusion tensors were calculated using the truncated hUev1a structure (residues 36-170).

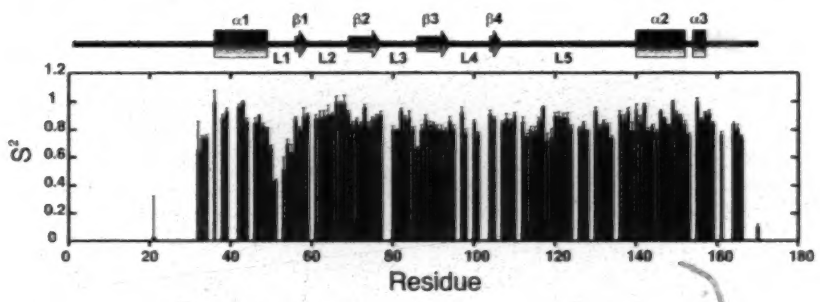

Figure 3.2: **Main Chain Dynamics for hUev1a.** Plot of main chain amide S^2 values for free hUev1a, calculated from data collected at 500 and 600 MHz.

3.4 Discussion

The observed average T_1, T_2, and NOE values at 500 (600) MHz were 562 ± 61 (721 ± 98) ms, 97 ± 45 (90 ± 41) ms, and 0.65 ± 0.24 (0.75 ± 0.17), respectively. The theoretical average T_1, T_2, and NOE values for the truncated, minimized average structure of hUev1a (residues 35-170) under a 500 (600) MHz field are 652 (844) ms, 88 (83) ms, and 0.74 (0.75), respectively.

Considering that the observed values closely match the theoretical values and that the theoretical values were calculated using the truncated average structure, we conclude that the N-terminal tail does not affect the rate of tumbling of the core region.

At magnetic fields of 500 and 600 MHz, the respective angles between the calculated and the theoretical D_{zz} are 11° and 6° (Figure 3.1). The theoretical D_{zz} was calculated by using the truncated average structure. The relatively small difference between the calculated and theoretical values supports the accuracy of the determined structure of hUev1a.

The S^2 values for main chain amide groups of hUev1a (Figure 3.2) are similar to those of free hMms2 [3]. For both hMms2 and hUev1a, the majority of residues have S^2 values around 0.82, while residues found in L1 and at the C-terminus display smaller S^2 values, indicating that the C-terminus and L1 are flexible. Given the empirical correlation between protein structure and main chain amide S^2 values [8], the similarity between S^2 values for hMms2 and hUev1a is consistent with the similarity of their tertiary structures.

The majority of S^2 values for hUev1a (~0.82) are typical for regions of classical secondary structure in proteins, including regions involved in the binding of hUbc13 and Ub. Therefore, a large unfavorable decrease in entropy for the main chain of hUev1a is not expected upon binding either hUbc13 or Ub. For example, we have estimated the entropy change for the main chain of hMms2 (~150 residues) upon Ub binding to be approximately 33 kJ mol^{-1} ($-T\Delta S$) [3]. In comparison, the per residue conformational entropy change for the protein main chain upon folding has been estimated to be around 3 kJ mol^{-1} $residue^{-1}$ [7].

Bibliography

[1] J. García de la Torre, M. L. Huertas, and B. Carrasco. HYDRONMR: Prediction of NMR Relaxation of Globular Proteins from Atomic-Level Structures and Hydrodynamic Calculations. *J. Magn. Reson.*, 147:138–146, 2000.

[2] S. W. Homans. Probing the Binding Entropy of Ligand-protein Interactions by NMR. *Chembiochem*, 6:1585–1591, 9.

[3] L. Spyracopoulos, M. J. Lewis, and L. F. Saltibus. Main Chain and Side Chain Dynamics of the Ubiquitin Conjugating Enzyme Variant Human Mms2 in the Free and Ubiquitin-Bound States. *Biochemistry*, 44:8770–8781, 2005.

[4] N. Tjandra, S. E. Feller, R. W. Pastor, and A. Bax. Rotational Diffusion Anisotropy of Human Ubiquitin from ^{15}NNMR Relaxation. *J. Am. Chem. Soc.*, 117:12562–12566, 1995.

[5] N. Tjandra, P. Wingfield, S. Stahl, and A. Bax. Anisotropic Rotational Diffusion of Perdeuterated HIV Protease from ^{15}N NMR Relaxation Measurements at Two Magnetic Fields. *J. Biomol. NMR*, 8:273–284, 1996.

[6] S. Wolfram. *The Mathematica Book*. Wolfram Media/Cambridge University Press, 3rd edition, 1996.

[7] D. W. Yang and L. E. Kay. Contributions to Conformational Entropy Arising from Bond Vector Fluctuations Measured from NMR-derived Order Parameters: Application to Protein Folding. *J. Mol. Biol.*, 263:369–382, 1996.

[8] F. Zhang and R. Bruschweiler. Contact Model for the Prediction of NMR N-H Order Parameters in Globular Proteins. *J. Am. Chem. Soc.*, 124:12654–12655, 2002.

Chapter 4

Protein-Protein Interactions of hUev1a with Ub and hUbc13

4.1 Introduction

hUbc13 and hUev1a dimerize and function as an E2 enzyme, catalyzing the formation of Lys^{63}-linked polyUb chains important in NF-κB, JNK, and p38 activation [1]. UEVs bind to both Ub and the E2, aligning Lys^{63} of Ub near the active site of the E2 [10, 6, 3]. The structures of hMms2 (a UEV) bound to hUbc13 or Ub have been determined by x-ray crystallography and NMR, respectively

In this chapter, we determine the regions of hUev1a that interact with hUbc13 and Ub by mapping hUev1a chemical shift changes upon titration with either protein.

4.2 Experimental Procedures

4.2.1 Cloning and Expression

The protocols for expression of unlabelled hUbc13 and Ub were identical to that for unlabelled hUev1a as detailed in Section 2.2.1.

4.2.2 Titration of hUbc13 into [U-^{15}N]-hUev1a

hUbc13 was titrated into a 300 μL sample of $\sim$0.5 mM [U-1^{15}N]-hUev1a in a Shigemi microcell NMR tube in the following manner. First, a 2D ^{1}H-^{15}N HSQC spectrum of [U-^{15}N]-hUev1a was collected in the absence of hUbc13. Subsequently, 0.4 mL of $\sim$1.5 mM hUbc13 was added to the sample and concentrated to 300 μL with a Biomax-10 Ultrafree-

0.5 centrifugal filter device to give a hUbc13/hUev1a ratio of approximately 2:1, and a 2D ^{1}H-^{15}N-HSQC NMR spectrum of the sample was acquired. An additional 0.2 mL of ~1.5 mM hUbc13 was added to the sample and concentrated to produce an NMR sample containing 3:1 hUbc13:hUev1a, and a 2D ^{1}H-^{15}N-HSQC NMR spectrum was collected. Main chain amide ^{1}H-^{15}N resonance peaks in the 2D ^{1}H-^{15}N HSQC NMR spectra for each of the titration points were assigned on the basis of proximity to resonance peaks in the 2D ^{1}H-^{15}N HSQC NMR spectrum for free hUev1a. Chemical shift changes for the main chain amide ^{1}H-^{15}N resonance peaks were calculated as previously described [5]. Chemical shift changes greater than the average chemical shift change plus one standard deviation ($\overline{\Delta\delta}$ + 1σ) were considered strongly significant, and chemical shift changes between $\overline{\Delta\delta}$ and ($\overline{\Delta\delta}$ + 1σ) were considered moderately significant.

4.2.3 Chemical shift mapping of [U-15N]-hUev1a upon titration with Ub

Chemical shift mapping of [U-^{15}N]-hUev1a upon titration with Ub was accomplished using previously published titration data [5], and main chain amide ^{1}H-^{15}N chemical shift assignments for hUev1a as determined in Section 2.2.2.

4.3 Results

4.3.1 Chemical shift mapping of [U-^{15}N]-hUev1a upon titration with hUbc13

From a total of 134 assignments for free Uev1a, 104 resonance peaks were assigned in the hUbc13-bound state. Unassigned residues included those whose resonance peaks vanished upon binding of hUbc13, or those that could not be unambiguously assigned. Two discrete peaks were observed for some of the resonances in the spectrum containing 2:1 hUbc13:hUev1a, indicating that the binding event occurs in slow exchange on the NMR timescale, and that hUev1a is not completely saturated with hUbc13. hUev1a may not be fully bound to hUbc13 at a 2:1 hUbc13:hUev1a ratio either due to an underestimation of hUbc13 concentration, or homodimerization of hUbc13.

The average change in chemical shift for the 104 resonance peaks is 0.04 $\pm$ 0.07 ppm.

hUev1a ^{1}H-^{15}N main chain amide resonances observed to undergo significant chemical shift changes upon addition of hUbc13 include (in order of increasing $\Delta\delta$): Phe^{38}, Cys^{94}, Leu^{44}, Glu^{42}, Arg^{70}, Asn^{37}, Lys^{33}, and Met^{66} (Figure 4.1A). Residues observed to undergo moderate chemical shift changes include (in order of increasing $\Delta\delta$): Lys^{97}, Val^{34}, Glu^{100}, Trp^{58}, Leu^{40}, Val^{56}, Gly^{95}, Trp^{71}, Thr^{67}, Val^{32}, Tyr^{98}, Glu^{45}, Glu^{46}, Arg^{39}, and Leu^{68} (Figure 4.1B). These residues are clustered around the $\alpha 1$ helix and the neighboring loop or strand regions (Figure 4.2A).

4.3.2 Chemical shift mapping of [U-^{15}N]-hUev1a upon titration with Ub

Main chain amide ^{1}H-^{15}N chemical shift changes for hUev1a upon titration with Ub are shown in Figure 4.1B. The average change in chemical shift is 0.05 ± 0.08 ppm for the 112 assigned resonance peaks. Residues whose chemical shift changes were found to be significantly affected upon titration with Ub include (in order of increasing $\Delta\delta$): Ile^{87}, Tyr^{88}, Val^{56}, Gly^{47}, Val^{51}, Thr^{55}, Ser^{57}, Lys^{49}, Met^{74}, Gly^{73}, and Trp^{58}. Main chain amide ^{1}H-^{15}N chemical shift changes for fifteen residues found to be moderately affected include (in order of increasing $\Delta\delta$): Ile^{75}, Glu^{61}, Arg^{70}, Gly^{77}, Met^{113}, Gln^{48}, Gln^{145}, Gly^{54}, Gly^{50}, Leu^{90}, Glu^{46}, Thr^{72}, Asn^{85}, Val^{142}, and Gly^{59}. The majority of residues whose main chain amide ^{1}H-^{15}N chemical shifts are strongly or moderately affected are localized to a surface of hUev1a that is comprised of the C-terminal end of helix $\alpha 1$, loop 1, and portions of the $\beta 1$, $\beta 2$, and $\beta 3$ strands (Figures 4.1B and 4.2C).

4.4 Discussion

4.4.1 Interaction with hUbc13

Atomic resolution structures for the complex between Mms2 and Ubc13 have been determined for both yeast and human proteins [7, 10]. Given the sequence and structural similarity between hMms2 and hUev1a, it is not surprising that hUev1a binds hUbc13 in a similar fashion to hMms2 as has recently been shown [12]. Residues that are within or proximal to the hUbc13 binding site in hMms2 are conserved in hUev1a [7]. Notably, Phe^{13} in hMms2, which participates in extensive hydrophobic contacts with hUbc13 [8],

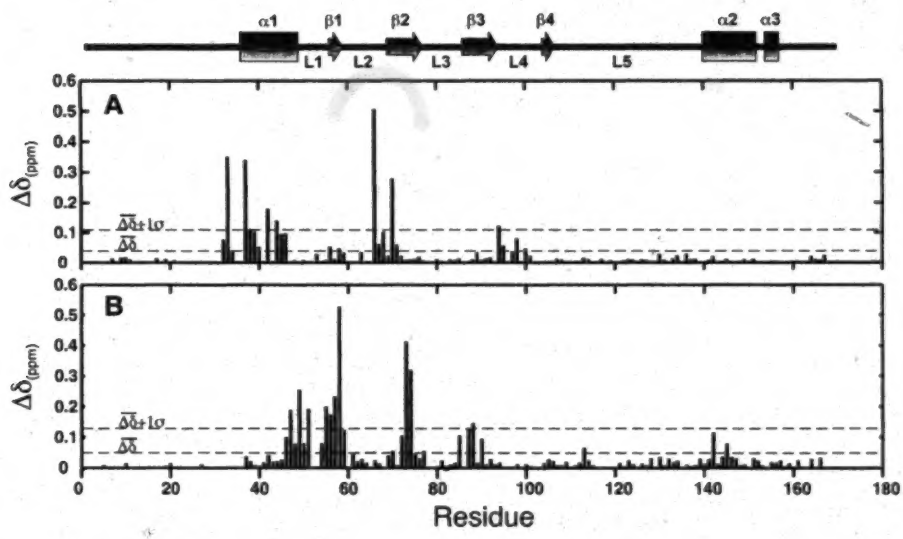

Figure 4.1: **Protein-Protein Interactions for hUev1a.** Comparison of main chain amide ^{1}H and ^{15}N chemical shifts of hUev1a in the presence or absence of hUbc13 (A) and Ub (B).

is conserved in hUev1a (Phe^{38}). The main chain amide ^{1}H-^{15}N chemical shift changes for hUev1a upon interaction with hUbc13 indicate that the binding interface is composed of residues from the N-terminus, helix α1, and L2 of hUev1a (Figure 4.2A). An alignment of the structure of hUev1a with the structure of hMms2 bound to hUbc13 (PDB ID: 1J7D), shows that the NMR chemical shift-based binding interface includes hUev1a residues are adjacent to, or within the vicinity of hUbc13 residues (Figure 4.2B). Furthermore, of the eight residues categorized as strongly affected upon binding of hUbc13, six are within 4 Å of the nearest hUbc13 atom, including residue Phe^{38}. These chemical shift data are consistent with the crystallographic structures of hMms2·hUbc13 and hUev1a·hUbc13 [7, 12].

The binding interface between hUev1a and hUbc13 contains hydrophobic interactions, electrostatic interactions at the periphery of the interface, and a buried salt-bridge (hUbc13: Glu^{55} - Arg^{70}) (Figure 4.3C, D). The K_D for the association of hUbc13 with hUev1a is 62 ± 6 nM (Trevor Moraes, personal communication), and 47 ± 7 nM for association with hMms2 [4], determined using isothermal titration calorimetry. These dissociation constants

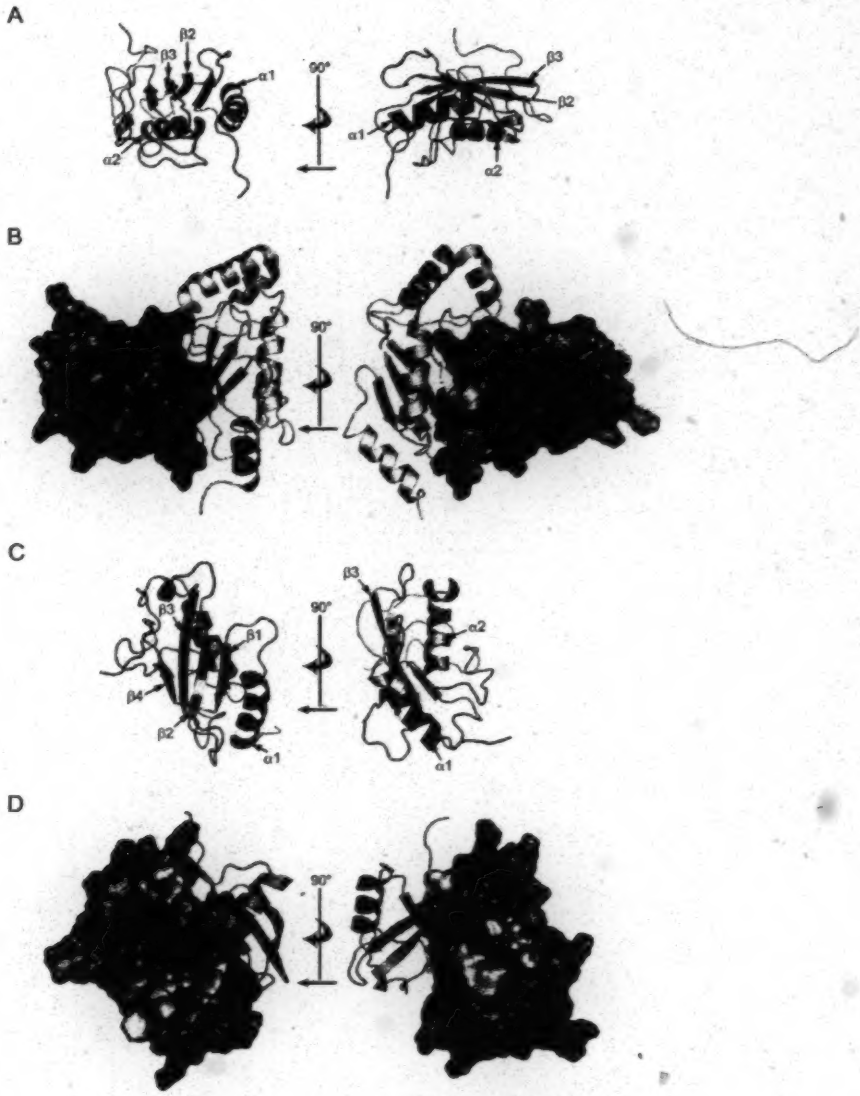

Figure 4.2: **Chemical Shift Maps for hUev1a upon Binding of Ub and hUbc13.** Cartoon representations of free hUev1a (A, C) and surface representations of hUev1a aligned to hMms2 in the hMms2-hUbc13 structure (B) and hUev1a aligned to hMms2 in the hMms2-Ub structure (D). hUev1a residues strongly ($\Delta\delta > \overline{\Delta\delta} + 1\sigma$) and moderately ($\overline{\Delta\delta} + 1\sigma \geq \Delta\delta > \overline{\Delta\delta}$) affected upon titration with hUbc13 (yellow) are colored in red and green, respectively (A, B). hUev1a residues significantly ($\Delta\delta > \overline{\Delta\delta} + 1\sigma$) and moderately ($\overline{\Delta\delta} + 1\sigma \geq \Delta\delta > \overline{\Delta\delta}$) affected upon titration with Ub (green) are colored in red and yellow, respectively (C, D).

correspond to $\Delta G°_{binding}$ values of -41.8 ± 0.2 and -42.5 ± 0.3 kJ M^{-1}, for binding of hUev1a and hMms2 to hUbc13, respectively. The similarity of the free energies of binding for hUev1a and hMms2 is consistent with the similarity in the binding sites of these proteins for hUbc13, as determined from chemical shift mapping.

4.4.2 Interaction with Ubiquitin

Employing the structure of hUev1a determined herein (see Chapter 2), the chemical shift changes for the main chain amide ^{1}H-^{15}N resonances of hUev1a upon binding of Ub indicate that the binding interface is composed of residues from L1, β1, β2, and the C-terminal end of α1 (Figure 4.2C). The binding interface contains several hydrophobic residues that are likely to be crucial in mediating the binding to Ub, including Met^{74}, Ile^{76}, Ile^{87}. The binding interface between hUev1a and Ub is predominantly hydrophobic (Figure 4.3A, B). Thus, given the similarity in sequence between hMms2 and hUev1a core regions, and the chemical shift data, the superposition of the structure of hUev1a determined herein to the structure of hMms2 bound to Ub (PDB ID: 1ZGU) is likely a reasonable model for the hUev1a·Ub interaction (Figure 4.2D).

4.4.3 Potential E3 Interactions

As described in greater detail in Section 1.5.1, TRAF6 and TRAF2 are ubiquitin ligases and function with the hUev1a·hUbc13 heterodimer to produce Lys^{63}-linked polyubiquitin chains essential for activation of NF-κB, JNK, and p38. TRAF6, a 522 residue protein, contains a RING domain (Section 1.3.4) that mediates physical interaction with hUbc13 [11]. TRAF2, a 501 residue protein, also contains a RING domain [9] that shares approximately 30% sequence identity with that of TRAF6 (Figure 4.4); thus the RING domain of TRAF2 may also interact with hUbc13.

The crystal structure of the E2·E3 complex composed of UbcH7, an E2, and c-Cbl, an E3, reveals the RING domain of c-Cbl forms a substantial interface with UbcH7 [13] (Figure 4.8A, PDB ID: 1FBV). Considering that the RING domain of c-Cbl shares sequence identities of 30 and 36% with the RING domains of TRAF6 and TRAF2 (Figure 4.4), respectively, and the sequences of hUbc13 and UbcH7 are 41% intentical (Figure 4.5), it is likely that the RING domains of TRAF2/6 bind hUbc13 in a fashion similar to that of c-Cbl

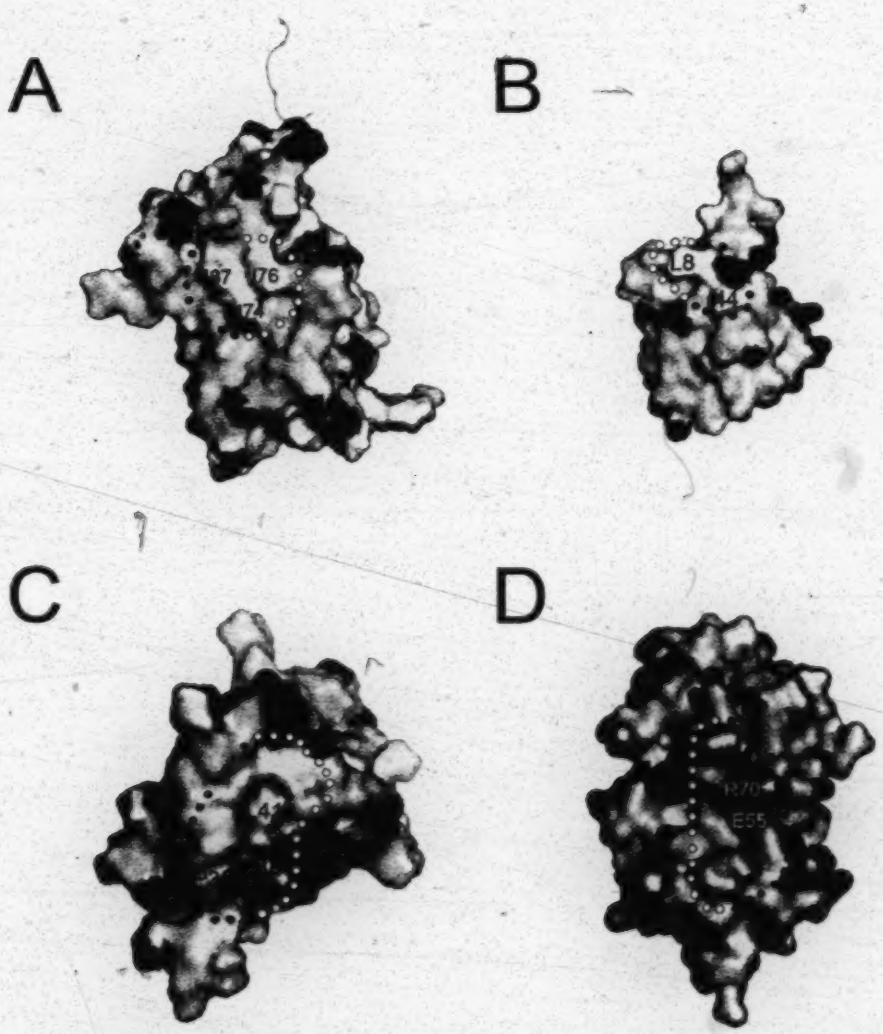

Figure 4.3: **Surface Representations of hUev1a and Cognate Protein Binding Partners.** (A) Ub-binding site of hUev1a, (B) hUev1a-binding site of Ub, (C) hUbc13-binding site of hUev1a, and (D) hUev1a-binding site of hUbc13. Binding surfaces are encompassed by filled black and white circles. For the respective interaction sites of protein binding partners, filled black circles in A or C align with filled black circles in B and D, respectively. Negatively charged atoms are colored red, positively charged atoms are colored blue, aliphatic/aromatic atoms (A, I, L, M, F, P, Y, V) from hydrophobic residues are colored yellow, and polar atoms are colored white.

and UbcH7.

To further explore this possibility, we aligned the structure of the RING domain of TRAF6 (Pascal Mercier, unpublished data) to the hMms2·hUbc13heterodimer (PDB ID: 1J7D, Figure 1.4B), using the c-Cbl·UbcH7 structure (Figure 4.8B). Analysis of the interfaces reveal that of the 15 UbcH7 residues within 6 Å of the c-Cbl RING domain, 7 are conserved in hUbc13(Figure 4.7). However, of the 19 c-Cbl RING domain residues within 6 Å of UbcH7, only 6 are conserved (Figure 4.6). Thus the TRAF6 RING domain may not bind to hUbc13 in a similar manner as c-Cbl·UbcH7.

Nevertheless, if TRAF6 indeed binds hUbc13 as c-Cbl binds UbcH7, then alignment of hUev1a to hMms2 in the hMms2·hUbc13 structure reveals that the N-terminal tail of hUev1a is positioned towards the RING domain (Figure 4.8B). Thus the tail may be involved in interactions with TRAF2/6, and could explain why hMms2, which lacks the tail, is not involved in TRAF2/6 polyubiquitination.

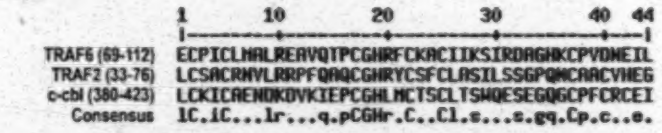

Figure 4.4: **Sequence Alignment of RING Domains from TRAF6, TRAF2, and c-Cbl.** The RING domains of TRAF6 (residues 69-112), TRAF2 (residues 33-76), and c-Cbl (residues 380-423) were aligned to each other. Residues colored in red indicate that the residue is conserved for all three proteins, while those in blue and black indicate that the position is conserved between two or none of the proteins, respectively. The sequences were aligned with the program Multalin [2].

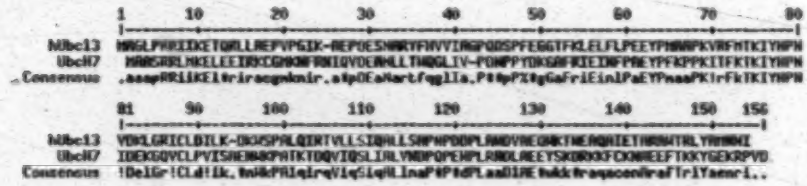

Figure 4.5: **Sequence Alignment of UbcH7 and hUbc13.** The amino acid sequences of UbcH7 and hUbc13 were aligned to each other. Residues colored in red and black indicate that the residue is conserved or not conserved, respectively. The sequences were aligned with the program Multalin [2].

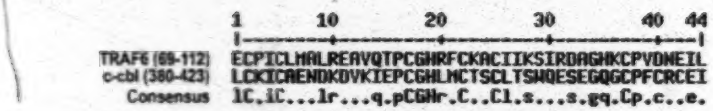

Figure 4.6: **Sequence Alignment of RING Domains from TRAF6 and c-Cbl.** The RING domains of TRAF6 (residues 69-112) and c-Cbl (residues 380-423) were aligned to each other. Residues of the RING domain of c-Cbl within 6 Å of UbcH7 (PDB ID: 1FBV) are colored in red. The sequences were aligned with the program Multalin [2].

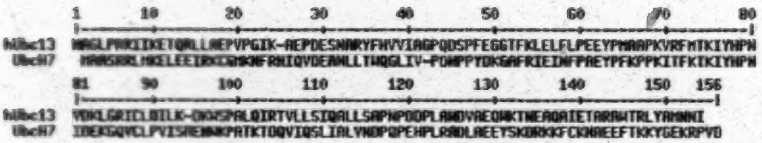
1 10 20 30 40 50 60 70 80
hUbc13 MAGLPARIIKETQRLLAEPVPGIK-AEPDESNARYFHVVIAGPQDSPFEGGTFKLELFLPEEYPMAAPKVRFMTKIYHPN
UbcH7 MAASRRLMKELEEIQKDPPSSCSAGPTGDDLFHWQATIMGPNDSAYQGGVFFLTIHFPTDYPFKPPKVAFTTRIYHPN
81 90 100 110 120 130 140 150 156
hUbc13 VDKLGRICLDILK-DKWSPALQIRTVLLSIQALLSAPNPDDPLANDVAEQWKTNEAQAIETARAWTRLYAMNNI
UbcH7 IDEKGQVCLPVISAENWKPATKTDQVIQSLIALVNDPQPEHPLRADLAEEYSKDRKKFCKNAEEFTKKYGEKRPVD

Figure 4.7: **Sequence Alignment of UbcH7 and hUbc13.** The amino acid sequences of UbcH7 and hUbc13 were aligned to each other. Residues of UbcH7 within 6 Å of the RING domain of c-Cbl (PDB ID: 1FBV) are colored in red. The sequences were aligned with the program Multalin [2].

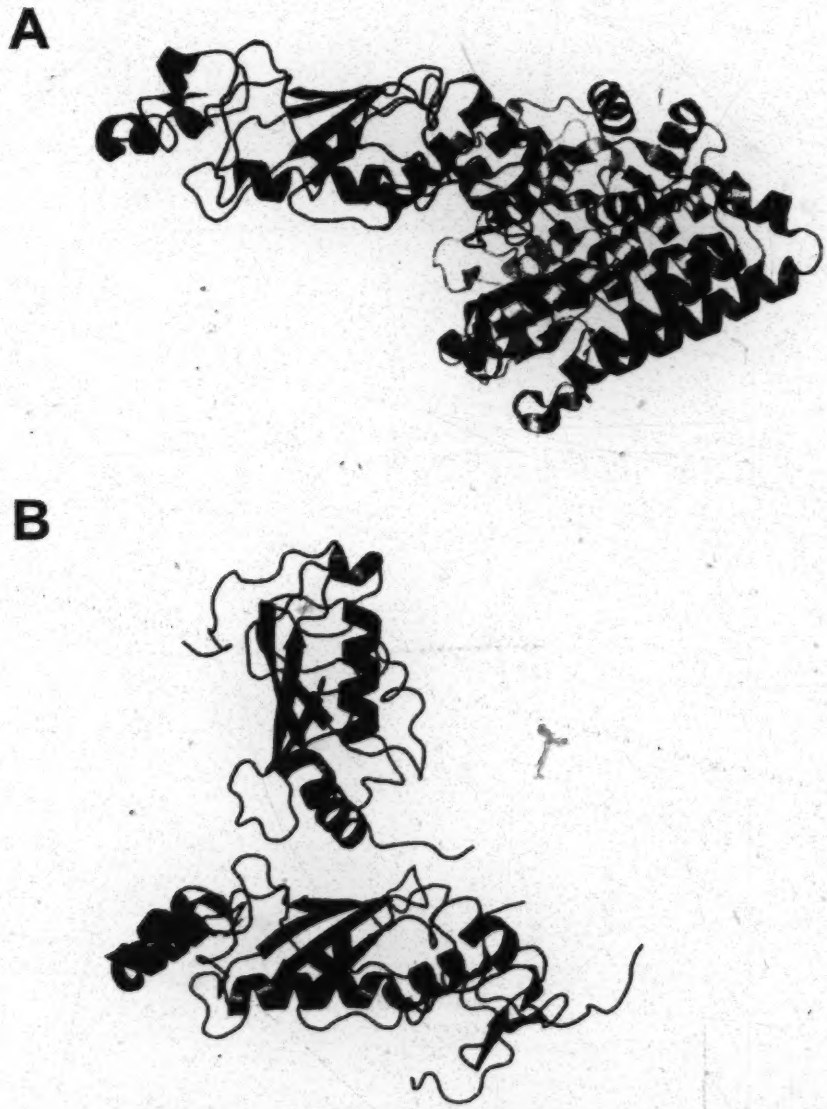

Figure 4.8: **Structure of the c-Cbl·UbcH7 Heterodimer and Model of the hUev1a·hUbc13·TRAF6 RING Domain Trimer.** (A) The crystal structure of the heterodimer composed of c-Cbl (pink and red) and UbcH7 (green). The RING domain of c-Cbl is shown in red. (B) A model of the trimer composed of hUev1a (blue), hUbc13 (green), and the RING domain of TRAF6 (red). Alignment of the structures were based upon the crystal structures of c-Cbl·UbcH7 and hMms2·hUbc13.

Bibliography

[1] Z. J. Chen. Ubiquitin Signalling in the NF-κB Pathway. *Nat. Cell Biol.*, 7:758–765, 2005.

[2] F. Corpet. Multiple Sequence Alignment with Heirarchical Clustering. *Nucl. Acids. Res.*, 16:10881–10890, 1988.

[3] M. J. Lewis, L. F. Saltibus, D. D. Hau, W. Xiao, and L. Spyracopoulos. Structural Basis for Non-covalent Interaction between Ubiquitin and the Ubiquitin Conjugating Enzyme Variant Human MMS2. *J. Biomol. NMR.*, 34:89–100, 2006.

[4] S. McKenna, J. Hu, T. Moraes, W. Xiao, M. J. Ellison, and L. Spyracopoulos. Energetics and Specificity of Interactions within Ub·Uev·Ubc13 Human Ubiquitin Conjugation Complexes. *Biochemistry*, 42:7922–7930, 2003.

[5] S. McKenna, T. Moraes, L. Pastushok, C. Ptak, W. Xiao, L. Spyracopoulos, and M. J. Ellison. An NMR-based Model of the Ubiquitin-bound Human Ubiquitin Conjugation Complex Mms2-Ubc13. *J. Biol. Chem.*, 278:13151–13158, 2003.

[6] S. McKenna, L. Spyracopoulos, T. Moraes, L. Pastushok, C. Ptak, W. Xiao, and M. J. Ellison. Noncovalent Interaction between Ubiquitin and the Human DNA Repair Protein Mms2 Is Required for Ubc13-mediated Polyubiquitination. *J. Biol. Chem.*, 276:40120–40126, 2001.

[7] T. F. Moraes, R. A. Edwards, S. McKenna, L. Pastushok, W. Xiao, J. N. M. Glover, and M. J. Ellison. Crystal Structure of the Human Ubiquitin Conjugating Enzyme Complex, hMms2-hUbc13. *Nat. Struct. Biol.*, 8:669–673, 2001.

[8] L. Pastushok, T. F. Moraes, M. J. Ellison, and W. Xiao. A Single Mms2 "Key" Residue Insertion into a Ubc13 Pocket Determines the Interface Specificity of a Human Lys^{63} Ubiquitin Conjugation Complex. *J. Biol. Chem.*, 280:17891–17900, 2005.

[9] M. Rothe, S. C. Wong, W. J. Henzel, and D. V. Goeddel. A Novel Family of Putative Signal Transducers Associated with the Cytoplasmic Domain of the 75 kDa Tumor Necrosis Factor Receptor. *Cell*, 78:681–692, 1994.

[10] A. P. VanDemark, R. M. Hofmann, C. Tsui, C. M. Pickart, and C. Wolberger. Molecular Insights into Polyubiquitin Chain Assembly: Crystal Structure of the Mms2/Ubc13 Heterodimer. *Cell*, 105:711–720, 2001.

[11] J. Wooff, L. Pastushok, M. Hanna, Y. Fu, and W. Xiao. The TRAF6 RING Finger Domain Mediates Physical Interaction with Ubc13. *FEBS*, 566:229–233, 2004.

[12] M. Zhang, M. Windheim, S. M. Roe, P. Cohen, C. Prodromou, and L. H. Pearl. Chaperoned Ubiquitylation - Crystal Structures of the CHIP U Box E3 Ubiquitin Ligase and a CHIP-Ubc13-Uev1a Complex. *Mol. Cell*, 20:525–538, 2005.

[13] N. Zheng, P. Wang, P. D. Jeffrey, and N. P. Pavletich. Structure of a C-Cbl-UbcH7 Complex: RING Domain Function in Ubiquitin-Protein Ligases. *Cell*, 102:533–539, 2000.

Chapter 5

Molecular Dynamics Simulations for the Ub·hUev1a·hUbc13~Ub Tetramer

5.1 Introduction

Though a model of the hUbc13·hUev1a·2Ub tetramer has been produced and the structures of the hMms2·Ub and hMms2·hUbc13 dimers have been determined, the atomic details concerning the catalysis of Ub conjugation have yet to be fully elucidated. It is known that Asn^{79} of hUbc13 is conserved, and essential for isopeptide bond formation [20]. On this basis, and the structure of hUbc13, it was proposed that the role of Asn^{79} is to stabilize the oxyanion intermediate that is formed on the thioester bond upon Lys^{63} attack [20].

In this chapter, we use the structures of hUev1a, the hMms2·Ub dimer, and the hUbc13·Ub dimer, in coodination with HADDOCK, a protein-protein docking software [8], to produce a tetramer composed of hUev1a, hUbc13 covalently bound to a donor Ub, and an acceptor Ub. A detailed analysis of the active site along with knowledge of basic catalytic mechanisms allow us to propose a chemical mechanism by which sidechain amine group of Lys^{63} of the acceptor Ub forms a covalent bond with the C-terminus of the donor Ub.

5.2 Experimental Procedures

5.2.1 Model-building for the hUev1a·(Ub-Gly-Gly^{76}~Cys^{87}-hUbc13)·Ub tetramer

In order to gain insight into the mechanism of catalysis of synthesis of polyUb chains by the hUbc13·hMms2 heterodimer, a model for the Ub·hUev1a·hUbc13 trimer was built

using the programs PyMol [7] and HADDOCK [8] by superimposing the structure of hUev1a minus the 35 flexible N-terminal residues onto the structure of hMms2 in the hMms2·hUbc13 heterodimer (PDB ID: 1J7D), and assuming that acceptor Ub binds to hUev1a in a similar fashion as hMms2 [11]. This model was then used to construct the Ub·hUev1a·hUbc13∼Ub tetramer. For the thioester bond between the C-terminus of donor Ub (. . .-Gly^{75}-Gly^{76}-COO-) and the side chain of the active site Cys^{87} from hUbc13, bond lengths and angles were estimated from the structure of S-methyl thioacetate, geometry optimized with the program Gaussian 03 [10] at the B3LYP/6-31G** level with stationary point verification using a frequency calculation [9]. Fixed partial charges for the main chain and side chain atoms of Ub-Gly^{76} and hUbc13-Cys^{87}, within a thioester-linked Cys-Gly model compound with capped N- and C-termini, were determined using two-stage RESP fits [1, 4] using the program Gaussian 03 (B3LYP/6-31G**//B3LYP/6-31G* level of theory) and the AMBER biomolecular simulation suite of programs [3, 6].

Following initial model building, the Ub·hUev1a·hUbc13∼Ub tetramer was subjected to energy minimization with the inclusion of a distance restraint between the ϵ-amino group of Ub-Lys^{63} and the carbonyl carbon of the thioester bond using the AMBER package. ΔpK_a values for Ub-Lys^{63}, Ub-Glu^{64}, and hUbc13-Asp^{81} were calculated from 200 ps restrained molecular dynamics simulations conducted at 300 K with the generalized Born implicit solvent model [13, 14, 17] using the AMBER suite of programs. Given that an unrestrained, nanosecond time scale molecular dynamics simulation is not practical in the present case, harmonic restraints were employed for all atoms except those from donor Ub thioester-linked to hUbc13, the loop (residues 61-66) containing residues Glu^{64} and Lys^{63} from acceptor Ub, active site residues from hUbc13 (residues 79-94), and the loop between hUbc13 α-helices 2 and 3 (residues 115-122). Moreover, a distance restraint between the amino nitrogen from Lys^{63} of the donor Ub and the carbonyl carbon of the thioester bond, between hUbc13 and the C-terminus of the acceptor Ub, was included. Additional details for the simulation include the use of the ff99 force field [19], a time step of 2 fs, covalent bonds to hydrogen were restrained using SHAKE [16], temperature was maintained using a Berendsen temperature bath [2], the cutoff for non-bonded interactions and generalized Born radii was 16 Å, salt concentration was 100 mM, and the initial generalized Born model [15].

5.3 Results

In the family of ten structures for the Ub·hUev1a·hUbc13 trimer generated with the HADDOCK docking protocol, there are no NOE violations greater than 0.1 Å, the backbone atoms from hUev1a, hUbc13, and Ub superimpose onto the average structure with rmsds of 0.41 ± 0.06, 0.31 ± 0.05, and 0.44 ± 0.07 Å, respectively. For the family of ten structures, 86.2/12.7 % of residues were determined to be in the most favored/additional allowed regions of the Ramachandran plot using the program PROCHECK-NMR.

The molecular dynamics simulation produced 2000 structures over a period of 200 ps. For each structure, the ΔpK_a of the sidechains of Ub-Lys^{63}, Ub-Glu^{64}, and hUbc13-Asp^{81} were calculated; the groups had average ΔpK_a values of 1 ± 4, -28 ± 8, and -31 ± 6, respectively. Furthermore, two angles, θ and ϕ, were also calculated for each structure. Angle θ is the angle formed between the ϵ-nitrogen of Ub-Lys^{63}, the thioester carbonyl carbon, and the respective carbonyl oxygen. Angle ϕ is the angle formed between the ϵ-nitrogen of Ub-Lys^{63}, the thioester carbonyl carbon, and the plane perpendicular to the plane formed by the thioester sulfur and the thioester carbonyl group. Angles θ and ϕ had average values of 56 ± 7 ° and (-3 ± 1) × 10 °, respectively (Figure 5.1).

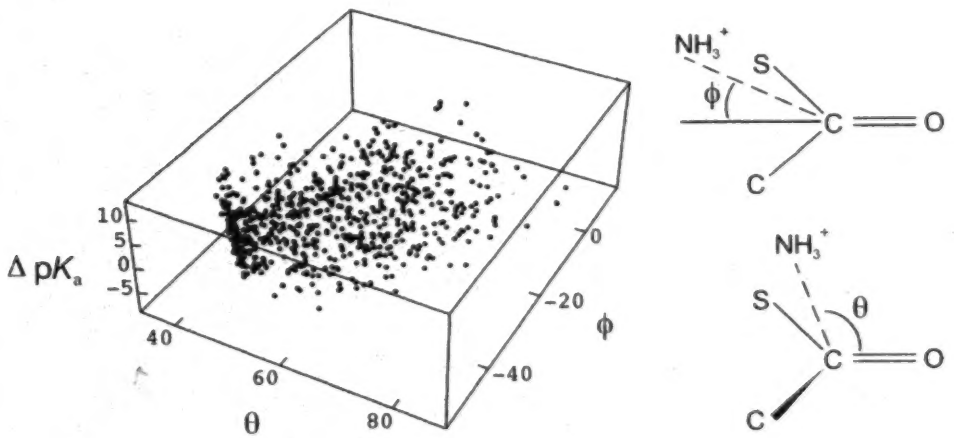

Figure 5.1: **Instantaneous ΔpK_a Values for the Lys^{63} ϵ-nitrogen of Acceptor Ub.** Instantaneous ΔpK_a values were calculated for the Lys^{63} ϵ-nitrogen of the acceptor Ub from a 200 ps restrained molecular dynamics simulation of the Ub·hUev1a·hUbc13~Ub tetramer. ΔpK_a values greater than 3.5 (blue) and less than -3.5 (red) are plotted against the θ and ϕ angles.

5.4 Discussion

Based on the similarity of Ub binding between hMms2 and hUev1a, our previous work involving chemical shift mapping of the interaction between Ub and the hMms2·hUbc13 heterodimer [12], and our structure of the hMms2·Ub complex [11], it is expected that the role of hUev1a is to bind Ub in such a manner as to position Lys^{63} of the acceptor Ub proximally to the active site cysteine of hUbc13. On the basis of NMR chemical shift mapping experiments presented in Chapter 4 and a recently determined structure for hUev1a·hUbc13 [23], it is likely that hUev1a binds Ub and hUbc13 in a similar fashion as hMms2. Therefore, we have used the structure of hUev1a determined in this study, and the structure of hMms2 bound to Ub [11], to develop a model for the interaction between acceptor Ub and hUev1a·hUbc13∼Ub (Figure 5.2), in order to assess the structural basis of catalysis.

Measurement of reaction rates and ab initio quantum mechanical studies in small thioacetate molecules [5, 21, 22] indicate that there are two important barriers that need to be overcome for aminolysis of the Ub∼hUbc13 thioester bond to account for observed enzyme-catalyzed rates. First, it is likely that the acceptor Ub Lys^{63} ϵ-amino group is deprotonated to promote nucleophilic attack of the carbonyl carbon of the thioester bond. Second, the negative charge on the carbonyl atom of the first tetrahedral transition state needs to be stabilized. Overcoming these barriers to the reaction is likely to lower the activation energy for the reaction and increase the enzyme-catalyzed rate.

One of the key structural aspects of our model is that Ub-Lys^{63} is placed in a catalytically competent position by a network of hydrogen bonds involving the side chain carboxyl groups of hUbc13-Asp^{81} and Ub-Glu^{64} (Figure 5.2B). It is generally assumed that deprotonation of acceptor Ub-Lys^{63} involves the side chain from an Asp or Glu residue acting as a general base. From the model presented herein, two likely candidates for a general base are hUbc13-Asp^{81} and acceptor Ub-Glu^{64}. The importance of Asp^{81} for catalysis has been demonstrated by the fact that Mms2·Ubc13-D81A has impaired catalysis of diUb and Mms2·Ubc13-D81R does not catalyze the synthesis of diUb [18].

In order to probe protein electrostatic interactions in and around the active site when acceptor Ub-Lys^{63} is proximal to the thioester bond, we have performed molecular dynamics simulations with a Ub·hUev1a·hUbc13∼Ub complex, where the distance between the

amino nitrogen of Lys^{63} of the donor Ub and the carbonyl carbon of the thioester bond is restrained to 3.0 Å (see Section 5.2 for further details). Given that there are no structural data for the Ub·hUev1a·hUbc13~Ub tetramer, this approach has the advantage of allowing conformational averaging in and around the active site, avoiding the pitfalls associated with using a single model structure. Whilst a fully unrestrained, long time scale molecular dynamics approach would be a more fundamental approach, it is too computationally expensive in the present case, given the size of the system.

ΔpK_a values for hUbc13-Asp^{81}, acceptor Ub-Glu^{64}, and acceptor Ub-Lys^{63}, were calculated as previously described [14, 17] for each step of the molecular dynamics simulation. The average ΔpK_a value for acceptor Ub-Lys^{63} over the course of the simulation is ~0.5. However, when the angle θ is approximately between 60° to 85° (Figure 5.1), many of the ΔpK_a values are large and negative, with an average value of -1.8 for θ greater than 70°. This suggests that as Ub-Lys^{63} approaches the thioester bond at values near the Bürgi-Dunitz angle (107°), deprotonation of the ϵ-amino group, and nucleophilic attack on the carbonyl carbon become possible, without the involvement of a general base. Furthermore, instantaneous ΔpK_a values for hUbc13-Asp^{81} and acceptor Ub-Glu^{64} do not show positive shifts during the course of the simulation, indicating that the environment of the active site does not favor protonation of either of these side chains.

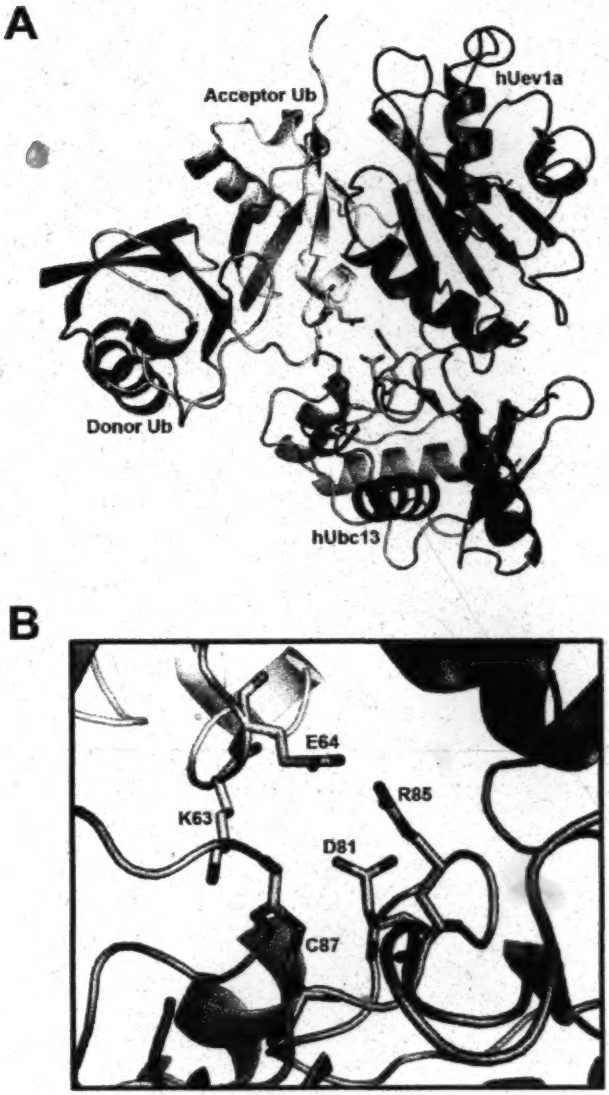

Figure 5.2: **Model for Synthesis of Lys^{63}-linked polyUb Chains.** (A) A model of the Ub·hUev1a·hUbc13~Ub complex. (B) Close-up of the active site of the Ub·hUev1a·hUbc13~Ub complex.

Bibliography

[1] C. I. Bayly, P. Cieplak, W. D. Cornell, and P. A. Kollman. A Well-behaved Electrostatic Potential Based Method Using Charge Restraints for Deriving Atomic Charges - the RESP Model. *J. Phys. Chem.*, 97:10269–10280, 1993.

[2] H. J. C. Berendsen, J. P. M. Postma, W. F. Vangunsteren, A. Dinola, and J. R. Haak. Molecular-dynamics with Coupling to an External Bath. *J. Chem. Phys.*, 81:3684–3690, 1984.

[3] D. A. Case, T. E. Cheatham, T. Darden, H. Gohlke, R. Luo, K. M. Merz, A. Onufriev, C. Simmerling, B. Wang, and R. J. Woods. The AMBER Biomolecular Simulations Programs. *J. Comput. Chem.*, 26:1668–1688, 2005.

[4] P. Cieplak, W. D. Cornell, C. Bayly, and P. A. Kollman. Application of the Multimolecule and Multiconformational RESP Methodology to Biopolymers - Charge Derivation for DNA, RNA, and Proteins. *J. Comput. Chem.*, 16:1357–1377, 1995.

[5] K. A. Conners and M. L. Bender. The Kinetics of Alkaline Hydrolysis and n-Butylaminolysis of Ethyl p-Nitrobenzoate and Ethyl p-Nitrothiobenzoate. *J. Org. Chem.*, 26:2498–2504, 1961.

[6] W. D. Cornell, P. Cieplak, C. I. Bayly, I. R. Gould, K. M. Merz, D. M. Ferguson, D. C. Spellmeyer, T. Fox, J. W. Caldwell, and P. A. Kollman. A 2nd Generation Force-Field for the Simulation of Proteins, Nucleic Acids, and Organic Molecules. *J. Am. Chem. Soc.*, 117:5179–5197, 1995.

[7] W. L. DeLano. The PyMOL Molecular Graphics System. http://www.pymol.org, 2002.

[8] C. Dominguez, R. Boelens, and A. M. Bonvin. HADDOCK: a Protein-protein Docking Approach Based on Biochemical or Biophysical Information. *J. Am. Chem. Soc.*, 125:1731–1737, 2003.

[9] J. B. Foresman and A. Frish. *Exploring Chemistry with Electronic Structure Methods.* Gaussian, Inc., 2nd edition, 1996.

[10] M. J. Frisch, G. W. Trucks, H. B. Schlegel, G. E. Scuseria, M. A. Robb, J. R. Cheeseman, J. A. Montgomery, Jr., T. Vreven, K. N. Kudin, J. C. Burant, J. M. Millam, S. S. Iyengar, J. Tomasi, V. Barone, B. Mennucci, M. Cossi, G. Scalmani, N. Rega, G. A.

Petersson, H. Nakatsuji, M. Hada, M. Ehara, K. Toyota, R. Fukuda, J. Hasegawa, M. Ishida, T. Nakajima, Y. Honda, O. Kitao, H. Nakai, M. Klene, X. Li, J. E. Knox, H. P. Hratchian, J. B. Cross, V. Bakken, C. Adamo, J. Jaramillo, R. Gomperts, R. E. Stratmann, O. Yazyev, A. J. Austin, R. Cammi, C. Pomelli, J. W. Ochterski, P. Y. Ayala, K. Morokuma, G. A. Voth, P. Salvador, J. J. Dannenberg, V. G. Zakrzewski, S. Dapprich, A. D. Daniels, M. C. Strain, O. Farkas, D. K. Malick, A. D. Rabuck, K. Raghavachari, J. B. Foresman, J. V. Ortiz, Q. Cui, A. G. Baboul, S. Clifford, J. Cioslowski, B. B. Stefanov, G. Liu, A. Liashenko, P. Piskorz, I. Komaromi, R. L. Martin, D. J. Fox, T. Keith, M. A. Al-Laham, C. Y. Peng, A. Nanayakkara, M. Challacombe, P. M. W. Gill, B. Johnson, W. Chen, M. W. Wong, C. Gonzalez, and J. A. Pople. Gaussian 03, Revision C.02. Gaussian, Inc., Wallingford, CT, 2004.

[11] M. J. Lewis, L. F. Saltibus, D. D. Hau, W. Xiao, and L. Spyracopoulos. Structural Basis for Non-covalent Interaction between Ubiquitin and the Ubiquitin Conjugating Enzyme Variant Human MMS2. *J. Biomol. NMR.*, 34:89–100, 2006.

[12] S. McKenna, T. Moraes, L. Pastushok, C. Ptak, W. Xiao, L. Spyracopoulos, and M. J. Ellison. An NMR-based Model of the Ubiquitin-bound Human Ubiquitin Conjugation Complex Mms2-Ubc13. *J. Biol. Chem.*, 278:13151–13158, 2003.

[13] J. Mongan and D. A. Case. Biomolecular Simulations at Constant pH. *Curr. Opin. Struc. Biol.*, 15:157–163, 2005.

[14] J. Mongan, D. A. Case, and J. A. McCammon. Constant pH Molecular Dynamics in Generalized Born Implicit Solvent. *J. Comput. Chem.*, 25:2038–2048, 2004.

[15] A. Onufriev, D. Bashford, and D. A. Case. Exploring Protein Native States and Large-scale Conformational Changes with a Modified Generalized Born Model. *Proteins*, 55:383–394, 2004.

[16] J. P. Ryckaert, G. Ciccotti, and H. J. C. Berenden. Numerical-integration of Cartesian Equations of Motion of a System with Constraints - Molecular Dynamics of N-alkanes. *J. Comput. Phys.*, 23:327–341, 1977.

[17] T. Simonson, J. Carlsson, and D. A. Case. Proton Binding to Proteins: pK(a) Calculations with Explicit and Implicit Solvent Models. *J. Am. Chem. Soc.*, 126:4167–4180, 2004.

[18] A. P. VanDemark, R. M. Hofmann, C. Tsui, C. M. Pickart, and C. Wolberger. Molecular Insights into Polyubiquitin Chain Assembly: Crystal Structure of the Mms2/Ubc13 Heterodimer. *Cell*, 105:711–720, 2001.

[19] J. M. Wang, P. Cieplak, and P. A. Kollman. How Well Does a Restrained Electostatic Potential (RESP) Model Perform in Calculating Conformational Energies of Organic and Biological Molecules? *J. Comput. Chem.*, 21:1049–1074, 2000.

[20] P. Y. Wu, M. Hanlon, M. Eddins, C. Tsui, R. S. Rogers, J. P. Jensen, M. J. Matunis, A. M. Weisman, C. P. Wolberger, and C. M. Pickart. A Conserved Catalytic Residue in the Ubiquitin-conjugating Enzyme Family. *EMBO J.*, 22:5241–5250, 2003.

[21] W. Yang and D. G. Drueckhammer. Computational Studies of the Aminolysis of Oxoesters and Thioesters in Aqueous Solution. *Org. Lett.*, 2:4133–4136, 2000.

[22] W. Yang and D. G. Drueckhammer. Understanding the Relative Acyl-Transfer Reactivity of Oxoesters and Thioesters: Computational Analysis of Transition State Delocalization Effects. *J. Am. Chem. Soc.*, 123:11004–11009, 2001.

[23] M. Zhang, M. Windheim, S. M. Roe, P. Cohen, C. Prodromou, and L. H. Pearl. Chaperoned Ubiquitylation - Crystal Structures of the CHIP U Box E3 Ubiquitin Ligase and a CHIP-Ubc13-Uev1a Complex. *Mol. Cell*, 20:525–538, 2005.

Chapter 6

Conclusion

6.1 Conclusion

This dissertation is based upon work focused on the structure and function of hUev1a. hUev1a, a ubiquitin conjugating enzyme variant, forms a heterodimer with hUbc13, a ubiquitin conjugating enzyme, to catalyze Lys^{63}-linked polyubiquitin chains on a number of target proteins. These polyubiquitin chains are important to the signal transduction cascades responsible for the activation of NF-κB, JNK, and p38 (Sections 1.5.1 and 1.5.1). Moreover, recent evidence suggests that hUev1a-mediated Lys^{63}-polyubiquitin chains may play a role in Parkinson's disease pathogenesis and/or the cellular machinery that handles misfolded protein (Sections 1.5.1 and 1.5.1). The studies contained herein address an important need to better understand the mechanisms of hUev1a function and the biological pathways in which it is involved.

Chapter 2 details the NMR-derived solution structure of hUev1a. The structure reveals that the first 34 residues, dubbed 'the N-terminal tail,' does not adopt regular structure and is therefore flexible. The remaining 136 residues form a core structure that is nearly identical to the crystal structure of hMms2. The structure and NMR data provide the basis for experiments detailed in subsequent chapters.

Chapter 3 involved the conformational dynamics of the backbone amide atoms of hUev1a. These experiments characterize the backbone flexibility of different regions in the protein, and serve to validate the overall fold of the determined structure. The backbone dynamics of hUev1a greatly resembles that of hMms2, where the core structure is highly ordered with the exception of the first loop. Agreement between the theoretical and ob-

served rotational diffusion tensor supports the verity of the determined structure.

Chapter 4 encompasses chemical shift mapping experiments that probe for regions of hUev1a affected by titration with either hUbc13 or Ub. The regions of hUev1a that are perturbed upon titration of hUbc13 or Ub are similar to the regions on hMms2 that form the interfaces with hUbc13 and Ub. Thus, it is likely that hUev1a binds hUbc13 and Ub similarly to hMms2. These data along with the structure of the TRAF6 RING domain, and insight gained from the c-Cbl·UbcH7 structure, were used to develop a model of a trimer consisting of hUev1a, hUbc13, and the TRAF6 RING domain was produced. The model revealed that the N-terminal tail of hUev1a is oriented towards the putative RING domain binding site; it is suspected that the tail of hUev1a may interact with the RING domain or adjacent domains of TRAF6, which could explain the exclusivity conferred to hUev1a as the UEV involved in TRAF6 polyubiquitination (as opposed to hMms2).

Chapter 5 described the construction of the tetramer model of Ub·hUev1a·hUbc13~Ub and the subsequent molecular dynamics simulation experiment that was performed with the model to explore the catalytic basis of ubiquitin conjugation. The results indicate that as the trajectory of the ϵ-nitrogen of Lys^{63} on the acceptor Ub approaches the Bürgi-Dunitz angle of 107°, relative to the carbonyl group in the thioester bond, the instantaneous pK_a of the Lys^{63} sidechain often shifts downwards as much as 8 pK_a units. This shift in pK_a could explain how the ϵ-nitrogen can be deprotonated, thus increasing its nucleophilicity prior to attack of the thioester carbonyl carbon. Furthermore, the experiment shows that positive ΔpK_a values for sidechains of hUbc13-Asp^{81} and acceptor Ub-Glu^{64} are not observed, indicating that it is unlikely that these groups serve as general bases to deprotonate the ϵ-nitrogen group of acceptor Ub-Lys^{63}; instead, the results surprisingly suggest that a general base is not required. The proximity between the sidechain of acceptor Ub-Lys^{63} to both hUbc13-Asp^{81} and acceptor Ub-Glu^{64} suggests that the Asp and Glu residues may facilitate orientation of acceptor Ub-Lys^{63} towards the active site thioester bond.

Many questions remain regarding how hUev1a, and not hMms2, is able to function in the polyubiquitination of TRAF2/6. There exist two factors that might explain the functional selectivity between the two UEV proteins: 1) the N-terminal tail that hUev1a possesses or 2) the 10 residues in the core that differ between the two proteins. Concerning the 10 core residues, 9 cluster to one side of the surface of the molecules (Figure 6.1). Notably,

Ser^{79}, Met^{97}, and Ala^{100} of hMms2 are substituted with Phe, Val, and Pro residues, respectively, in hUev1a, creating a distinct hydrophobic patch that is found only on the hUev1a surface (Figure 6.1). This hydrophobic patch may be responsible for interactions with E3s.

Alternatively, the flexible N-terminal tail of hUev1a might be the factor responsible for TRAF association with the hUev1a·hUbc13 heterodimer. As described in Section 4.4.3, analysis of the E2·E3 structures indicates that the hUev1a tail may be proximal to the RING domain of TRAF6 and therefore may be involved in recognition interactions. A recent study has revealed that truncated hUev1a, which lacks the first 30 residues, behaves similarly to hMms2 *in vitro*, colocalizing with hUbc13 into nuclei upon DNA damage [1]. Thus, the N-terminal tail of hUev1a is proving to be the determining factor. However, that the different core residues may play a role cannot be ruled out. An experiment involving the measurement of activity of NF-κB activation in cells containing hUev1a versus cells containing hMms2 fused with the tail of hUev1a would answer the importance of the different core residues; if the activities are similar, then the tail is the only selectivity factor.

In addition to questions concerning the functional selectivity between hUev1a and hMms2, details concerning the mechanism of ubiquitin conjugation still remain. For example, *in vitro* evidence shows that the hUev1a·hUbc13 heterodimer builds polyUb chains that are covalently linked to hUev1a, presumably on one of the four lysines found in the N-terminal tail (Trevor Moraes, unpublished data). Further experimentation, such as mutation of the tail Lys residues, may determine if ubiquitin conjugation to the tail is important for TRAF ubiquitination. Moreover, the observation of polyUb chains attached to hUev1a raises the question of whether the polyUb chain is built first, then attached to the protein substrate. This is opposed to the conventional theory where Ub molecules are sequentially attached to the substrate. The mechanism of polyUb chain elongation still needs to be addressed. A recent review proposes four possible models for polyubiquitin-chain sythesis, which three could apply to the hUev1a-involved systems [2] (Figure 6.2). However, none of the models have strong experimental suppport.

It is unclear whether hUev1a is essential for conjugation of the initial Ub molecule on the target substrate. If so, what is the chemical and/or structural mechanism? This question also ties into the question of where the site(s) of polyubiquitination are on the TRAF proteins. Should the involvement of hUev1a prove to be significant in Parkinson's

disease and handling of misfolded proteins (outlined in Sections 1.5.1 and 1.5.1), these questions would also apply.

Currently, our lab has determined the structure of the RING domain of TRAF6 (unpublished data) and has found, through chemical shift mapping experiments, that it likely binds to hUbc13 as similarly observed between c-Cbl and UbcH7. Furthermore, we are in the process of determining the NMR structure of the trimer composed of the acceptor Ub, hMms2, and hUbc13. Once determined, the structure will provide a higher resolution view of the interactions between each component in the trimer.

In summary, the work discussed in this dissertation, which includes investigation of the structure and function of hUev1a, sheds further light on Lys^{63}-linked polyubiquitination and provides a basis for future work into this system.

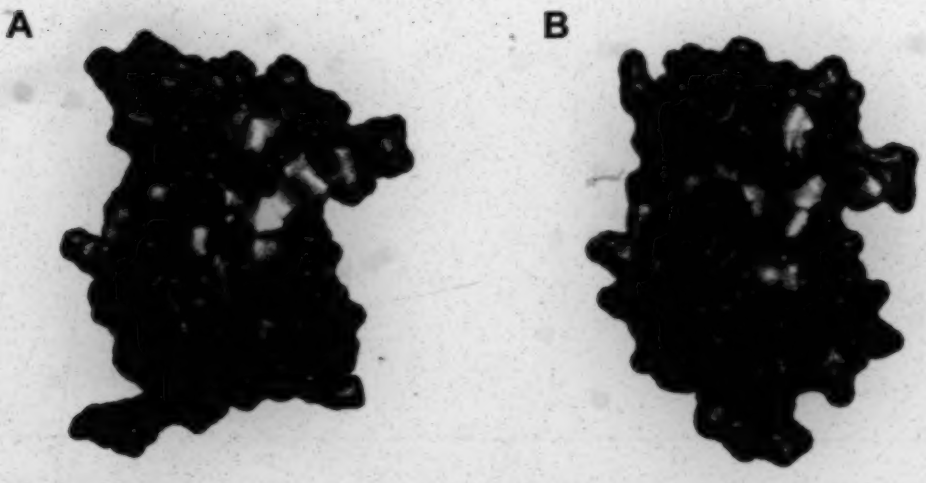

Figure 6.1: **Differences in Core Residues Between hUev1a and hMms2.** Surface representations of hUev1a (A) and hMms2 (B). Positions of sequence dissimilarity between the two structures are denoted by white and yellow, and indicates polar and hydrophobic groups, respectively. The dissimilar residues did not contain any charged amino acids.

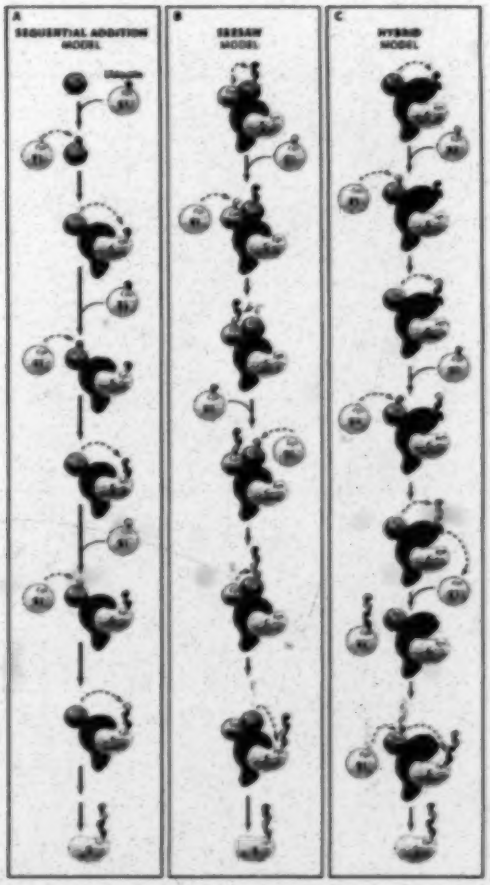

Figure 6.2: **Models for Polyubiquitin-Chain Synthesis.** (A) Sequential addition model. Ub molecules are added one at a time, first to a lysine on the substrate protein (S) and then to a specific lysine in the Ub at the distal end of the growing Ub chain. A RING E3 is depicted and is assumed to remain associated with the substrate through multiple rounds of Ub addition. (B) Seesaw model. Ub chains are built by a pair of E2s (either a homo- or heterodimer), which pass the growing chainback and forth between the two E2 active sites, before being transferred to the substrate. During chain assembly, the attacking lysine is always on a monomeric Ub that is in thioester linkage to an E2. The order of Ub addition is opposite to that in the other three models (compare colors). (C) Hybrid model. The Ub chain is assembled prior to transfer to the substrate, but a noncovalent interaction between (poly)Ub and a site in the E2 or E3 (the latter is depected) positions it for nucleophilic attack on the E2~Ub thioester, much as in the sequential addition model. At some point, the free end of the Ub chain must be activated by E1 and transferred to the E2 cysteine before the final transfer of the chain to the substrate. Reprinted from *Cell*, 124, Hochstrasser, M., Lingering Mysteries of Ubiquitin-Chain Assembly, 27-34, 2006, with permission from Elsevier.

Bibliography

[1] P. L. Andersen, H. Zhou, L. Pastushok, T. Moraes, S. McKenna, B. Ziola, M. J. Ellison, V. M. Dixit, and W. Xiao. Distinct Regulation of Ubc13 Functions by the Two Ubiquitin-Conjugating Enzyme Variants Mms2 and Uev1a. *J. Cell Bio.*, 147:138–146, 2000.

[2] M. Hochstrasser. Lingering Mysteries of Ubiquitin-Chain Assembly. *Cell*, 124:27–34, 2006.

Appendix A

hUev1a Chemical Shifts

The six tables in this chapter contain the chemical shifts for the atoms of hUev1a. All values were recorded to three decimal places, but, due to formatting complications, values ending in one or more zeroes do not have the specified zeroes displayed.

Table A.1: Backbone Amide ^{15}N and ^{1}H Chemical Shifts.

Residue		N	H_N
1	Met	123.213	
2	Pro		
3	Gly	109.46	8.518
4	Glu	120.511	8.093
5	Val	121.386	8.148
6	Gln	123.844	8.379
7	Ala	124.957	8.304
8	Ser	114.601	8.206
9	Tyr	121.691	7.966
10	Leu	122.399	7.9
11	Lys	121.322	8.059
12	Ser	115.988	8.145
13	Gln	121.785	8.274
14	Ser	116.533	8.223
15	Lys	122.962	8.266
16	Leu	122.723	8.205
17	Ser	115.88	8.225
18	Asp	122.385	8.341
19	Glu	120.742	8.358
20	Gly	109.281	8.411
21	Arg	119.945	7.917
22	Leu	123.029	8.235
23	Glu	122.998	8.251

Continued on next page

Table A.1 – continued from previous page

Residue		N	H_N
24	Pro		
25	Arg	120.52	8.406
26	Lys	121.662	8.176
27	Phe	120.337	8.138
28	His		7.0
29	Cys		
30	Lys		
31	Gly	110.168	8.432
32	Val	119.089	7.831
33	Lys	125.16	8.329
34	Val	124.198	8.304
35	Pro		
36	Arg	123.7	8.602
37	Asn	115.239	8.432
38	Phe	118.236	7.577
39	Arg	119.617	8.08
40	Leu	119.765	8.657
41	Leu	120.566	8.275
42	Glu	121.837	7.802
43	Glu	120.378	8.501
44	Leu	125.207	9.103
45	Glu	120.372	8.007
46	Glu	119.226	8.441
47	Gly	107.372	8.408
48	Gln	119.29	7.887
49	Lys	118.939	7.623
50	Gly	107.041	7.854
51	Val	115.756	8.321
52	Gly	112.647	8.705
53	Asp	119.564	8.17
54	Gly	107.486	8.342
55	Thr	109.825	8.103
56	Val	111.07	7.285
57	Ser	115.861	8.901
58	Trp	119.563	7.885
59	Gly	104.778	8.579
60	Leu	121.663	8.273
61	Glu	123.742	8.419
62	Asp	117.615	7.966
63	Asp	123.821	8.492
64	Glu	117.225	8.356
65	Asp	118.526	7.662

Continued on next page

Table A.1 – continued from previous page

Residue		N	H_N
66	Met	126.367	8.603
67	Thr	109.538	8.368
68	Leu	117.211	7.77
69	Thr	113.568	7.955
70	Arg	119.094	7.134
71	Trp	126.694	9.716
72	Thr	117.206	9.88
73	Gly	107.842	8.434
74	Met	122.952	8.993
75	Ile	121.652	8.826
76	Ile	126.72	8.579
77	Gly	117.621	9.774
78	Pro		
79	Pro		
80	Arg	113.132	9.149
81	Thr	105.366	7.428
82	Ile	121.864	8.607
83	Tyr	119.314	7.324
84	Glu	118.62	7.293
85	Asn	117.557	8.534
86	Arg	121.481	8.186
87	Ile	120.941	8.105
88	Tyr	127.514	9.349
89	Ser	117.507	9.294
90	Leu	124.383	9.143
91	Lys	121.415	9.255
92	Ile	124.271	8.705
93	Glu	126.631	9.269
94	Cys	126.53	9.343
95	Gly	111.186	8.042
96	Pro		
97	Lys	114.82	8.693
98	Tyr	125.564	7.754
99	Pro		
100	Glu	125.309	8.893
101	Ala	121.279	7.153
102	Pro		
103	Pro		
104	Phe	120.024	8.395
105	Val	126.765	8.341
106	Arg	122.717	8.597
107	Phe	124.622	9.649

Continued on next page

Table A.1 – continued from previous page

Residue		N	H_N
108	Val	122.945	9.332
109	Thr	116.639	7.558
110	Lys	121.679	8.367
111	Ile	120.608	8.0
112	Asn	124.879	8.636
113	Met	127.405	8.907
114	Asn	125.509	8.516
115	Gly	111.058	8.627
116	Val	118.424	7.698
117	Asn	129.124	8.732
118	Ser	123.368	8.99
119	Ser	116.971	8.927
120	Asn	116.894	7.24
121	Gly	108.627	7.889
122	Val	122.147	8.068
123	Val	130.631	8.194
124	Asp	129.537	8.794
125	Pro		
126	Arg	111.88	7.904
127	Ala	119.012	7.797
128	Ile	117.013	7.087
129	Ser		
130	Val	113.805	7.557
131	Leu	114.178	7.035
132	Ala	124.886	8.576
133	Lys	118.163	8.229
134	Trp	122.301	7.047
135	Gln	123.958	5.177
136	Asn	116.945	8.499
137	Ser	109.017	6.601
138	Tyr	123.054	7.253
139	Ser	107.729	6.418
140	Ile	123.78	9.657
141	Lys	118.009	7.669
142	Val	116.808	6.927
143	Val	119.172	7.585
144	Leu	117.108	8.012
145	Gln	116.369	8.668
146	Glu	120.988	8.278
147	Leu	120.448	8.24
148	Arg	117.643	7.915
149	Arg	119.06	8.033

Continued on next page

Table A.1 – continued from previous page

Residue		N	H_N
150	Leu	121.922	8.368
151	Met	122.291	7.65
152	Met	109.924	7.261
153	Ser	115.532	7.794
154	Lys		
155	Glu	116.795	9.125
156	Asn	115.852	7.53
157	Met	113.779	7.887
158	Lys	119.139	8.535
159	Leu	125.277	7.578
160	Pro		
161	Gln	121.029	8.695
162	Pro		
163	Pro		
164	Glu	122.935	8.528
165	Gly	112.454	8.937
166	Gln	119.244	7.459
167	Cys	119.651	8.666
168	Tyr	120.447	8.412
169	Ser		
170	Asn	125.797	8.132

Table A.2: ^{13}C Chemical Shifts. Groups marked with an asterisk (*) denote that the group is stereospecifically labelled, where the first and second values corresponds to the 'R' and 'S' groups, respectively. C_δ and C_ϵ chemical shifts for Phe and Tyr residues are located in Table A.6

Residue		C_α	C_β	C_γ	C_δ	C_ϵ
1	Met	53.399	32.433	32.178		
2	Pro	63.758	32.152	27.471	50.781	
3	Gly	45.472				
4	Glu	56.74	30.426	36.385		
5	Val	62.733	32.701	(21.200, 20.889)*		
6	Gln	56.109	29.296	33.872		
7	Ala	53.297	19.164			
8	Ser	58.962	63.519			
9	Tyr	58.464	38.378			
10	Leu	55.611	42.26	26.697	(24.982, 23.397)	

Continued on next page

Table A.2 – continued from previous page

Residue		C_α	C_β	C_γ	C_δ	C_ϵ
11	Lys	56.932	32.861	24.823	29.183	42.143
12	Ser	58.871	63.634			
13	Gln	56.275	29.394	33.881		
14	Ser	58.748	63.891			
15	Lys	56.318	33.044	24.63	29.067	42.134
16	Leu	55.453	42.386	26.936	(24.995, 23.440)	
17	Ser	58.39	63.914			
18	Asp	54.802	41.25			
19	Glu	57.36	30.005	36.385		
20	Gly	45.69				
21	Arg	56.217	30.916	27.065	43.392	
22	Leu	55.036	42.513	26.933	(25.023, 23.481)*	
23	Glu	54.456	30.04	36.133		
24	Pro	63.566	32.095	27.388	50.783	
25	Arg	56.458	30.66	27.188	43.429	
26	Lys	56.449	33.127	24.746	29.134	42.172
27	Phe	57.698	39.719			
28	His	56.263	31.027			
29	Cys					
30	Lys	56.786	32.953	24.788	29.129	42.29
31	Gly	45.35				
32	Val	62.086	32.941	(21.264, 20.536)		
33	Lys	56.094	32.944	24.948	29.152	42.44
34	Val	60.014	33.066	(21.48, 20.815)*		
35	Pro	63.774	32.571		51.185	
36	Arg	60.56	31.178		43.632	
37	Asn	56.826	37.245			
38	Phe	60.932	38.761			
39	Arg	57.506	28.504		40.597	
40	Leu	58.582	43.021	28.193	(26.311, 23.900)*	
41	Leu	58.188	41.715	26.985	(25.380, 23.379)*	
42	Glu	60.071	29.587	36.861		
43	Glu	61.678	29.523	38.435		
44	Leu	58.821	42.89	27.301	(24.73, 25.935)*	
45	Glu	59.665	29.495	36.284		
46	Glu	59.7	30.04	36.832		
47	Gly	45.357				
48	Gln	57.875	28.764	34.27		
49	Lys	57.982	33.247	25.143	29.387	42.23
50	Gly	45.093				
51	Val	61.32	33.389	(21.855, 20.445)*		
52	Gly	46.724				

Continued on next page

Table A.2 – continued from previous page

Residue		C_α	C_β	C_γ	C_δ	C_ϵ
53	Asp	53.554	41.052			
54	Gly	46.222				
55	Thr	64.236	70.536	22.577		
56	Val	59.405	36.007	(22.569, 19.48)*		
57	Ser	57.778	65.359			
58	Trp	57.906	32.262			
59	Gly	45.157				
60	Leu	55.039	42.541	26.6	(25.190, 22.732)*	
61	Glu	59.049	30.308	36.959		
62	Asp	52.698	43.021			
63	Asp	56.063	40.621			
64	Glu	56.185	29.497	36.74		
65	Asp	53.581	40.396			
66	Met	56.456	32.056	32.368		17.447
67	Thr	62.449	70.13	21.626		
68	Leu	56.417	39.897	27.295	(27.158, 24.825)*	
69	Thr	66.164	69.253	21.2		
70	Arg	57.211	31.002	28.525	43.326	
71	Trp	56.786	31.321			
72	Thr	60.051	70.628	21.6		
73	Gly	44.255				
74	Met	54.691	36.387	32.041		16.875
75	Ile	60.612	44.937	(27.533, 18.100)	16.04	
76	Ile	60.343	37.707	(28.008, 17.197)	12.8	
77	Gly	44.88				
78	Pro	61.739	31.021			
79	Pro	62.708	32.643	27.27	51.1	
80	Arg	57.487	26.626	27.93	43.453	
81	Thr	60.124	74.71	22.72		
82	Ile	60.632	39.955	(28.113, 16.470)	14.91	
83	Tyr	56.849	38.948			
84	Glu	57.943	30.886	35.446		
85	Asn	55.376	37.443			
86	Arg	56.725	31.711	28.661	44.214	
87	Ile	60.735	38.609	(27.837, 17.950)	13.2	
88	Tyr	58.386	40.817			
89	Ser	57.513	64.603			
90	Leu	56.324	46.579	29.661	(25.636, 26.441)*	
91	Lys	55.857	35.435	25.575	29.055	42.072
92	Ile	59.95	42.769	(29.451, 19.379)	15.438	
93	Glu	54.555	32.949	36.75		
94	Cys	58.266	27.871			

Continued on next page

Table A.2 – continued from previous page

Residue		C_α	C_β	C_γ	C_δ	C_ϵ
95	Gly	45.745				
96	Pro	65.086	32.691	27.124	49.949	
97	Lys	54.882	32.699	25.374	28.904	42.248
98	Tyr	57.848	39.947			
99	Pro	63.915	32.306	24.638	49.26	
100	Glu	58.297	28.911	36.271		
101	Ala	48.207	20.72			
102	Pro	59.307	30.868	25.951	49.858	
103	Pro	61.696	32.451	24.93	48.911	
104	Phe	56.972	40.819			
105	Val	61.253	34.724	(22.161, 21.381)*		
106	Arg	53.821	34.261	26.345	44.11	
107	Phe	60.018	39.708			
108	Val	64.896	32.967	(21.054, 22.175)*		
109	Thr	63.355	70.808	22.864		
110	Lys	58.769	33.121	25.15	29.956	42.128
111	Ile	60.261	41.8	(30.326, 13.772)	14.068	
112	Asn	50.793	38.926			
113	Met	56.301	37.1	31.986		18.191
114	Asn	56.274	38.477			
115	Gly	45.212				
116	Val	61.079	32.863	(20.776, 22.057)*		
117	Asn	54.627	39.037			
118	Ser	60.555	63.555			
119	Ser	60.244	64.006			
120	Asn	52.588	39.922			
121	Gly	46.77				
122	Val	65.496	32.158	(21.753, 22.863)*		
123	Val	62.461	32.109	(22.405, 23.200)*		
124	Asp	51.15	41.707			
125	Pro	64.131	32.252	27.173	51.065	
126	Arg	57.446	30.002	27.097	43.367	
127	Ala	52.691	21.11			
128	Ile	57.712	38.033	(26.825, 18.032)	10.7	
129	Ser	62.919	62.448			
130	Val	64.093	31.397	(21.206, 20.646)		
131	Leu	56.355	41.859	27.48	(22.978, 25.176)*	
132	Ala	55.059	19.127			
133	Lys	53.673	31.079	24.628	29.316	42.273
134	Trp	59.737	30.665			
135	Gln	52.317	31.694	32.646		
136	Asn	54.05	37.437			

Continued on next page

Table A.2 – continued from previous page

Residue		C_α	C_β	C_γ	C_δ	C_ε
137	Ser	57.656	63.023			
138	Tyr	53.813	34.96			
139	Ser	56.305	65.31			
140	Ile	67.05	37.702	(29.150, 17.100)	11.729	
141	Lys	59.908	31.465	23.525	29.427	41.577
142	Val	65.767	32.415	(20.323, 22.900)*		
143	Val	67.117	31.491	(21.108, 23.999)*		
144	Leu	58.243	41.366	26.69	(27.888, 22.957)*	
145	Gln	59.472	28.55	35.201		
146	Glu	58.534	28.819	35.907		
147	Leu	58.431	41.976	26.943	(26.614, 23.058)*	
148	Arg	59.403	29.579		43.415	
149	Arg	59.613	30.124	27.968	43.011	
150	Leu	57.695	41.594	27.2	(25.908, 22.800)*	
151	Met	59.383	32.345	34.135		18.374
152	Met	55.396	33.763	32.704		17.553
153	Ser	58.694	64.41			
154	Lys	60.047	32.346	24.688	29.401	42.047
155	Glu	58.888	28.972	36.279		
156	Asn	54.313	41.055			
157	Met	59.742	33.419	31.313		17.575
158	Lys	55.138	33.053	25.315	29.427	42.162
159	Leu	53.484	41.485	26.786	(26.786, 22.885)*	
160	Pro	62.961	31.83	27.718	50.276	
161	Gln	52.636	30.221	33.971		
162	Pro	61.13	30.422	26.845	50.292	
163	Pro	63.146	32.251	27.9	50.5	
164	Glu	57.7	30.07	36.27		
165	Gly	45.399				
166	Gln	56.378	30.004	34.53		
167	Cys	57.419	31.582			
168	Tyr	60.233	38.932			
169	Ser	58.354	64.081			
170	Asn	54.953	40.567			

Table A.3: $^1H_\alpha$ and $^1H_\beta$ Chemical Shifts. Groups that should contain two values (eg. the H_β resonances of Tyr), but have one value missing indicate that one of the two was unassigned or that the group is degenerate.

Residue		H_α	H_β
1	Met	4.857	(1.981, 2.090)
2	Pro	4.419	(1.940, 2.329)
3	Gly	4.419	
4	Glu	4.314	(1.993, 2.033)
5	Val	4.059	2.077
6	Gln	4.283	(1.983, 2.100)
7	Ala	4.25	1.36
8	Ser	4.321	(3.867, 3.830)
9	Tyr	4.542	(, 3.053)
10	Leu	4.221	(1.613, 1.537)
11	Lys	4.271	(1.795, 1.877)
12	Ser	4.412	(2.905, 3.097)
13	Gln	4.349	(1.993, 2.149)
14	Ser	4.434	(, 3.887)
15	Lys	4.366	(1.875, 1.770)
16	Leu	4.367	(1.584, 1.651)
17	Ser	4.447	(, 3.899)
18	Asp	4.625	(2.671, 2.731)
19	Glu	4.225	(1.968, 2.099)
20	Gly	(3.793, 3.937)	
21	Arg	4.326	(1.778, 1.854)
22	Leu	4.36	(1.594, 1.648)
23	Glu	4.587	(1.910, 2.022)
24	Pro	4.373	(1.894, 2.266)
25	Arg	4.206	(, 1.744)
26	Lys	4.231	(, 1.651)
27	Phe	4.569	(3.075, 2.959)
28	His	4.607	(3.029, 3.102)
29	Cys		
30	Lys	4.28	(1.799, 1.875)
31	Gly	(3.978, 3.926)	
32	Val	4.125	2.061
33	Lys	4.36	(, 1.741)
34	Val	4.379	2.062
35	Pro	4.446	(, 2.462)
36	Arg	4.044	(, 1.751)
37	Asn	4.341	(2.798, 2.863)

Continued on next page

Table A.3 – continued from previous page

Residue		H_α	H_β
38	Phe	4.33	(3.178, 3.277)
39	Arg	4.451	(, 2.141)
40	Leu	4.377	(2.165, 1.955)
41	Leu	4.332	(1.568, 1.988)
42	Glu	4.263	(2.506, 2.265)
43	Glu	4.455	(2.253,)
44	Leu	4.592	(2.140, 2.474)
45	Glu	4.139	(2.237, 2.285)
46	Glu	4.125	(2.439, 2.482)
47	Gly	(2.324, 2.782)	
48	Gln	4.086	(2.095, 2.25)
49	Lys	4.175	(, 1.969)
50	Gly	(3.668, 4.115)	
51	Val	4.484	2.319
52	Gly	(3.873, 4.163)	
53	Asp	4.63	(2.692, 3.026)
54	Gly	(3.955, 4.085)	
55	Thr	4.028	4.224
56	Val	5.483	2.317
57	Ser	4.747	(3.823, 3.684)
58	Trp	5.768	(3.225, 3.632)
59	Gly	(4.009, 4.353)	
60	Leu	3.654	(1.114, 1.052)
61	Glu	3.916	(1.631, 1.787)
62	Asp	4.676	(2.488, 2.761)
63	Asp	4.268	(, 2.615)
64	Glu	4.259	(2.21, 1.919)
65	Asp	4.643	(2.700, 3.205)
66	Met	4.395	(2.196, 2.121)
67	Thr	4.495	4.42
68	Leu	3.638	(2.277, 1.830)
69	Thr	4.415	3.95
70	Arg	4.916	(1.866, 2.011)
71	Trp	5.097	(3.075, 3.381)
72	Thr	5.236	4.239
73	Gly	(5.48, 3.384)	
74	Met	5.744	(1.909, 1.981)
75	Ile	4.83	1.555
76	Ile	4.814	1.825
77	Gly	(4.220, 4.359)	
78	Pro	4.887	(, 2.143)
79	Pro	4.449	(1.920, 2.414)

Continued on next page

Table A.3 – continued from previous page

Residue		H_α	H_β
80	Arg	3.91	(2.029, 2.207)
81	Thr	4.889	4.568
82	Ile	4.225	1.65
83	Tyr	4.379	(3.642, 2.554)
84	Glu	3.556	(2.343, 2.137)
85	Asn	4.227	(3.037, 3.183)
86	Arg	4.36	(1.379, 2.219)
87	Ile	4.438	1.658
88	Tyr	4.629	(3.100, 2.971)
89	Ser	5.401	(3.822, 3.957)
90	Leu	5.212	(0.797, 1.424)
91	Lys	5.04	(1.521, 1.968)
92	Ile	5.043	1.553
93	Glu	5.555	(, 2.078)
94	Cys	4.083	(1.941, 2.878)
95	Gly	(4.093, 4.3690)	
96	Pro	4.303	(1.964, 2.453)
97	Lys	4.57	(, 2.032)
98	Tyr	4.638	(3.138, 2.797)
99	Pro	3.672	(1.184, 2.371)
100	Glu	4.302	(2.186, 2.29)
101	Ala	4.522	1.139
102	Pro	2.228	(, 1.560)
103	Pro	4.746	(, 1.545)
104	Phe	4.654	(3.213, 3.03)
105	Val	4.512	1.608
106	Arg	5.063	(1.519, 1.582)
107	Phe	4.469	(3.087, 3.991)
108	Val	4.237	1.972
109	Thr	4.511	4.276
110	Lys	3.858	(, 1.245)
111	Ile	4.299	1.476
112	Asn	5.25	(2.693, 2.925)
113	Met	4.076	(1.54, 1.327)
114	Asn	4.425	(2.630, 3.042)
115	Gly	(3.595, 4.195)	
116	Val	4.351	1.945
117	Asn	4.542	(2.975, 3.451)
118	Ser	4.548	(, 4.163)
119	Ser	4.709	(3.984, 3.957)
120	Asn	4.385	(2.572, 3.039)
121	Gly	(4.287, 3.327)	

Continued on next page

Table A.3 – continued from previous page

Residue		H_α	H_β
122	Val	3.618	2.086
123	Val	4.186	1.932
124	Asp	4.8	(2.768, 3.004)
125	Pro	4.269	(1.935, 2.365)
126	Arg	4.016	(, 1.855)
127	Ala	4.306	1.53
128	Ile	4.509	2.051
129	Ser	4.096	(3.911, 4.012)
130	Val	4.055	1.951
131	Leu	4.835	(1.488, 2.336)
132	Ala	4.026	1.496
133	Lys	4.717	(1.769, 1.932)
134	Trp	4.629	(2.905, 3.694)
135	Gln	4.26	(0.410, 1.640)
136	Asn	4.283	(2.754, 2.607)
137	Ser	4.223	(3.615, 3.901)
138	Tyr	4.468	(1.395, 2.224)
139	Ser	5.077	(3.728, 3.916)
140	Ile	2.975	0.691
141	Lys	2.792	(0.7240, 1.011)
142	Val	3.571	1.901
143	Val	3.342	2.251
144	Leu	3.85	(1.305, 1.774)
145	Gln	3.889	(2.198, 1.915)
146	Glu	4.341	(1.918, 2.043)
147	Leu	3.985	(1.017, 2.044)
148	Arg	4.189	(1.602, 1.921)
149	Arg	4.017	(2.02, 1.927)
150	Leu	4.112	(1.497, 1.945)
151	Met	3.768	(1.778, 2.296)
152	Met	4.458	(2.268,)
153	Ser	4.47	(4.247, 4.189)
154	Lys	4.062	(1.904, 1.982)
155	Glu	4.158	(, 1.991)
156	Asn	5.28	(2.856, 3.690)
157	Met	4.48	(, 2.272)
158	Lys	4.484	(1.697, 2.04)
159	Leu	4.33	(1.175, 1.690)
160	Pro	4.346	(1.859, 2.245)
161	Gln	4.618	(1.755, 2.376)
162	Pro	4.787	(1.716, 2.363)
163	Pro	4.321	(1.696, 2.372)

Continued on next page

Table A.3 – continued from previous page

Residue		H_α	H_β
164	Glu	4.03	(, 1.916)
165	Gly	(4.202, 3.741)	
166	Gln	4.376	(1.829, 1.876)
167	Cys	5.223	(2.923, 2.829)
168	Tyr	4.334	(3.279, 2.774)
169	Ser	4.53	(, 3.968)
170	Asn	4.537	(2.734, 2.809)

Table A.4: $^1H_\gamma$, $^1H_\delta$, and $^1H_\epsilon$ Chemical Shifts. Groups that should contain two values (eg. the H_γ resonances of Lys), but have one value missing indicate that one of the two was unassigned or that the group is degenerate. Groups marked with an asterisk (*) denote that the group is stereospecifically labelled, where the first and second values corresponds to the 'R' and 'S' groups, respectively. For Ile H_γ values, the first two values are for the CG1 protons while the third value is for that of the CG2 proton. $^1H_\delta$ and $^1H_\epsilon$ chemical shifts for Tyr and Phe residues are located in Table A.6.

Residue		H_γ	H_δ	H_ϵ
1	Met	(2.656, 2.579)		
2	Pro	(2.032, 2.090)	(3.721, 3.870)	
3	Gly			
4	Glu	(2.228, 2.265)		
5	Val	(0.930, 0.955)*		
6	Gln	(, 2.367)		(7.457,)
7	Ala			
8	Ser			
9	Tyr			
10	Leu	1.49	(0.901, 0.856)	
11	Lys	(, 1.457)	(, 1.712)	(, 3.001)
12	Ser			
13	Gln	(, 2.338)		(7.445,)
14	Ser			
15	Lys	(, 1.441)	(, 1.694)	(, 2.998)
16	Leu	1.62	(0.915, 0.867)	
17	Ser			
18	Asp			
19	Glu	(, 2.285)		

Continued on next page

Table A.4 – continued from previous page

Residue		H_γ	H_δ	H_ϵ
20	Gly			
21	Arg	(, 1.604)	(, 3.195)	
22	Leu	1.607	(0.907, 0.851)*	
23	Glu	(, 2.257)		
24	Pro	(2.003,)	(3.694, 3.814)	
25	Arg	(, 1.595)	(, 3.169)	
26	Lys	(1.24, 1.317)	(, 1.623)	(, 2.947)
27	Phe			
28	His			
29	Cys			
30	Lys	(1.429, 1.477)	(, 1.697)	(, 2.996)
31	Gly			
32	Val	(0.900, 0.888)		
33	Lys	(, 1.319)	(, 1.648)	(, 2.962)
34	Val	(1.013, 0.970)*		
35	Pro		(3.642, 3.961)	
36	Arg		(3.274, 3.479)	
37	Asn		(7.523, 6.782)	
38	Phe			
39	Arg		(3.415, 3.633)	
40	Leu	1.893	(1.185, 0.913)*	
41	Leu	1.93	(0.913, 0.951)*	
42	Glu	(2.492, 2.164)		
43	Glu	(2.782, 2.191)		
44	Leu	1.647	(0.979, 0.941)*	
45	Glu	(2.337, 2.474)		
46	Glu	(2.611, 2.544)		
47	Gly			
48	Gln	(2.424, 2.625)		(7.319, 6.815)
49	Lys	(1.655, 1.54)	(, 1.75)	(, 3.016)
50	Gly			
51	Val	(1.086, 1.109)*		
52	Gly			
53	Asp			
54	Gly			
55	Thr	1.198		
56	Val	(1.002, 1.016)*		
57	Ser			
58	Trp			
59	Gly			
60	Leu	0.882	(0.473, -0.154)*	
61	Glu	(, 2.074)		

Continued on next page

Table A.4 – continued from previous page

Residue		H_γ	H_δ	H_ϵ
62	Asp			
63	Asp			
64	Glu	(2.305, 2.143)		
65	Asp			
66	Met	(2.557, 2.765)		2.078
67	Thr	1.289		
68	Leu	1.533	(0.970, 0.925)*	
69	Thr	1.16		
70	Arg	(, 1.551)	(, 3.258)	
71	Trp			
72	Thr	1.17		
73	Gly			
74	Met	(2.497, 2.303)		1.915
75	Ile	(1.623, , 0.848)	0.805	
76	Ile	(1.150, 1.629, 0.974)	0.833	
77	Gly			
78	Pro			
79	Pro	(, 2.119)	(3.920, 3.639)	
80	Arg	(1.602, 1.633)	(3.23, 3.314)	
81	Thr	1.339		
82	Ile	(1.396, 1.195, 0.334)	0.844	
83	Tyr			
84	Glu	(2.106, 2.327)		
85	Asn		(7.703, 6.956)	
86	Arg	(1.402, 1.713)	(3.29, 3.357)	
87	Ile	(1.058, 1.566, 0.789)	0.838	
88	Tyr			
89	Ser			
90	Leu	0.949	(0.439, -0.389)*	
91	Lys	(, 1.423)	(1.747, 1.584)	(2.926, 2.977)
92	Ile	(1.355, 0.865, 0.633)	0.659	
93	Glu	(2.048, 2.25)		
94	Cys			
95	Gly			
96	Pro	(2.052, 1.973)	(3.674, 3.719)	
97	Lys	(1.369, 1.410)	(, 1.636)	(, 2.963)
98	Tyr			
99	Pro	(1.705, 1.631)	(3.672, 3.296)	
100	Glu	(2.298, 2.409)		
101	Ala			
102	Pro	(2.048, 1.758)	(3.5, 3.272)	
103	Pro		(2.555, 2.445)	

Continued on next page

Table A.4 – continued from previous page

Residue		H_γ	H_δ	H_ϵ
104	Phe			
105	Val	(0.532, 0.685)*		
106	Arg	(1.657, 1.285)	(3.091, 3.187)	
107	Phe			
108	Val	(1.121, 0.973)*		
109	Thr	1.526		
110	Lys	(-0.389, 0.475)	(, 1.341)	(2.555, 2.631)
111	Ile	(0.592, 1.53, -0.098)	-0.342	
112	Asn		(8.07, 7.024)	
113	Met	(2.146, 2.324)		1.8
114	Asn		(6.848, 7.557)	
115	Gly			
116	Val	(0.695, 0.645)*		
117	Asn		(7.145, 7.682)	
118	Ser			
119	Ser			
120	Asn		(7.235, 6.593)	
121	Gly			
122	Val	(0.941, 0.933)*		
123	Val	(0.705, 0.972)*		
124	Asp			
125	Pro	(1.991, 2.112)	(4.132, 4.222)	
126	Arg	(, 1.728)	(3.292, 3.218)	
127	Ala			
128	Ile	(1.194, 1.611, 0.897)	0.69	
129	Ser			
130	Val	(0.688, 0.732)*		
131	Leu	1.62	(0.941, 0.855)*	
132	Ala			
133	Lys	(, 1.416)	(, 1.690)	(, 2.979)
134	Trp			
135	Gln	(1.640, 1.686)		(6.833, 6.644)
136	Asn		(8.537, 6.689)	
137	Ser			
138	Tyr			
139	Ser			
140	Ile	(1.419, -0.13, 0.180)	-0.704	
141	Lys	(0.895, 1.021)	(1.693, 1.578)	(2.741, 2.908)
142	Val	(0.455, 0.9260)*		
143	Val	(0.760, 1.148)*		
144	Leu	1.736	(1.029, 0.658)*	
145	Gln	(2.620, 2.305)		(6.765, 7.314)

Continued on next page

Table A.4 – continued from previous page

Residue		H_γ	H_δ	H_ϵ
146	Glu	(2.278, 2.148)		
147	Leu	1.821	(0.575, 0.778)*	
148	Arg		(, 3.264)	
149	Arg	(1.737, 1.560)	(3.303, 3.119)	
150	Leu	1.858	(1.035, 0.948)*	
151	Met	(1.22, 2.539)		1.249
152	Met	(2.706, 2.561)		2.162
153	Ser			
154	Lys	(, 1.559)	(, 1.765)	(, 3.057)
155	Glu	(2.275, 2.336)		
156	Asn		(7.504, 7.870)	
157	Met	(2.467, 2.823)		2.187
158	Lys	(, 1.412)	(, 1.715)	(, 3.012)
159	Leu	1.88	(1.012, 0.929)*	
160	Pro	(2.022, 2.055)	(3.976, 3.571)	
161	Gln	(2.495, 1.888)		(7.649, 8.551)
162	Pro	(1.604, 1.765)	(, 3.526)	
163	Pro	(2.013, 1.954)	(3.792, 3.326)	
164	Glu	(2.208, 2.243)		
165	Gly			
166	Gln	(2.257, 2.440)		(7.534, 6.886)
167	Cys			
168	Tyr			
169	Ser			
170	Asn		(7.507, 6.845)	

Table A.5: Aromatic Sidechain ^{13}C, ^{15}N, and ^{1}H Chemical Shifts.

Residue		Ring $^{13}C/^{15}N$	Chemical Shift	Ring ^{1}H	Chemical Shift
9	Tyr	C2,6	(133.139, 133.139)	H2,6	(7.098, 7.098)
		C3,5	(118.297, 118.297)	H3,5	(6.808, 6.808)
27	Phe	C2,6		H2,6	(7.178, 7.178)
		C3,5		H3,5	
		C4		H4	
38	Phe	C2,6		H2,6	(7.272, 7.272)
		C3,5		H3,5	
		C4		H4	
58	Trp	C2	127.689	H2	7.289

Continued on next page

Table A.5 – continued from previous page

Residue		Ring $^{13}C/^{15}N$	Chemical Shift	Ring ^{1}H	Chemical Shift
		C4		H4	7.139
		C5	120.892	H5	6.914
		C6	124.107	H6	7.021
		C7	114.127	H7	7.338
		N1	126.762	HN1	9.899
71	Trp	C2	127.292	H2	7.144
		C4		H4	7.432
		C5		H5	7.001
		C6	123.332	H6	7.182
		C7	115.007	H7	7.379
		N1	129.341	HN1	9.56
83	Tyr	C2,6		H2,6	(7.281, 7.281)
		C3,5		H3,5	(6.731, 6.731)
98	Tyr	C2,6	(132.947, 131.653)	H2,6	(6.993, 6.626)
		C3,5	(119.674, 119.198)	H3,5	(6.5, 6.840)
104	Phe	C2,6		H2,6	(7.220, 7.22)
		C3,5		H3,5	(7.305, 7.305)
		C4		H4	7.292
107	Phe	C2,6	(132.063, 132.063)	H2,6	(7.295, 7.295)
		C3,5	(130.801, 130.801)	H3,5	(6.748, 6.748)
		C4	128.341	H4	6.556
134	Trp	C2	127.549	H2	6.612
		C4		H4	
		C5	121.105	H5	6.667
		C6	124.133	H6	6.762
		C7	115.708	H7	6.927
		N1	133.962	HN1	10.013
138	Tyr	C2,6		H2,6	(6.740, 6.740)
		C3,5		H3,5	(6.796, 6.796)
168	Tyr	C2,6		H2,6	(7.166, 7.166)
		C3,5		H3,5	(6.780, 6.780)

Table A.6: Sidechain Amide ^{15}N, and ^{1}H Chemical Shifts.

Residue		$^{15}ND2/^{15}NE2$	$^{1}HD/^{1}HE$
6	Gln	112.204	(7.457, 0.001)
13	Gln	112.373	(7.445, 0.001)
37	Asn	111.384	(7.523, 6.782)
48	Gln	111.147	(7.319, 6.815)
85	Asn	113.018	(7.703, 6.956)
112	Asn	110.446	(8.07, 7.024)
114	Asn	114.139	(6.848, 7.557)
117	Asn	114.407	(7.145, 7.682)
120	Asn	108.236	(7.235, 6.593)
135	Gln	111.891	(6.833, 6.644)
136	Asn	113.295	(8.537, 6.689)
145	Gln	109.981	(6.765, 7.314)
156	Asn	117.145	(7.504, 7.870)
161	Gln	124.302	(7.649, 8.551)
166	Gln	111.238	(7.534, 6.886)
170	Asn	112.4	(7.507, 6.8450)

Appendix B

Python Scripting

Over the course of my training, I've used the Python programming language to create numerous scripts that were absolutely essential for many tasks, including data processing and writing PyMol scripts. Below is an example of one such script. Dubbed 'Superanalyzer.py,' the script does a number of things with the output from AMBER molecular dynamics simulations. It pulls out the energy values from 'prot' and 'unprot' files for K63. With these values, it calculates the respective ΔpK_a. Once all the ΔpK_as have been calculated, the mean and standard deviation for the ΔpK_a are calculated. Also, for each PDB file, the script calculates angles θ and ϕ, and the distances between the C_δ of E64 and sidechain nitrogen of K63, C_γ of D81 and sidechain nitrogen of K63, thioester carbonyl carbon and sidechain nitrogen of K63, and thioester carbonyl oxygen and sidechain nitrogen of K63. All the ΔpK_a, angle, and distance values are tabulated and written into an output file dubbed 'analysis.txt.'

```
#!/usr/bin/python

import re

import sys

import os

import math

from Numeric import *

path = './'

name = 'K63_'

if (sys.argv[2] == None):
    print "Error!  Please imput number of structures within command"
    sys.exit(1)

number = int(sys.argv[2])
x = int(sys.argv[1])

end = number+1

pkas = open("%sanalysis.txt"%(path),"w")

prot={}
unprot={}

y=x
z=x
while (y != end):
    pout = open("%s%sprot.out%s"%(path,name,y),"r")
    for line in pout.readlines():
        matchone = re.search("( Etot    = )( +[^ ]+ +)(EKtot    = )( +[^ ]+
+)(EPtot      = )( +)([^ ]+)(.*)",line)
        if (matchone != None):
            prot[y]=float(matchone.group(7))
            #print "prot"
            #print prot[y]
    unpout=open("%s%sunprot.out%s"%(path,name,y),"r")
    for line in unpout.readlines():
        matchtwo = re.search("( Etot    = )( +[^ ]+ +)(EKtot    = )( +[^ ]+
+)(EPtot      = )( +)([^ ]+)(.*)",line)
        if (matchtwo != None):
            unprot[y]=float(matchtwo.group(7))
            #print "unprot"
            #print unprot[y]
    y=y+1
#print prot
#print unprot
deltapkas={}


while (z != end):
    print z
    pka = -(((prot[z] - unprot[z])-(-15.21))/1.374643301)
    deltapkas[z]=pka
```

```
    print deltapkas[z]
    #pkas.write("%s                %s\n"%(z,pka))
    z=z+1

pkanumbers=prot.keys()
deltapkatotal=0
numberofstructs=0
for num in pkanumbers:
    deltapkatotal = deltapkatotal+deltapkas[num]
    numberofstructs = numberofstructs+1
mean = float(deltapkatotal/numberofstructs)

squareddev=0

for num in pkanumbers:
    squareddev= squareddev+((mean-deltapkas[num])**2)

stddev=(squareddev/(numberofstructs-1))**0.5
end=int(sys.argv[2])

start = int(sys.argv[1])

name = 'QMcharge.pdb.'

endx = end+1

angles = {}
anglestwo={}
bin1 = []
bin2 = []
bin3 =[]

while (start != endx):
    pdb = open("%s%s%s"%(path,name,start),"r")
    print start
    for line in pdb.readlines():
        match = re.search("([^ ]+ +[^ ]+ +[^ ]+ +[^ ]+ +[^ ]+)( +)([^ ]+)(
+)([^ ]+)( +)([^ ]+)( +)(.*)",line)
        if (match != None):
            atom = match.group(1)
            xcoord=float(match.group(3))
            ycoord=float(match.group(5))
            zcoord=float(match.group(7))

            if (atom == 'ATOM   5815  NZ  LYS   352'):
                lysx = xcoord
                lysy = ycoord
                lysz = zcoord
            if (atom == 'ATOM   7311  C   GLY   441'):
                glycx = xcoord
                glycy = ycoord
                glycz = zcoord
                if (atom == 'ATOM   7312  O   GLY   441'):
                glyox = xcoord
                glyoy = ycoord
                glyoz = zcoord
            if (atom == 'ATOM   7308  CA  GLY   441'):
                glycax = xcoord
                glycay = ycoord
```

```
                glycaz = zcoord

    lysorix = (lysx - glycx)
    lysoriy = (lysy - glycy)
    lysoriz = (lysz-glycz)
    glyoorix = (glyox - glycx)
    glyooriy = (glyoy - glycy)
    glyooriz = (glyoz - glycz)

    glycarix = (glycax - glycx)
    glycariy = (glycay - glycy)
    glycariz = (glycaz - glycz)
    firstcrossx =(glyooriy*glycariz-glyooriz*glycariy)
    firstcrossy =-(glyoorix*glycariz-glyooriz*glycarix)
    firstcrossz =(glyoorix*glycariy-glyooriy*glycarix)

    secondcrossx =(glyooriy*firstcrossz-glyooriz*firstcrossy)
    secondcrossy =-(glyoorix*firstcrossz-glyooriz*firstcrossx)
    secondcrossz =(glyoorix*firstcrossy-glyooriy*firstcrossx)

    norm = (secondcrossx**2 + secondcrossy**2 + secondcrossz**2)**(0.5)
    dotprodtwo = (secondcrossx*lysorix + secondcrossy*lysoriy + secondcrossz*
lysoriz)

    dotprod = (lysorix*glyoorix + lysoriy*glyooriy + lysoriz*glyooriz)
    normlys = (lysorix**2 + lysoriy**2 + lysoriz**2)**(0.5)
    normgly = (glyoorix**2 + glyooriy**2 + glyooriz**2)**(0.5)
        angle1 = arccos(dotprod/(normlys*normgly))*(180.0/3.14159)
    angle2 = arccos(dotprodtwo/(normlys*norm))*(180.0/3.14159)

    angles[start] = angle1
    anglestwo[start]=(90 - angle2)
    bin1.append(angle1)
    start = start+1

#print bin1

end=int(sys.argv[2])

start = int(sys.argv[1])

name = 'QMcharge.pdb.'

endx = end+1

bin1 = []
bin2 = []
bin3 =[]
G76COK63N = {}
while (start != endx):
    pdb = open("%s%s%s"%(path,name,start),"r")
    for line in pdb.readlines():
        match = re.search("([^ ]+ +[^ ]+ +[^ ]+ +[^ ]+ +[^ ]+)( +)([^ ]+)(
+)([^ ]+)( +)([^ ]+)( +)(.*)",line)
        if (match != None):
            atom = match.group(1)
            xcoord=float(match.group(3))
            ycoord=float(match.group(5))
            zcoord=float(match.group(7))
```

```
            if (atom == 'ATOM   5815  NZ  LYS   352'):
                lysx = xcoord
                lysy = ycoord
                lysz = zcoord
            if (atom == 'ATOM   7311  C   GLY   441'):
                glyx = xcoord
                glyy = ycoord
                glyz = zcoord
    distance = ((lysx - glyx)**2 + (lysy - glyy)**2 + (lysz - glyz)**2)**(
0.5)
    G76COK63N[start] = distance
    start = start+1

end=int(sys.argv[2])

start = int(sys.argv[1])

name = 'QMcharge.pdb.'

endx = end+1

bin1 = []
bin2 = []
bin3 =[]

E64K63={}

while (start != endx):
    pdb = open("%s%s%s"%(path,name,start),"r")
    for line in pdb.readlines():
        match = re.search("([^ ]+ +[^ ]+ +[^ ]+ +[^ ]+ +[^ ]+)( +)([^ ]+)(
+)([^ ]+)( +)([^ ]+)( +)(.*)",line)
        if (match != None):
            atom = match.group(1)
            xcoord=float(match.group(3))
            ycoord=float(match.group(5))
            zcoord=float(match.group(7))

            if (atom == 'ATOM   5815  NZ  LYS   352'):
                lysx = xcoord
                lysy = ycoord
                lysz = zcoord
            if (atom == 'ATOM   5831  CD  GL4   353'):
                glyx = xcoord
                glyy = ycoord
                glyz = zcoord
    distance = ((lysx - glyx)**2 + (lysy - glyy)**2 + (lysz - glyz)**2)**(
0.5)
    E64K63[start]=distance
    start=start+1

end=int(sys.argv[2])

start = int(sys.argv[1])

name = 'QMcharge.pdb.'

endx = end+1
```

```
bin1 = []
bin2 = []
bin3 =[]

D81K63={}

while (start != endx):
    pdb = open("%s%s%s"%(path,name,start),"r")
    for line in pdb.readlines():
        match = re.search("([^ ]+ +[^ ]+ +[^ ]+ +[^ ]+ +[^ ]+)( +)([^ ]+)(
+)([^ ]+)( +)([^ ]+)( +)(.*)",line)
        if (match != None):
            atom = match.group(1)
            xcoord=float(match.group(3))
            ycoord=float(match.group(5))
            zcoord=float(match.group(7))

            if (atom == 'ATOM   5815  NZ  LYS   352'):
                lysx = xcoord
                lysy = ycoord
                lysz = zcoord
            if (atom == 'ATOM   3618  CG  AS4   220'):
                glyx = xcoord
                glyy = ycoord
                glyz = zcoord
    distance = ((lysx - glyx)**2 + (lysy - glyy)**2 + (lysz - glyz)**2)**(
0.5)
    D81K63[start]=distance
    start=start+1

end=int(sys.argv[2])

start = int(sys.argv[1])

name = 'QMcharge.pdb.'

endx = end+1

bin1 = []
bin2 = []
bin3 =[]

G760K63N={}

while (start != endx):
    pdb = open("%s%s%s"%(path,name,start),"r")
    for line in pdb.readlines():
        match = re.search("([^ ]+ +[^ ]+ +[^ ]+ +[^ ]+ +[^ ]+)( +)([^ ]+)(
+)([^ ]+)( +)([^ ]+)( +)(.*)",line)
        if (match != None):
            atom = match.group(1)
            xcoord=float(match.group(3))
            ycoord=float(match.group(5))
            zcoord=float(match.group(7))

            if (atom == 'ATOM   5815  NZ  LYS   352'):
                lysx = xcoord
                lysy = ycoord
                lysz = zcoord
```

```
            if (atom == 'ATOM   7312  O   GLY   441'):
                glyx = xcoord
                glyy = ycoord
                glyz = zcoord
    distance = ((lysx - glyx)**2 + (lysy - glyy)**2 + (lysz - glyz)**2)**(
0.5)
    G76OK63N[start]=distance
    start=start+1


pkas.write("Structure       DeltaPKA       Angle1       Angle2
E64-K63       D81-K63       G76C-K63N       G76O-K63N\n")

for num in pkanumbers:
    pkas.write("%s          %.3f          %.3f          %.3f
%.3f          %.3f          %.3f          %.3f          %.3f          \n"%(num,deltapkas[num
],angles[num],anglestwo[num],E64K63[num],D81K63[num],G76COK63N[num],G76OK63N
[num]))
pkas.write("\n\nmean = %s\nstd.dev. = %s\ntotal structures = %s\n"%(mean,
stddev,numberofstructs))
```